

CORIOLIS VIBRATORY MEMS GYRO DRIVE AXIS CONTROL WITH
PROXY-BASED SLIDING MODE CONTROLLER

A THESIS SUBMITTED TO
THE GRADUATE SCHOOL OF NATURAL AND APPLIED SCIENCES
OF
MIDDLE EAST TECHNICAL UNIVERSITY

BY

DERYA ÜNSAL ÖZTÜRK

IN PARTIAL FULFILLMENT OF THE REQUIREMENTS
FOR
THE DEGREE OF DOCTOR OF PHILOSOPHY
IN
ELECTRICAL AND ELECTRONIC ENGINEERING

JUNE 2022

Approval of the thesis:

**CORIOLIS VIBRATORY MEMS GYRO DRIVE AXIS CONTROL WITH
PROXY-BASED SLIDING MODE CONTROLLER**

submitted by **DERYA ÜNSAL ÖZTÜRK** in partial fulfillment of the requirements
for the degree of **Doctor of Philosophy in Electrical and Electronic Engineering,**
Middle East Technical University by,

Prof. Dr. Halil Kalıpçılar
Dean, Graduate School of **Natural and Applied Sciences** _____

Prof. Dr. İlkey Ulusoy
Head of the Department, **Electrical and Electronic
Engineering** _____

Prof. Dr. Aydan M. Erkmén
Supervisor, **Electrical and Electronic Engineering, METU** _____

Examining Committee Members:

Prof. Dr. Kemal Leblebiciođlu
Electrical and Electronic Engineering, METU _____

Prof. Dr. Aydan M. Erkmén
Electrical and Electronic Engineering, METU _____

Prof. Dr. Afşar Saranlı
Electrical and Electronic Engineering, METU _____

Prof. Dr. Mustafa Dođan
Control and Automation Engineering, ITU _____

Assist. Prof. Dr. Murat Üçüncü
Electrical and Electronic Engineering, Baskent University _____

Date: 20.06.2022

I hereby declare that all information in this document has been obtained and presented in accordance with academic rules and ethical conduct. I also declare that, as required by these rules and conduct, I have fully cited and referenced all material and results that are not original to this work.

Name Last name : Derya Ünsal Öztürk

Signature :

ABSTRACT

CORIOLIS VIBRATORY MEMS GYRO DRIVE AXIS CONTROL WITH PROXY-BASED SLIDING MODE CONTROLLER

Ünsal Öztürk, Derya
Doctor of Philosophy, Electrical and Electronic Engineering
Supervisor : Prof. Dr. Aydan Erkmen

June 2022, 134 pages

This thesis investigates controller design on the drive axis of MEMS gyroscopes. To increase the performance of gyros, modeling errors, mechanical imperfections, and sensor parameter changes due to the change of environmental factors should be eliminated. The tracking parameters of the closed loop MEMS gyro is strongly related to the performance of the controller on the drive axis. This controller should be robust to disruptive effects and modeling errors. This study uses “Weighted Feed Forward Controller” and “Proxy Based Sliding Mode Controller” methods to control the drive axis. Weighted Feedforward Controllers are used to change the places of zeros to increase error performance and response time. Both methods are robust to model uncertainty and disruptive effects on simulation environments. However, experiments prove that “Proxy Based Sliding Mode Controller” performance overwhelms the other methods. Sliding Mode Controller and PID controller are implemented to compare both methods is based on simulation and experimental data.

Keywords: Gyroscope, Feedforward, Sliding Mode Control, MEMS

ÖZ

VEKİL TABANLI KAYAN KIPLİ KONTROL İLE CORİOLİS TİTREŞİMLİ MEMS DÖNÜÖLÇER SÜRME EKSENİ KONTROLÜ

Ünsal Öztürk, Derya
Doktora, Elektrik ve Elektronik Mühendisliği
Tez Yöneticisi: Prof. Dr. Aydan Erkmen

Haziran 2022, 134 sayfa

Bu tez çalışması, MEMS dönüölçerin sürme eksenini için denetleyici tasarımı konusunu tartışmaktadır. Dönüölçerlerin başarımının iyileştirilmesi için modelleme hataları, mekanik üretim bozuklukları, sensör parametrelerinin çevresel faktörlerle değişmesi ve mekanik- termal gürültü etkilerinin bastırılması gerekmektedir. Kapalı döngü bir MEMS dönüölçerin takip performansı sürme eksenindeki denetleyicinin performansı ile büyük ölçüde ilişkilidir. Sürme eksenini denetimi için kullanılacak denetleyici bozucu etkiler ve modelleme hataları altında kararlı ve gürbüz olmalıdır. Bu çalışma, sürme eksenini denetimi için “Ağırlıklandırılmış İleri Beslemeli Denetim” yöntemini ve “Vekil Tabanlı Kayan Kipli Kontrol” yöntemlerini önermektedir. Ağırlıklandırılmış İleri Beslemeli Denetim yönteminde hata başarımı ve yanıt hızını arttırmak için denetim döngüsünün sıfırlarının yerleşimi değiştirilmektedir. Önerilen her iki yöntem de simulasyon ortamında model belirsizlikleri ve bozucu etkilere karşı gürbüzlük sağlarken deneysel veriler Vekil Tabanlı Kayan Kipli Kontrol yönteminin üstünlüğünü ortaya koymaktadır. Önerilen yöntemlere ek olarak, başarımlarını karşılaştırmak üzere kayan kipli denetleyici ve PID denetleyici sürme eksenini denetleyicisi olarak geliştirilmiştir. Çalışma sonuçları, simulasyon verileri ve deneysel verilerle karşılaştırmalı olarak verilmiştir.

Anahtar Kelimeler: Dönüölçer, İleri Besleme, Kayan Kipli Denetim, MEMS, Vekil Tabanlı Kayan Kipli Kontrol

To my family

ACKNOWLEDGMENTS

The author wishes to express his deepest gratitude to her supervisor Prof. Dr. Aydan Erkmen, for her guidance, advice, criticism, encouragement, and insight throughout the research.

The author would also like to thank Prof. Dr. Kemal Leblebiciođlu and Prof. Dr. Mustafa Dođan for their suggestions and comments.

The author also wishes to thank her colleague Bađıř Altınöz for his support, encouragement, and friendship.

The author would like to express her special thanks to her family for their love, endless support, and patience. Finally, the support provided by ROKETSAN Inc. to this thesis is greatly acknowledged.

TABLE OF CONTENTS

ABSTRACT	v
ÖZ.....	vi
ACKNOWLEDGMENTS	ix
TABLE OF CONTENTS	x
LIST OF TABLES	xiii
LIST OF FIGURES	xiv
LIST OF ABBREVIATIONS	xix
LIST OF SYMBOLS.....	xx
CHAPTERS	
1 INTRODUCTION.....	1
1.1 Problem Definition	3
1.2 Objectives and Goals	6
1.3 Methodology.....	7
1.4 Contributions of the Thesis.....	10
1.5 Outline of the Thesis.....	11
2 MEMS GYROSCOPE TECHNOLOGY	13
2.1 Gyroscope Performance Metrics	14
2.1.1 Bias	14
2.1.2 Scale Factor Error.....	16
2.1.3 Misalignment.....	17
2.1.4 G-Dependent Bias	18
2.1.5 Noise.....	18
2.2 Gyroscope Classification	19

2.2.1	Performance Classification	20
2.2.2	Structural Classification.....	21
2.3	Coriolis Vibratory MEMS Gyroscope (CVG MEMS) Operating Principle 23	
2.4	Dynamic Model.....	29
2.5	MEMS Gyro Structure	30
2.6	MEMS Technology Trends.....	32
3	MEMS GYROSCOPE DRIVE AXIS CONTROL TECHNIQUES	37
3.1	Closed Loop Control Structure	37
3.2	Sliding Mode Control: A Background Overview	39
3.2.1	Sliding Surface.....	41
3.2.2	Controller Rule.....	44
3.2.3	Our Proposed SMC Design for the Gyro Drive Axis Control Problem 49	
3.2.4	Chattering Minimization by Fat-Boundary Layer Sliding Mode Controller	51
3.3	Proxy-Based Sliding Mode Control: A Background Overview.....	53
3.3.1	Our Proposed of PBSMC Design to Gyro Drive Axis Control Problem 54	
3.4	Feedforward Controller: A Background Overview.....	58
3.4.1	Our Proposed of Weighted Feedforward Controller Design to Gyro Drive Axis Control Problem	60
4	SIMULATION AND EXPERIMENTAL RESULTS	67
4.1	Gyro Dynamic Model.....	67
4.2	Simulation Results.....	69

4.2.1	PID Controller Results	69
4.2.2	Sliding Mode Controller and Sliding Mode Controller with Boundary Layer Results	72
4.2.3	Proxy-Based Sliding Mode Controller Results	75
4.2.4	Weighted Feedforward Controller Results	78
4.2.5	Simulation Result Comparison of Controller Performances	82
4.3	Experimental Results	88
4.3.1	Experimental Setup	88
4.3.2	PID Controller Results	91
4.3.3	Sliding Mode Controller and Sliding Mode Controller with Boundary Layer Results	92
4.3.4	Proxy-Based Sliding Mode Controller Results	95
4.3.5	Weighted Feedforward Controller Results	98
4.3.6	Experimental Result Comparison of Controller Performances	101
5	SENSIVITY ANALYSIS.....	107
5.1	Error Performance Comparison for Different Noise Levels.....	107
5.2	Controller Performance Comparison for Different SMC Parameters	115
5.3	Error Performance Comparison for Different Angular Rate Input.....	120
6	CONCLUSIONS AND FUTURE WORK.....	125
6.1	Conclusions.....	125
6.2	Future Works	126
	REFERENCES	127
	CURRICULUM VITAE	133

LIST OF TABLES

TABLES

Table 2.1 Gyroscope Performance Classification.....	20
Table 3.1 PBSMC Behaviors According to Parameters	57
Table 4.1. MEMS Gyro Parameters.....	68
Table 4.2 Simulation Parameters	69
Table 4.3 PID Controller Parameters	70
Table 4.4 SMC and SMC-BL Parameters.....	72
Table 4.5 W-FF Controller Parameters (PID Controller Parameters and Weighting Coefficients).....	79
Table 4.6 Error Performance and Convergence Time for Controllers.....	87
Table 4.7 Angular Rate Measurement Total Error Comparison.....	88
Table 4.8 Rate Table Properties.....	88
Table 4.9 Error Performance and Convergence Time for Controllers.....	105
Table 4.10 Angular Rate Measurement Total Error Comparison.....	106
Table 5.1 Error Performance Comparison for Different Noise Power Level	113
Table 5.2 Angular Rate Total Error Comparison for Different Input Rates	120

LIST OF FIGURES

FIGURES

Figure 2.1 Representation of bias and scale factor (Emcore Navigation, 2020).....	15
Figure 2.2 Bias over temperature (Cui et al., 2019)	15
Figure 2.3 Representation of Ideal, Actual and Linear Fit Scale Factor (Figure is taken from (Vectornav Navigation, 2020))	17
Figure 2.4 Scale factor over temperature example (Cui et al., 2019).....	17
Figure 2.5 Representation of Misalignment (Adopted from(Looney, 2015)	18
Figure 2.6 MEMS Gyro Structural Classification, (Adopted from (Apostolyuk, 2016))	22
Figure 2.7 DTG Configuration (Adopted from (El-Sheimy & Youssef, 2020)).....	23
Figure 2.8 2-DOF Gyroscope Model.....	24
Figure 2.9 A Generic MEMS Gyro Structure	25
Figure 2.10 Representation of the Position vector Relative to the Inertial Frame A and the Rotating Reference Frame B (Adopted from (Acar & Shkel, 2008)).....	26
Figure 2.11 Representation of the gyroscope frame rotating with respect to the inertial frame (Adopted from (Acar & Shkel, 2008)).....	27
Figure 2.12 Proof Mass TFG and Lumped Model (Adopted from (Acar & Shkel, 2008))	29
Figure 2.13 A typical MEMS Gyro Functional Block Diagram (Analog Devices ADXRS645 Data Sheet).....	31
Figure 2.14 MEMS Packaging Example (Kyocera Industries, 2022)	32
Figure 2.15 Wire -bonding Example (Warren, 2009)	32
Figure 2.16 Development of gyro technology over the years (Damiano & Girardin, 2020).....	33
Figure 2.17. Gyro Performance vs Cost Technology Classification (Damiano & Girardin, 2020)	34
Figure 2.18. The future of gyro technology (Damiano & Girardin, 2020).....	35
Figure 3.1 Gyro Drive Axis Control Loop	37

Figure 3.2 Phase Plane (adopted from Yasin et al., 2018).....	44
Figure 3.3 Sliding Mode Controller Structure	45
Figure 3.4 Representation of Chattering on the Sliding Surface (Adopted from (Tanakitkorn et al., 2018)).....	48
Figure 3.5 Sliding Mode Controller for Gyro Drive Axis Control Problem	49
Figure 3.6 Representation of Boundary Layer on the Sliding Surface (Adopted from (Erbatur & Çallı, 2009)).....	51
Figure 3.7 Representation of Saturation Function (Adopted from (Erbatur & Çallı, 2009)).....	52
Figure 3.8 Physical Interpretation of Proxy Based Sliding Mode Control (Kikuuwe & Fujimoto, 2006)	53
Figure 3.9 Block Diagram of Control Loop with PBSMC (Gu et al., 2015).....	54
Figure 3.10 Proxy-Based Sliding Mode Controller Working Principle	54
Figure 3.11 Proxy-Based Sliding Mode Controller Design for Gyro Drive Axis ..	57
Figure 3.12 Disturbance Feedforward Controller	59
Figure 3.13 Setpoint/2-DOF Feedforward Controller	59
Figure 3.14 Example application for feedforward and W-FF controller	62
Figure 3.15 Pole-Zero Analysis for feedback control with PID controller.....	63
Figure 3.16 Pole-Zero Analysis for feedfoward control, $K1 > K2$	63
Figure 3.17 Pole-Zero Map Analysis for feedfoward control, $K2 > K1$	64
Figure 3.18 Step responses for PID, FF and W-FF.....	64
Figure 3.19. Weighted Feedforward Controller for Drive-Axis Control.....	65
Figure 4.1 Signal Processing Loop for Angular Rate Estimation.....	68
Figure 4.2. PID Controller Tracking Performance for Drive Axis Control.....	70
Figure 4.3. Controller Tracking Error Performance PID.....	71
Figure 4.4. Angular Rate Measurement with PID Controller (for 10 deg/s)	71
Figure 4.5. SMC and SMC-BL Tracking Performance for Drive Axis Control.....	73
Figure 4.6. SMC and SMC-BL Controller Tracking Error Performance	74
Figure 4.7. Angular Rate Measurement with SMC and SMC-BL (for 10 deg/s)...	75
Figure 4.8. PBSMC Tracking Performance for Drive Axis Control	76

Figure 4.9. PBSMC Tracking Error Performance	77
Figure 4.10. Angular Rate Measurement with PBSMC (for 10 deg/s)	78
Figure 4.11. W-FF Tracking Performance for Drive Axis Control.....	80
Figure 4.12. W-FF Controller Tracking Error Performance	81
Figure 4.13. Angular Rate Measurement with W-FF (for 10 deg/s).....	82
Figure 4.14. Controller Tracking Performance for Drive Axis Control (Initial Phase)	83
Figure 4.15. Controller Tracking Performance for Drive Axis Control (Steady State Phase)	84
Figure 4.16. Controller Error Comparison (Initial Phase).....	85
Figure 4.17. Controller Error Comparison (Steady State Phase)	86
Figure 4.18 Angular Rate Measurement Comparisons (for 10 deg/s).....	87
Figure 4.19. Experimental Setup	89
Figure 4.20. Experimental Setup -Data Monitoring and Logging.....	89
Figure 4.21. Reference Vibration Signal in Real Application.....	90
Figure 4.22. PID Tracking Performance for Drive Axis Control-Experimental Data	91
Figure 4.23. PID Controller Tracking Error Performance -Experimental Data	91
Figure 4.24. Angular Rate Measurement with PID - Experimental Data (for 10 deg/s)	92
Figure 4.25. SMC and SMC-BL Tracking Performance for Drive Axis Control-Experimental Data	93
Figure 4.26. SMC and SMC-BL Controller Tracking Error Performance - Experimental Data	94
Figure 4.27. Angular Rate Measurement with SMC and SMC-BL - Experimental Data (for 10 deg/s).....	95
Figure 4.28. PBSMC Tracking Performance for Drive Axis Control-Experimental Data.....	96
Figure 4.29. PBSMC Tracking Performance for Drive Axis Control-Experimental Data.....	97

Figure 4.30. Angular Rate Measurement with PBSMC - Experimental Data (for 10 deg/s).....	98
Figure 4.31.W-FF Tracking Performance for Drive Axis Control-Experimental Data.....	99
Figure 4.32.W-FF Controller Tracking Error Performance -Experimental Data .	100
Figure 4.33.Angular Rate Measurement with W-FF - Experimental Data (for 10 deg/s).....	101
Figure 4.34. Controller Tracking Performance for Drive Axis Control – Experimental Data	102
Figure 4.35. Controller Error Comparison (Initial Phase) – Experimental Data..	103
Figure 4.36. Controller Error Comparison (Steady State Phase) – Experimental Data	104
Figure 4.37 Angular Rate Measurement Comparison-Experimental Data	105
Figure 5.1 Controller Tracking Performance for Drive Axis Control – 0.5 PSD (Initial Phase).....	108
Figure 5.2 Controller Tracking Performance for Drive Axis Control – 0.5 PSD (Steady State Phase).....	109
Figure 5.3 Error Comparisons – 0.5 PSD (Initial Phase).....	110
Figure 5.4 Controller Tracking Performance for Drive Axis Control – 1.5 PSD .	111
Figure 5.5 Error Comparisons – 1.5 PSD (Initial Phase).....	112
Figure 5.6 Controller Tracking Performance for Drive Axis Control – 40 kHz Reference Vibration Signal Frequency	114
Figure 5.7 Error Comparisons – 40 kHz Reference Vibration Signal Frequency	114
Figure 5.8 Effect of λ on the SMC Tracking Performance	115
Figure 5.9 Effect of λ on the SMC Error Performance	116
Figure 5.10 Effect of Q on the SMC Tracking Performance	117
Figure 5.11 Effect of Q on the SMC Error Performance	118
Figure 5.12 Effect of ϕ on the SMC Tracking Performance	119
Figure 5.13 Effect of ϕ on the SMC Error Performance	120

Figure 5.14 Controller Tracking Performance for Drive Axis Control – Experimental Data 20 deg/s input rate	121
Figure 5.15 Error Comparisons - Experimental Data 20 deg/s input rate	122
Figure 5.16 Angular Rate Measurement Comparison-Experimental Data 20 deg/s input rate	123

LIST OF ABBREVIATIONS

ABBREVIATIONS

ADC: Analog to Digital Converter

ARW: Angular Random Walk

ASIC: Application Specific Integrated Circuit

CVG: Coriolis Vibratory Gyroscope

DOF: Degree of Freedom

DSBDC : Double Side Band Suppressed Carrier

DTG: Dynamically Tuned Gyro

FF: Feedforward

HRG: Hemispherical Resonator Gyroscope

LPF: Low Pass Filter

MEMS: Micro Electro Mechanical Systems

NA : Not Applicable

PBPMC: Proxy-Based Sliding Mode Controller

PID: Proportional Integral Derivative

SMC: Sliding Mode Controller

TFG: Tuning Fork Gyro

W-FF: Weighted Feedforward

LIST OF SYMBOLS

SYMBOLS

Ω : Angular Rate

ϕ : Boundary Layer Thickness

sgn : Signum Function

λ : Sliding Surface Coefficient

CHAPTER 1

INTRODUCTION

Today, navigation systems are critical components for safety navigation on land, sea and especially on air platforms. Navigation systems use gyroscope measurements to generate attitude, acceleration, and angular rate data and make use of different types of gyroscopes that are generally classified according to their technologies and error performances (Groves P.D., 2003; Passaro et al., 2017). Gyroscope error characteristics directly affect navigation and flight control performance. For example, attitude of rolling aircraft is calculated based on the x-axis gyro measurement and the attitude is sensitive to gyro errors. (Shi et al., 2011) Similarly, direction cosine matrix and quaternion vector are calculated according to gyro measurements, frame transformations are made according to direction cosine matrix, and quaternions and accuracy of gyro measurement directly affects the estimation accuracy of position and velocity. On the other hand, attitude determination has become quite crucial for some applications such as mobile mapping (photogrammetry or scanning), airborne reconnaissance (pointing of cameras to a specific location on the ground) and motion compensation applications (ensure airborne mapping camera points vertically to the ground and marine mapping is not distorted by wave movement) (Hexagon, 2022). Finally, gyro performance has a crucial role on gimbal stabilization applications. With the introduction of gimbals into many systems, the need for cheap, small, and high-performance gyros has increased.

The gyroscope market is growing up, powered by widespread research and implementations on missiles, autonomous vehicles, robots, and mobile phones, all of which are demanding greater precision and even-smaller devices. Different types

of gyros (Ring Laser, Fiber Optic, MEMS (Micro Electro Mechanical Systems), Quartz, Cold Atom) are generally used in various applications and are classified according to bias and bias stability performances.

Gyros which have bias stability between 0.01 deg/h and 1 deg/h are defined as navigation grade. Bias stability between 1 deg/h and 10 deg/h represents tactical grade and greater than 10 deg/h represents control/industrial grade. FOG (Fiber Optic Gyro) and RLG (Ring Laser Gyro) technologies provide navigation and tactical grade performances. While gyroscope drift dominates the definition of grade, all platforms have their own requirements such as bandwidth, vibration and shock, power consumption, etc. Therefore, users can not use a gyro for navigating a ship and the same system for guiding a missile.(Moyer, 2020)

Tactical grade gyros are especially preferred in long-term navigation and stabilization applications that currently require small dimensions, low power consumption, and low cost (Passaro et al., 2017). Navigation grade sensors are preferred for long-term mission plannings (airplanes, strategic missiles, UAVs, underwater vehicles,etc.). Navigation grade sensors are expensive, production processes are complex and production volumes are small. On the other hand, three major technologies in inertial sensing (FOG, RLG and MEMS) have enabled advances in military and commercial capabilities.

Control grade gyros are widely used in commercial applications such as mobile phones, automotive, camera stabilization, etc. MEMS sensor technology dominates the control grade sensor industry. Since, MEMS technology stands out with its manufacturability, low cost and performance improvements based on high precision, low noise readout circuits and control and compensation electronics. While early MEMS technology presented control grade error performance but in recent years, new trends (new manufacturing techniques, closed-loop sensor and circuit designs, etc.) in MEMS technology provides tactical grade error performance. As a result of that, MEMS sensors can be used in long term navigation applications and precious flight control applications.

A brief history of MEMS technology is as follows.

The first prototype of MEMS gyro was developed in Drapper Labs in 1991. ((Greiff et al., n.d.) In the same decade, British Aerospace Systems, Murata and Berkeley University developed simulators with various performance characteristics. Later on, commercial companies like Samsung and Bosch made investments in this topic. At the beginning of 2000's, Analog Devices produced and introduced an integrated dual resonator gyro into the market (Geen et al., 2002).

Since 1990 to 2000, different fabrication methods have been developed to increase sensor performance. In 2007, Researchers from Georgia Tech University developed high-performance MEMS gyro with ASIC design. (Acar & Shkel, 2008)

In the rest of 2000s from all over the world, lots of companies started to develop and produce MEMS gyro. With the help of the rising technology, the proliferation of ASIC usage and controlled development and production techniques, performance of sensors are upgraded.(Acar & Shkel, 2008)

In the later stages of the 2000s, in addition to the developments in production technology, algorithms started to run on the sensors. This has opened up new opportunities for increasing sensor performances. Based on this point, in this thesis, controller algorithms are proposed to increase the performance and robustness of a MEMS gyroscope.

1.1 Problem Definition

MEMS gyros have less stability over temperature, humidity and stress, some of which can be compensated for software with calibration tests and algorithms. Additionally, MEMS gyro technology offers more integration error as compared to FOG or RLG. And, MEMS technology often has varied performance across lots of units due to the variations on the process and raw material. Therefore, various methods should be developed in order to standardize sensor performance and upgrade the stability and robustness.

Although MEMS technology provided control/industrial grade performance at the beginning, nowadays it tries to find a place in larger areas using the advantage of size, power consumption and low cost. Therefore, MEMS technology has moved to control grade to tactical and navigation grade.

Mechanical sensing elements of MEMS gyros are required to provide excellent performance, stability, and robustness to meet expected specifications such as bias instability, linearity and bandwidth. Fabrication imperfections and variations and fluctuations in the environmental conditions (ambient temperature and/or pressure) during the operation time of these devices introduce significant errors, which typically require electronic compensation. (Acar & Shkel, 2008). For example, gyro quadrature errors can be orders of magnitude larger than the angular rate measurement component and in open-loop applications and this can cause delusive effects on the dynamic range of the readout circuit (Raman et al., 2009).

Researchers have developed various methods for MEMS sensors to reach tactical and navigation grade performance with upgrading stability and robustness. The basis of these methods consists of compensating the effects of mechanical imperfections, environmental condition dependent parameter variations and mechanical–thermal noises that cause performance degradation.

Some of these compensation methods are constructed over hardware such as multiple proof mass usage for better noise performance and bias instability, electrostatic tuning for frequency mismatch, and multi degree of freedom mechanical structures for compensating external effects (Pistorio et al., 2021; Saqib et al., 2018; Trusov et al., 2009). Other methods are based on algorithmic methods using the controller. (Wang et al., 2007, Batur et al., 2006, Fei & Yuan, 2013, Xia et al., 2016) Instead of modifying sensor design, those methods use controller electronics. Controller based methods are mostly used to compensate for the effects of changing parameters on the system dynamics due to temperature, environmental factors, etc.; thus, it is aimed to increase the robustness of the sensor. Hardware changes in the design appear as more complex, costly, and long-term solutions to implement. Therefore,

controller-based methods are preferred as they are easier to implement. And gyros with such controller-based designs are also called closed-loop gyros.

As an example from real applications, the performances of an open-loop gyro and a closed-loop gyro can be compared. Analog Devices ADXRS646 open loop MEMS gyro (300 deg/s measurement range) has 12°/h bias stability and 19.5 °/s temperature bias drift.(Analog Devices, 2017). On the other hand, Tronics Gypro3300 closed loop MEMS gyro (300 deg/s measurement range has 10°/h bias stability and 0.02 °/s temperature bias drift.(Tronics, 2021)

MEMS gyroscopes generally use a vibrating mechanical element (proof mass) as a sensing element for detecting the angular velocity. Vibrating MEMS gyroscopes mainly consist of three frames that are mechanically connected by springs, which are drive axis, sense axis and proof mass.

During the operation, the driving frame is constantly vibrated by means of piezoelectric, electromagnetic or electrostatic actuation mechanisms to ensure regular movement in the drive axis. The proof mass vibrates in line with the drive and sense frame and transmits rotation-induced energy to the sense mode. The transferred energy is proportional to the magnitude of the rotation and creates a displacement in the sensor axis.

Based on this working principle, measurement accuracy of a MEMS gyro is directly related to how well the drive axis movement matches the reference vibration signal.

The vibration signal applied to drive axis determines the displacement of proof mass along drive axis. To determine the angular rate, the demodulation of proof mass displacement along the sense axis and the vibration on drive axis are used. Performance increase is related to how perfect displacement of the proof mass along drive axis (minimum error between reference vibration and drive axis displacement) is. However, the presence of unavoidable errors in the manufacturing process, and the influence of the outside ambient temperature result in mechanical coupling

between two axes, mechanical–thermal noises, and environmental condition dependent parameter variations.

Related to this topic, the current and popular problem today is to design the best possible controller for closed loop gyroscopes. It is also an important issue that the designed controller to be designed can be used in practical applications.

This thesis proposes new generation and optimal controllers for this problem.

1.2 Objectives and Goals

The main objective of this thesis is to design a drive axis controller which performs the reference vibration movement in the closest form under all adversary effects by designing a drive axis controller.

Researchers have recently proposed various methods for MEMS gyro control such as PLL controller, adaptive controller, PID controller and sliding mode controller. PLL method proposed by (Wang et al., 2007) and (Batur et al., 2006) compares performances of a model referenced based feedback control and sliding mode control to control the MEMS gyroscope. (Batur et al., 2006) shows that the sliding mode control gives better results than the adaptive feedback control. Dynamic Sliding Mode Control method with a switching function is developed by (Fei & Yuan, 2013) Additionally, University of California at Berkeley researchers use adaptive control strategy, RMIT University works on Tri-axial adaptively controlled algorithm and, Cleveland State University works on adaptive disturbance rejection for MEMS gyro control. (Xia et al., 2016) Backstepping-Based Recurrent Type-2 Fuzzy SMC for three axis gyroscope is proposed by (Asad et al., 2017) and, a new robust sliding mode controller which provides a solution for chattering problem is proposed by (Rahmani et al., 2020).

These methods are effective but they cause process load and they are not easy to implement. FPGA based processors added to system to meet the process load of the control algorithms. These high capacity processor usage causes an increase in size

and cost of the sensor, whilst MEMS industry needs small and low-cost sensor solutions. Therefore, optimizing the process load and sensor features (performance, size and cost) becomes a critical need.

MEMS gyroscope has a controller on the drive axis in the methods involving controller electronics. The performance of MEMS gyroscope is strongly related to the drive axis tracking/control performance.

It is expected that the controller or controllers to be developed in this context will be affected minimally by the changes and uncertainties in the model. In addition, it should be aimed to prevent a decrease in its performance under various environmental effects. Additionally, it is essential that the proposed method can be used in real applications without incremental size, power consumption, and cost.

In summary, the proposed method must maintain stability and robustness in the presence of disturbance and modeling errors with low cost and size.

The goal of this thesis is to increase the gyro performance by designing a controller for drive axis controller which provides robustness, low cost, small size and high performance.

1.3 Methodology

Feedback control is the most popular and easily implementable control method for many applications. Many different feedback controller laws can be listed in the literature. The proportional integral derivative control function is the most popular choice in the industry. If the controller gains do not tuned properly, closed loop system can become unstable. Additionally, noise amplification can be observed due to derivative process.

In the literature, control algorithms and closed-loop solutions are proposed to overcome gyro drive axis controller design problem. (Asad et al., 2017; Batur et al., 2006; Fei & Yuan, 2013; Rahmani et al., 2020; Wang et al., 2007; Xia et al., 2016)

Some of them offer model based algorithms, while others propose model-free solutions.

Model-based controller algorithm design has three design phases. Moreover, these controllers work correctly when the model of a system is well known (or it can be estimated). Therefore, the first phase of the design is plant modeling. System identification applications form the basis of the plant modeling phase. The second phase is controller analysis and synthesis in this phase; controller parameters are selected and tuned according to the plant model. Furthermore, the final phase is simulation studies which are implemented to verify the controller performance. Real time application of the controller can be implemented after completion of these steps. Various studies show that model-based controllers offer robust solutions when system identification performance is good. (Cerone et al., 2007)

When a model of a system is well known (or it can be estimated) it can be used to improve the performance of a control system by adding a feedforward function. The feedforward function is basically an inverse model of the process. When this is used together with a more traditional feedback function the overall system can outperform more traditional controllers function such as the PID controller. In this thesis, assuming that the gyroscope design parameters are known, it was decided that one of the controllers to be developed in this thesis study would be a model-based controller, a feedforward controller. Feedforward controller does not need high processing power and it provides robust solutions in noisy environments. Therefore, feedforward controller is chosen for the gyro drive axis control problem.

On the other hand, the model based controller's performance is directly related to system identification performance. For our gyro drive axis controller design problem, if the gyro model can not be estimated accurately, expected performance parameters can not be reached with the selected control method. Because of that, a modified version of the feedforward controller is needed and developed in the scope of this thesis. In the modified version, weighting coefficients are added to both feedforward and feedback controller to increase the robustness against disturbances

and a feedforward controller can be designed to achieve fast tracking by eliminating effects of model uncertainties with weight coefficients.

Alternative controller methods that can be robust against the uncertainties in the model due to the structure of the gyro have also been investigated. In this context, studies have been started with the sliding mode control, which provides high performance against model uncertainties. In this context, studies have been started with the sliding mode control, which provides high performance against model uncertainties. Due to various drawbacks of the sliding mode control, it is decided to design a proxy based sliding mode controller, which is the extended version of SMC and PID controller.

Sliding mode control is a high speed switched feedback control. Each feedback path gains are switched between two values according to a rule that depends on the value of the system state at each instant (Durmaz, 2009). The main drawback of sliding mode controller is chattering phenomena. One of the essential features of this controller is that it is robust against model uncertainties, parameter variations and external disturbances.

Proxy-based sliding mode control is an extension of PID and SMC. This method combines PID control and SMC algebraically to reduce chattering effect. PID controller defines low/local dynamics and SMC specifies high/global dynamics of the system. Finally, PBSMC system provides overdamped response without sacrificing tracking accuracy. PBSMC is also robust against model uncertainties, parameter variations without chattering problem and does not cause high processing power. Due to the differences between theoretical applications and real applications PBSMC is the most suitable method for gyro drive axis control applications.

Weighted feedforward controller and proxy-based sliding mode controller are applied as a drive axis controller to maintain the proof mass to oscillate in the x-direction at a given frequency and amplitude. For the weighted feedforward controller, the desired motion trajectory is the reference input for the whole controller and the inverse of the gyro transfer function is the controller function for

the feedforward path. Also, there is a PID controller on the feedback path and the performance of the controller loop is optimized with the controllers' weight parameters. Also, feedforward controller does not require highly capable processors, it is easy to implement.

In addition to the weighted feedforward controller and proxy-based sliding mode controller methods, PID controller, sliding mode controller, proxy based sliding mode controller implemented to compare the performance of each controller.

1.4 Contributions of the Thesis

In the literature, several controllers are proposed in order to improve MEMS sensor performance with eliminating disturbance effects.(Asad et al., 2017; Batur et al., 2006; Bu et al., 2021; Fei & Yuan, 2013; Grinberg et al., 2016; Raman et al., 2009; Xia et al., 2016) Most of them either uses the traditional controllers such as PID controller ,SMC and sigma-delta force feedback. However, traditional controllers cannot meet robustness, delay and steady-state error requirements. Although, successful results are obtained with adaptive control algorithms,PLLs and disturbance rejection algorithms for gyro drive axis control, these methods needs additional hardware and processors due to process loads.

One of the contribution of this study is to design a feedforward control with weighting coefficients for MEMS gyro drive axis control to improve the tracking performance. The feedforward method has not been applied as a gyro drive axis controller before. On the other hand, the weighted feedforward method was developed and implemented within the scope of this thesis study. It is applied, and superiorities over the conventional techniques are presented in this study.

The second and the main contribution of this thesis is the adaptation of proxy based sliding mode controller for the Coriolis Vibratory MEMS gyro drive axis control problem. The advantage of this method is that it can be developed independently of the gyro model. As a result, if the gyro model is not well defined or the model varies

a lot environmental effects and/or mechanical imperfections, this method can serve as a solution.

PBSMC has not been implemented on MEMS applications before. The proof mass movement tracking performance and disturbance rejection capability of the proxy based sliding mode control are compared with that of conventional PID control, SMC, and SMC-BL. Simulation results show that system error and gyroscope total error is reduced by 49.52% and 12.03%, respectively, compared to the sliding mode controller. Simulation results are supported with the experimental data, and experimental results clearly demonstrate the superiority of the proxy-based sliding mode controller.

The improvement on the proof mass tracking performance directly improves the gyro measurement performance by reducing total bias, scale factor error. And these improvements directly upgrade platforms' navigation and flight control performance.

1.5 Outline of the Thesis

This thesis is composed of six chapters.

In this first chapter of the thesis, problem definition and objectives are defined. Additionally, methodology and contributions to the literature are also included in this chapter.

The second chapter of this thesis provides the theoretical background about the structure of MEMS gyro. Additionally, the measurement principle of Coriolis vibratory gyro and dynamic model of vibratory MEMS gyro are described. Moreover, technology trends for MEMS gyro technology are overviewed.

In Chapter 3, classical control techniques for a Coriolis vibratory MEMS gyro drive axis are presented, including closed loop architectures; on top of this general background layout, the outstanding features of our approaches with the innovative

contributions are detailed. Our proxy-based sliding mode controller and weighted feedforward controller features are explained within this scope, giving sliding mode control and boundary layer sliding mode control and our proxy-based sliding mode control design.

Chapter 4 provides the simulation and experimental studies. The experimental setup is described in detail, giving our gyro design parameters with full justifications. Controller performance comparisons, angular rate measurements with our proposed controllers, and measurement accuracies are thoroughly discussed in Chapter 4.

Chapter 5 conducts an in depth sensitivity analysis under different noise level, angular rate and frequency to determine the sensitivity of the controllers to changing parameters. And sensitivity characteristics are provided in Chapter 5. Similarly, experimental studies are performed with different test scenarios under parameter variations change and the associated sensitivity results are discussed in this chapter.

Chapter 6 concludes the thesis with suggestions for future research works.

CHAPTER 2

MEMS GYROSCOPE TECHNOLOGY

Gyroscope is a sensor that measures angular rate typically in the unit of degrees per second or radians per second. (“IEEE Standard for Sensor Performance Parameter Definitions IEEE Electron Devices Society Sponsored by the Microelectromechanical Systems Standards Development Committee,” 2017). On the other hand, the acronym MEMS represents a broad group of silicon-based sensors made by semiconductor wafer manufacturing processes. (Fitzgerald, 2021) Moreover, a MEMS gyroscope transduces Coriolis forces into an electrical output proportional to changes in angular acceleration. Since we have a Coriolis vibratory MEMS gyroscope prototype with an ongoing design process, vibratory gyroscope model is used in this thesis work. All vibratory gyroscopes are based on the transfer of energy between two vibration modes (drive and sense mode) of a structure caused by Coriolis acceleration.(Preethi et al., n.d.)

This chapter gives theoretical background about MEMS gyroscope types and their performance, together with its metrics classifications, working principle, their dynamics and gyroscope subsystems. Section 2.1 summarizes gyroscope performance metrics and gyroscope classification is provided in Section 2.2. Section 2.3 gives the Coriolis vibratory MEMS gyro operating principle. Dynamic model of a MEMS gyroscope is presented in Section 2.4. And this chapter continues with MEMS gyro structure and ends with MEMS technology trends.

2.1 Gyroscope Performance Metrics

Various types of performance parameters are used to determine the measurement accuracy of sensors. The definitions of these performance parameters have been determined by based on IEEE standards ((IEEE 528-2019, 2019; IEEE 1431-2004, 2010)) and sensor manufacturers also make the performance classifications according to values of the defined parameters. Types of performance parameters can vary according to sensor technologies (MEMS (Micro Electronic Mechanical Systems), FOG (Fiber Optic Gyroscope), RLG (Ring Laser Gyroscope), etc.). The effects of the parameters on the angular rate measurement vary according to the definitions of the parameters. For example, while the effect of bias is constant under constant temperature, the effect of scale factor error becomes significant with increasing angular rate.

This section describes performance parameters specific to MEMS gyroscope technology. Besides, measurement model according to the performance parameters are provided in this section.

2.1.1 Bias

The gyroscope bias can be defined as the gyroscope output under 0 deg/s angular rate. Representation of bias is given in Figure 2.1. The bias term contains different types of bias parameters such as

- Bias repeatability
- In-run bias stability
- Bias over temperature

Gyro bias repeatability is defined as the residual output bias error, including the effects of turn-off and turn-on, time, and temperature variations. This measure represents the statistical expected value for output bias error at any given time and thermal condition (Honeywell Aerospace, 2017). Especially, silicon based gyros

have different bias performances under different temperature conditions. This is due to changes in silicon structure with temperature.

In-run bias stability/bias instability is a measure of how the bias will drift while operating under power. It is computed over a specified sample time and averaging time interval. Unit of bias is degree/hour or radian/hour. Representation of bias and scale are depicted in Figure 2.1.

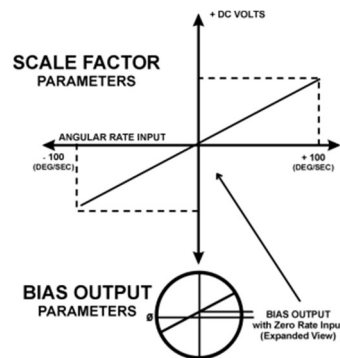


Figure 2.1 Representation of bias and scale factor (Emcore Navigation, 2020)

Gyro performance degrades over temperature. Parameters sensitive to temperature include noise, bias offset, and scale factor. Calibration is the traditional method for compensating the bias temperature variations. Some fitting and polynomial based methods are used in these compensation algorithms. These compensation algorithms can reduce the bias effect but cannot zeroize it. The proposed control algorithms will support these calibration algorithms to minimize the temperature dependent bias variation. An example of bias over temperature is given in Figure 2.2.

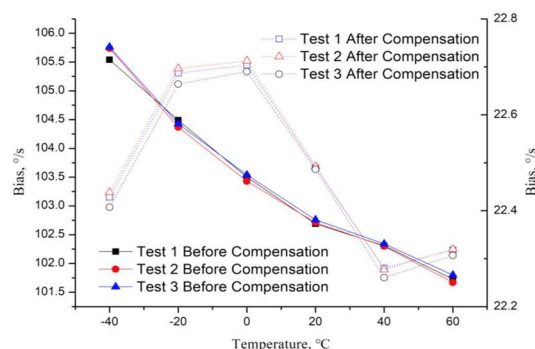


Figure 2.2 Bias over temperature (Cui et al., 2019)

2.1.2 Scale Factor Error

The scale factor is a parameter used to convert the sensor voltage output, which is determined by the input angular rate, to the physical angular rate value. Moreover, scale factor varies with time and temperature. The unit of the scale factor is mV/degree/s, and every gyro has an ideal scale factor value.

Representation of ideal and actual scale factor is given in Figure 2.3. The magnitude of the scale factor error is expressed in parts per million (ppm). Scale factor error is the difference between the ideal scale factor and actual scale factor.

Like bias, scale factor repeatability is defined as the residual output SF error, the effects of turn-off and turn-on, time, and temperature variations. (Honeywell Aerospace, 2017) Additionally, scale factor contains asymmetry and nonlinearity terms.

Effects of scale factor error become observable under high angular rate input. Because the scale factor is used as a multiplier in the conversion sensor voltage output to physical angular rate value. It can easily be observed from Eq.(2.1) gyro measurement equation.

On the other hand, characteristics of scale factor error change according to the input angular rate. This change causes deviation from the nominal scale factor, and this error term is called linearity error. Linearity may be limited by capacitive nature of MEMS sensors in which output is inversely proportional to the gap change in the sense capacitor.(Wang, 2013) The gap change is directly related to movement of proof mass.

Additionally, scale factor varies with temperature. Therefore, polynomial based compensation algorithms are used to compensate the effect of temperature variations. But these algorithms cannot completely solve the problem. An example of scale factor temperature variation and compensation results is given in Figure 2.4.

Linearity problems and temperature dependent errors changes can be minimized by adding a controller to the gyro drive axis.

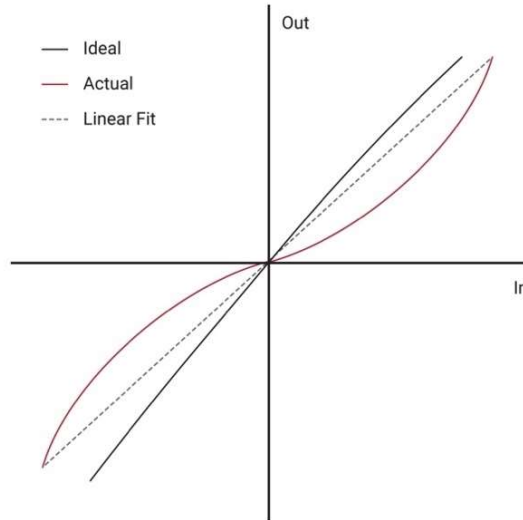


Figure 2.3 Representation of Ideal, Actual and Linear Fit Scale Factor (Figure is taken from (Vectornav Navigation, 2020))

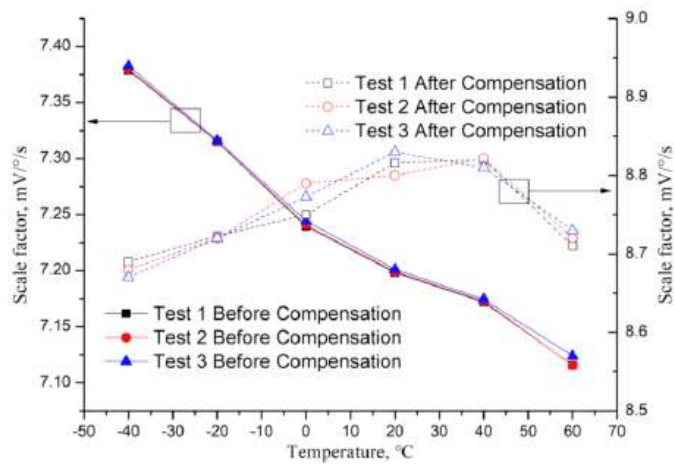


Figure 2.4 Scale factor over temperature example (Cui et al., 2019)

2.1.3 Misalignment

The misalignment error is the sum of the errors caused by the fact that the sensor sensitive axis cannot be placed directly on the measurement/sensitivity axis and the

deviation of the sensor from the ideal axis of the sensitive axis due to manufacturing. In summary, sensor misalignment describes the angular difference between each gyroscope's actual sensitivity axis and the system defined ideal sensor sensitivity axis. Representation of misalignment is given in Figure 2.5. Due to misalignment error, the measurement is affected by the movements in the orthogonal axes of the sensor, leading to gyroscope performance degradation. Unit of misalignment is milliradian.

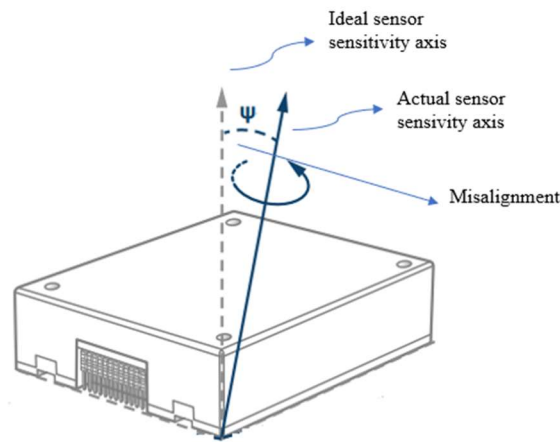


Figure 2.5 Representation of Misalignment (Adopted from(Looney, 2015))

2.1.4 G-Dependent Bias

MEMS gyroscopes are sensitive to linear accelerations due to asymmetrical design and manufacturing tolerances. This bias component is proportional to the acceleration applied in any direction. Unit of this g-dependent bias is degrees/second/g or radians/second/g.

2.1.5 Noise

Noise can be defined as random variation of a measured output when a sensor is subjected to a constant input at constant conditions and is usually characterized by either a standard deviation value or a RMS value.(Vectornav Navigation, 2020)

Electronic component based noises and mechanical-thermal noises are the sources of sensor noise. When a noisy output of a sensor is integrated, there is a drift will be observed over time. This drift is called angular random walk (ARW). ARW is the angular error buildup with time due to white noise in angular rate expressed in $^{\circ}/\sqrt{\text{hr}}$. (Honeywell Aerospace, 2017)

Bias, scale factor, misalignment, and g-dependent bias determine the total deterministic error of a gyro measurement. A gyro measurement equation is given in Eq.(2.1). Noise represents the stochastic error part of the gyro measurement,

$$\tilde{w}_x = (1 + S_x)w_x + B_x + B_{Gx}a_x + n_x \quad (2.1)$$

Where

\tilde{w}_x : gyro measurement output w_x : real angular rate

B_x : bias , B_{Gx} : g-dep bias coeff., S_x : scale factor error, n_x : sensor noise

Especially, scale factor error linearity and temperature dependent variations can be improved with the use of controller. Additionally, noise parameter can be upgraded by using controller. The control loop bandwidth determine dynamic movement measurement capability of a gyro. Consequently, sensor measurement noise power and bandwidth can be adjusted according to the controller.

2.2 Gyroscope Classification

Gyros can be classified in two different ways. The first classification is determined according to the performance parameters and the second classification is determined by the gyro structure. Performance classification is given in Section 2.2.1 and structural classification is given in Section 2.2.2.

2.2.1 Performance Classification

In the literature and industry, performance classes are listed as strategic grade, navigation grade, tactical grade, and control grade. Bias, scale factor and angular random walk are the key parameters for this classification. Table 2.1 shows the gyroscope performance classification. The control grade can also be defined as automotive class in some sources. MEMS gyro technology started with the control grade. Tactical grade products have been achieved with the developments in design and production processes and, navigation grade products began to appear.

Table 2.1 Gyroscope Performance Classification

Class of Gyroscope	<i>Bias</i> (deg/h)	<i>Scale</i> Factor(ppm)	<i>Angular Random Walk</i> deg/sqrt(hr)
Strategic Grade	< 0.01	< 10	< 0.005
Navigation Grade	0.01-1	10-100	0.005-0.04
Tactical Grade	1-10	100-1000	0.04-0.5
Control Grade	10-10000	1000-10000	> 0.5

In general, MEMS type gyroscopes constitute control class gyroscopes and are preferred for automobile applications, short range missile navigation and control systems, cell phones, and wearable technologies.

On the other hand, FOGs, RLGs, and new generation MEMS gyros can be considered as the tactical grade gyro class. Tactical grade gyros are used in tactical missile navigation and autopilot applications, oil and gas exploration, pipeline laying, drilling guidance, and non-magnetic north finding applications.

Navigation grade gyros are suitable for long range or long time navigation such as aircraft, land and marine vehicles, and ballistic missiles. FOGs and RLGs are preferred for these applications.

Strategic grade gyroscopes are very costly and are used in limited applications. Generally, they are used for satellite and star tracking applications. Until recently, mechanical gyroscopes dominated this class. However, recent developments in FOG technology have shown that FOGs can also be used in this class.(Wheeler & Digonnet, 2021)

2.2.2 Structural Classification

The first level of structural classification is determined according to the movement of the sensitive element (The component on which the theoretical measurement setup is made). This movement can be specified as oscillatory or rotary. Mathematical models of dynamics of oscillatory and rotary gyroscopes are derived according to their operating principles.

Oscillatory/linear vibratory type gyroscope are used in this thesis work and derivation of linear vibratory gyroscopes will be provided in Section 2.3.

In the case of an oscillatory gyroscope, a Coriolis force is induced due to linear drive oscillations, while in a rotary gyroscope, a Coriolis torque is induced due to rotary drive oscillations.(Acar & Shkel, 2008)

In the next step, classification is made according to design of proof mass which is the sensitive element. The classification here is determined by the mass distribution such as continuous and discrete (lumped mass). The third level classification is made for systems with discrete mass distribution. Classification at this level is determined by the mass number. Nowadays, the widely used number is four for multiple mass structure gyros. In the final stage, primary and secondary movements of the proof mass determine the classification. Movements can be linear or rotational or both linear and rotary. (Ex. Primary linear, secondary rotational or both linear or both rotational) (Apostolyuk, 2016)

Classification summary and examples for these classifications are presented in Figure 2.6.

First level separation is done based on the nature of the sensitive element motion. Sensitive element motion can be either oscillatory or rotary.

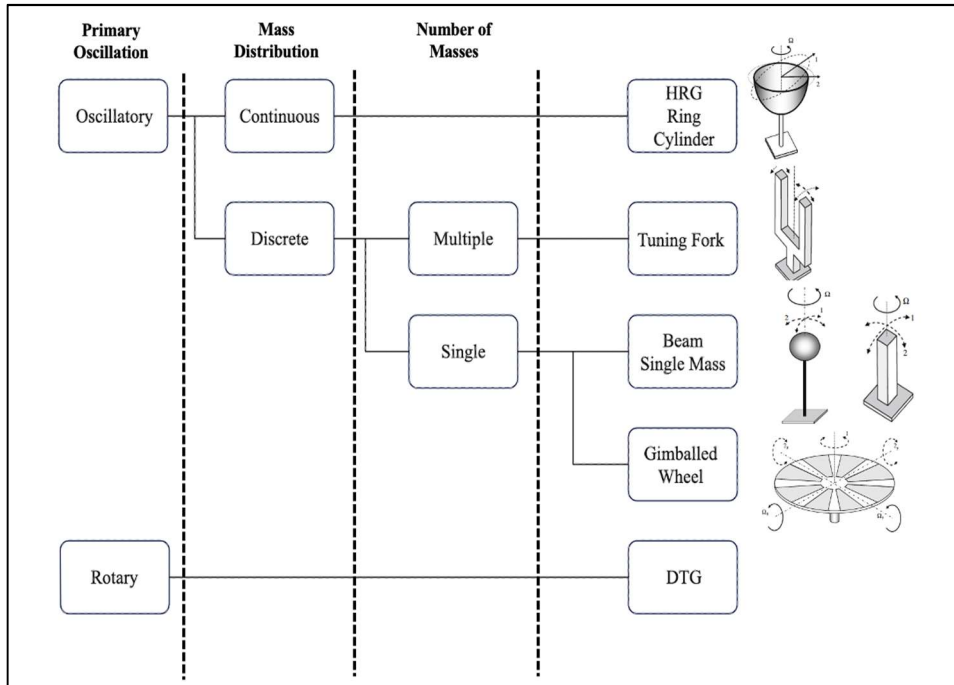


Figure 2.6 MEMS Gyro Structural Classification, (Adopted from (Apostolyuk, 2016))

The second level defines the general approach to design the sensitive element. In particular, the design of the vibration sensitive element may be based on a continuously vibrating environment or discrete. Corresponding mathematical models are based either on partial differential equations, namely modified wave equation, or systems of ordinary differential equations.(Apostolyuk, 2016)

The third level determines the discrete masses branch of the classification. It is based on a single or multiple series of vibrating masses.

Finally, Coriolis vibratory gyroscope sensitive elements can be classified based on the combination of types of motions, utilized in primary and secondary motions: linear and rotational.

Example representations of gyro types according to the classification are given in the Figure 2.6.

Additionally, an example of a rotary vibratory gyroscope, dynamically tuned gyroscope is given in Figure 2.8.

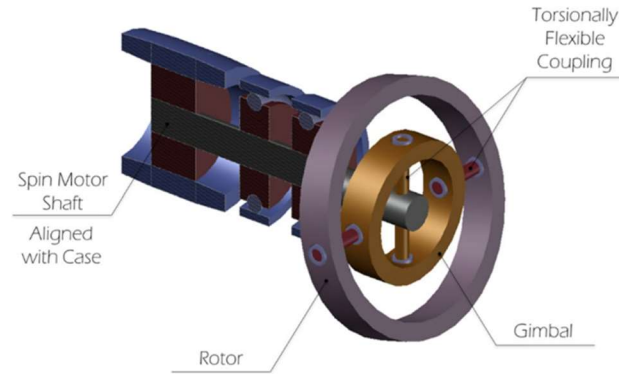


Figure 2.7 DTG Configuration (Adopted from (El-Sheimy & Youssef, 2020))

Dynamically tuned gyroscopes basically operates using a highly spinning mass.

The gyroscopic precession effect that occur due to the external torques acting upon a spinning mass. Torques are deliberately applied to the rotating mass using restraint means as hinges. Consequently, the spinning mass precession is defined as a measure of the angular rate, which is measured by using appropriate pick-off means. ((El-Sheimy & Youssef, 2020))

2.3 Coriolis Vibratory MEMS Gyroscope (CVG MEMS) Operating Principle

According to Figure 2.6 Coriolis Vibratory MEMS gyroscope belongs to oscillatory discrete distributed beam single mass. Gyro modeling and mathematical motion equations are derived according to this classification. Details about the CVG MEMS structure and operation principle are provided in this section.

CVG MEMS gyroscopes mainly consist of three frames that are mechanically connected by springs, which are driving frame, sensing frame and proof mass. as simply visualized as a two degree-of freedom spring-mass-damper system (Qing Zheng et al., 2009) in Figure 2.8.

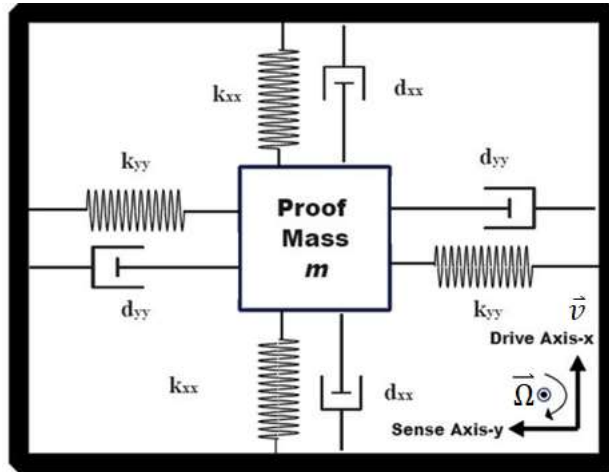


Figure 2.8 2-DOF Gyroscope Model

Regardless of its type, the main component of a vibratory MEMS gyro is its motion sensitive element. The main idea behind vibrating gyro is that they replace the continuously rotating rotors with vibrating components. Angular velocity creates motion on the second axis because of the Coriolis effect. This type of gyroscopes is called as Coriolis vibratory gyroscope.

The sensitive element of Coriolis vibratory gyroscope is named as proof mass. Proof mass oscillates on primary and secondary axis that are orthogonal. Primary oscillation is generated on primary axis intentionally. Because of the Coriolis effect generated by angular velocity, oscillation generated on the second axis. Using the oscillation on the second axis, angular velocity measured. Coriolis effect is represented with an imaginary Coriolis force F_C :

$$F_C = -2m\vec{\Omega} \times \vec{v} \quad (2.1)$$

Where,

$\vec{\Omega}$: external/axial angular rate

\vec{v} : vector of the primary motion/oscillation

m : mass

During the operation, the driving frame is constantly vibrated by means of piezoelectric, electromagnetic or electrostatic actuation mechanisms to ensure

regular movement in the primary axis. The proof mass vibrates in line with the primary and secondary frame and transmits rotation-induced energy to the sense mode (motion in the secondary axis). The transferred energy is proportional to the magnitude of the rotation/angular rate (Ω) and creates a displacement in the secondary axis. This displacement is perceived as rotation by the sense mode of gyroscope, with piezoelectric, optical, piezo-resistive or capacitive sensor mechanisms (Patel & McCluskey, 2012)

In the remaining part of the thesis, the primary axis will be defined as the drive axis and the secondary axis as the sense axis. Sense axis and drive axis are shown in Figure 2.8 and 2.9.

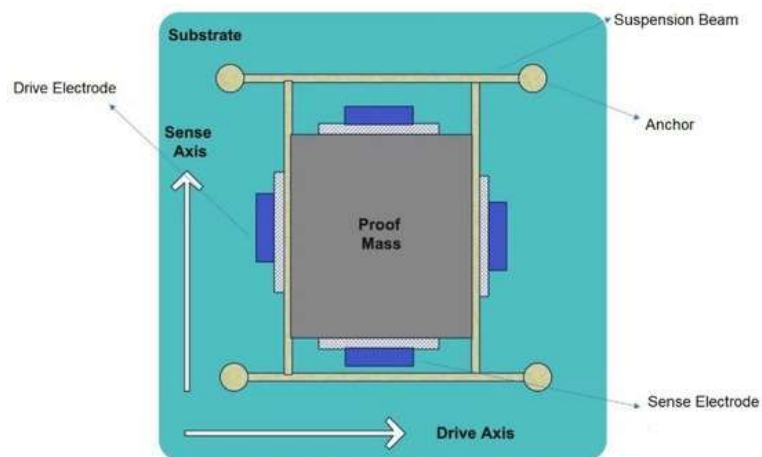


Figure 2.9 A Generic MEMS Gyro Structure

A generic MEMS gyro structure is given in Figure 2.9; a proof mass is suspended above a substrate using a suspension system comprised of flexible beams, anchored to the substrate. There are two sets of electrodes used to excite and detect the output signal. One set of electrodes is needed to excite the drive axis oscillator (desired trajectory/reference vibration) and another set of electrodes detects the sense axis response. (Acar & Shkel, 2008)

To describe the operating dynamics of a MEMS gyro, it is necessary to describe the rotation induced Coriolis force acting on a mass/structure observed in a rotating reference frame.

What we need is to calculate the total force acting on the proof mass. For this, it is suggested to calculate acceleration based on the position vector. Vector and axes definitions for the respective calculations are given in Figure 2.10.

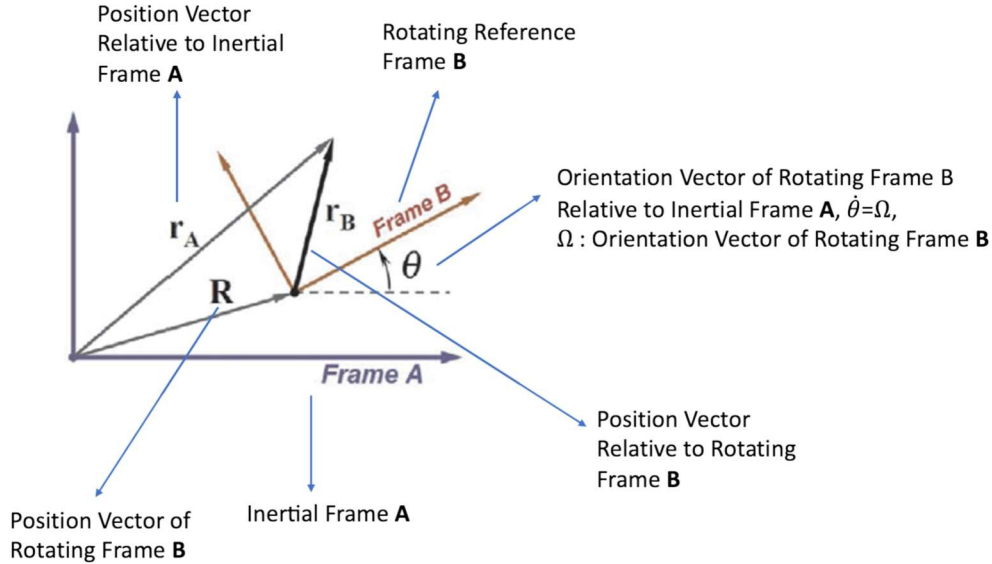


Figure 2.10 Representation of the Position vector Relative to the Inertial Frame A and the Rotating Reference Frame B (Adopted from (Acar & Shkel, 2008))

Frame A is the stationary frame and Frame B is the rotating reference frame. We are trying to find a_A , the acceleration vector with respect to inertial frame A and it can be derived taking the second time derivative of the position vector r_A . Equations which are derived according to the Figure 2.10 are given below:

$$r_A(t) = R(t) + r_B(t) \quad (2.2)$$

$$\dot{r}_A(t) = \dot{r}_B(t) + \dot{\theta} \times r_B(t) \quad (2.3)$$

$$\ddot{r}_A(t) = \ddot{R}(t) + \ddot{r}_B(t) + \dot{\theta} \times r_B(t) \quad (2.4)$$

$$\begin{aligned} \ddot{r}_A(t) = & \ddot{R}(t) + \ddot{r}_B(t) + \dot{\theta} \times \dot{r}_B(t) + \dot{\theta} \times (\dot{\theta} \times r_B(t)) + \ddot{\theta} \times r_B(t) \\ & + \dot{\theta} \times r_B(t) \end{aligned} \quad (2.5)$$

Eq. (2.5) gives the acceleration of a mass moving with the rotating reference frame.

Eq. (2.5) is arranged according to the acceleration terms and given in Eq.(2.6):

Here, the three terms in Eq. (2.6) are defined as follows:

1: Local Acceleration

2: Centripetal Acceleration

3: Coriolis Acceleration, **amplitude is directly related to angular rate**

$$a_A = \underbrace{A + a_B}_{1} + \underbrace{\dot{\Omega} \times r_B}_{2} + \underbrace{\Omega \times (\Omega \times r_B)}_{2} + \underbrace{2\Omega \times v_B}_{3} \quad (2.6)$$

$\dot{\theta} = \Omega$: angular rate vector of rotating reference frame B

a_A : acceleration vector with respect to the rotating inertial frame A

a_B : acceleration vector with respect to the rotating reference frame B

v_B : velocity vector with respect to the rotating reference frame B

Coriolis acceleration is the primary mechanism that scales and converts the rotation rate of the rotating reference frame B into a fictitious inertial force when observed in the rotating frame. (Acar & Shkel, 2008)

When applied to the position vector of a vibratory gyroscope proof mass, this analysis yields the dynamics of the gyroscope attached to a rotating object. When the derivation defined above is applied to CVG, the total force acting on the proof mass is calculated as in Eq.(2.7).

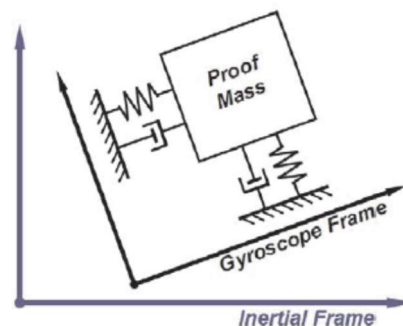


Figure 2.11 Representation of the gyroscope frame rotating with respect to the inertial frame (Adopted from (Acar & Shkel, 2008))

Total force excited on the proof mass is given below:

$$F = m[A + a_B + \dot{\Omega} \times r_B + \Omega \times (\Omega \times r_B) + 2\Omega \times v_B] \quad (2.7)$$

m : The mass of the proof mass

A : The linear acceleration

Ω : the angular velocity of the rotating gyroscope frame

v_B : the velocity vector of the proof mass with respect to the reference frame

a_B : acceleration vectors of the proof mass with respect to the reference frame

In a z-axis gyroscope, the two principle oscillation directions are the drive direction along the x-axis (drive axis) and the sense direction along the y-axis (sense axis). The dynamic model of a MEMS gyro can be constructed by decomposing the motion into the principal oscillation directions. It is assumed that linear accelerations are negligible:

$$m\ddot{x} + d_{xx}\dot{x} + (k_{xx} - m(\Omega_y^2 + \Omega_z^2))x + m(\Omega_x\Omega_y - \dot{\Omega}_z)y = u_x + 2m\Omega_z\dot{y} \quad (2.8)$$

$$\begin{aligned} m\ddot{y} + d_{yy}\dot{y} + (k_{yy} - m(\Omega_x^2 + \Omega_z^2))y + m(\Omega_x\Omega_y + \dot{\Omega}_z)x \\ = u_y - 2m\Omega_z\dot{x} \end{aligned} \quad (2.9)$$

Under the assumption that $\Omega_x^2 \approx \Omega_y^2 \approx \Omega_z^2 \cong 0$ (negligible components), $\dot{\Omega}_z \equiv \dot{\Omega} \approx 0$ (constant angular rate) and sense mode response's amplitude (amplitude of Coriolis term $2m\Omega_z\dot{y}$) is smaller than the drive motion, the simplified dynamic 2-DOF equations of CVG can be defined as:

$$m\ddot{x} + d_{xx}\dot{x} + k_{xx}x = u_x \quad (2.10)$$

$$m\ddot{y} + d_{yy}\dot{y} + k_{yy}y = u_y - 2m\Omega\dot{x} \quad (2.11)$$

u_x, u_y : External driving forces

This section summarizes the theoretical basis of the dynamic model of a gyro. In the following section the dynamic model of a MEMS gyro with error parameters (quadrature errors, mechanical imperfection effects) will be provided.

2.4 Dynamic Model

Some gyroscopes have more than one proof mass. Derived dynamical models are valid for all type MEMS gyroscope types. The model is named as “lumped mathematical model” and derivations and assumptions are given below.

2- proof mass TFG example is presented in Figure 2.12. Lumped model of TFG is the same as the traditional single proof mass gyro.

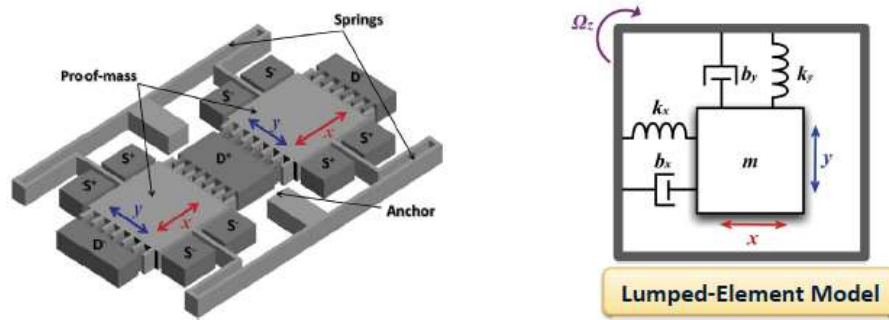


Figure 2.12 Proof Mass TFG and Lumped Model (Adopted from (Acar & Shkel, 2008))

The lumped mathematical model of a vibrating gyroscope is given in Eq. (2.12) and Eq. (2.13). These equations are constructed over Eq. (2.10) and Eq. (2.11) by adding effects of quadrature errors, mechanical imperfection effects.

$$m\ddot{x} + d_{xx}\dot{x} + k_{xx}x + d_{xy}\dot{y} + k_{xy}y = u_x + 2m\Omega\dot{y} \quad (2.12)$$

$$m\ddot{y} + d_{yy}\dot{y} + k_{yy}y + d_{xy}\dot{x} + k_{xy}x = u_y - 2m\Omega\dot{x} \quad (2.13)$$

m is the mass of the proof mass (the mass is restricted to move in x,y plane), x and y are the coordinates of the proof mass and k_{xx}, k_{yy} are the spring coefficients. The parameters d_{xx}, d_{yy} represent the damping, u_x, u_y are electrostatic driving forces

(control input). $2m\Omega\dot{y}$ and $2m\Omega\dot{x}$ are the coupling forces due to the Coriolis effect and d_{xy} and k_{xy} are coupling quadrature and spring errors due to the manufacturing imperfections.

The lumped model can be converted into a parameter dependent model where these parameters are the quality factor and natural frequency characterizing the gyro.

$$\ddot{x} + \frac{\omega_{nx}}{q_x} \dot{x} + \omega_{nx}^2 x + \frac{\omega_{nxy}}{q_{xy}} \dot{y} + \omega_{nxy}^2 y = \frac{u_x}{m} + 2\Omega\dot{y} \quad (2.14)$$

$$\ddot{y} + \frac{\omega_{ny}}{q_y} \dot{y} + \omega_{ny}^2 y + \frac{\omega_{nxy}}{q_{xy}} \dot{x} + \omega_{nxy}^2 x = \frac{u_y}{m} - 2\Omega\dot{x} \quad (2.15)$$

Where,

$$\omega_{nx} = \sqrt{\frac{k_{xx}}{m}}, \quad \frac{\omega_{nx}}{q_x} = \frac{d_{xx}}{m}, \quad \omega_{ny} = \sqrt{\frac{k_{yy}}{m}}, \quad \frac{\omega_{ny}}{q_y} = \frac{d_{yy}}{m}, \quad \frac{\omega_{nxy}}{q_{xy}} = \frac{d_{xy}}{m}$$

In this thesis, simulation models are generated based on Eq. (2.12) and Eq. (2.13). Drive and sense axis characteristics and the closed loop performance of the gyro control loop are observed based on Eq. (2.14) and Eq. (2.15).

2.5 MEMS Gyro Structure

A MEMS gyroscope composed of 3 main components which are;

1. Sensor
2. Read-out Circuit
3. Case / Package

Sensing element measures angular velocity by using Coriolis effect, is composed of mass-spring-damper which is given in Figure 2.8.

The readout circuit generates necessary oscillation/vibration on the drive axis and senses the oscillation on the second axis. And angular velocity is calculated by demodulation of the signal on sense axis. Current-voltage conversions and reference

signal and drive axis displacement signal comparisons are performed on the readout circuit.

On readout circuit ASIC (Application Specific Integrated Circuit) design is preferred due to its size advantage. ASIC is a microchip designed for a special application such as sensor detector, cell phones, etc. The main advantage of ASIC is size because all of the circuits are on the same chip. Readout circuit is composed of two parts: drive axis readout circuit and sense axis readout circuit. Noise from the circuit may affect the angular velocity measurement signal. For accurate measurement, the noise level in the circuit must be lower than the signal level generated by the Coriolis effect. To acquire amplitude of angular rate, low noise, high resolution, and sensitive detection mode readout circuit is required.

A typical MEMS gyro functional diagram is shown in Figure 2.13. Mechanical sensor part represent sensor, remaining parts and components represent the readout circuit part. This sensor is an open-loop structure and has an analog output.

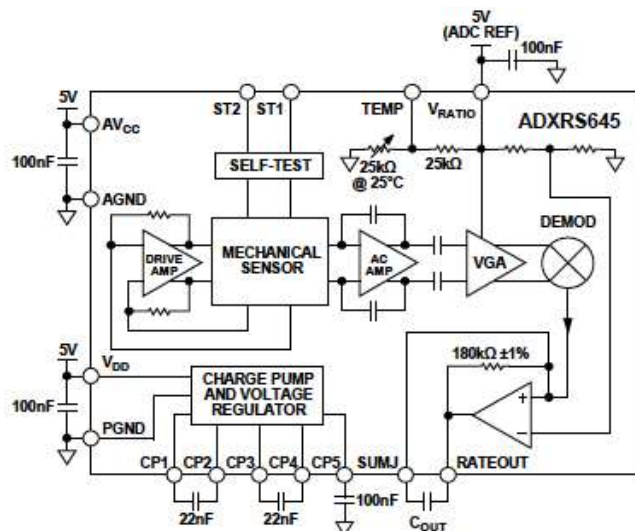


Figure 2.13 A typical MEMS Gyro Functional Block Diagram (Analog Devices ADXRS645 Data Sheet)

Case/package is used to protect the components of the gyroscope from external effects. External connection interface is also supplied by the case. The placement of sensor over electronics and wiring are features of the case. To improve the performance of the sensor, vacuum is required which is a specification of the case.

Various types of packaging technologies such as ceramic, hermetic, metal packaging are used in MEMS industry.

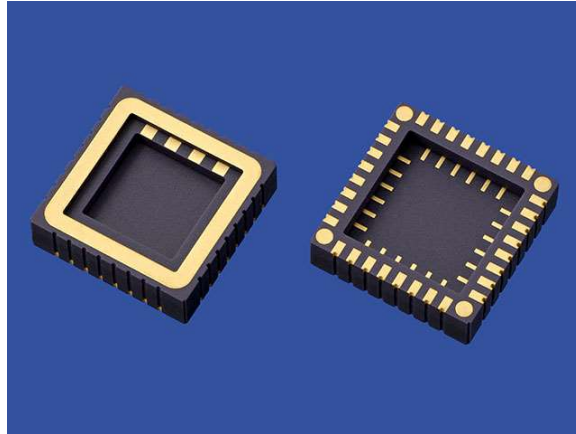


Figure 2.14 MEMS Packaging Example (Kyocera Industries, 2022)

Wiring between sensor-readout circuit and readout circuit-case is produced by a special process called wire-bonding. A wire-bonding application is presented in Figure 2.16.

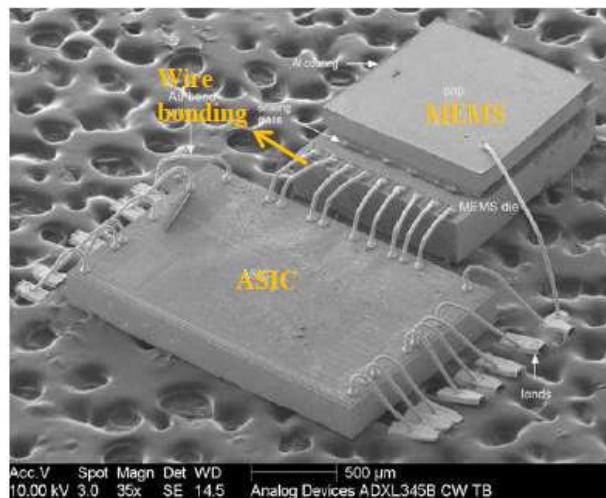


Figure 2.15 Wire -bonding Example (Warren, 2009)

2.6 MEMS Technology Trends

According to the literature and research driving the industry, it is clear that MEMS sensors will dominate the market. The main reason of this tendency is that MEMS

sensors are widely used on many new applications each day. Figure 2.14 shows the widely used sensor technologies according to years.

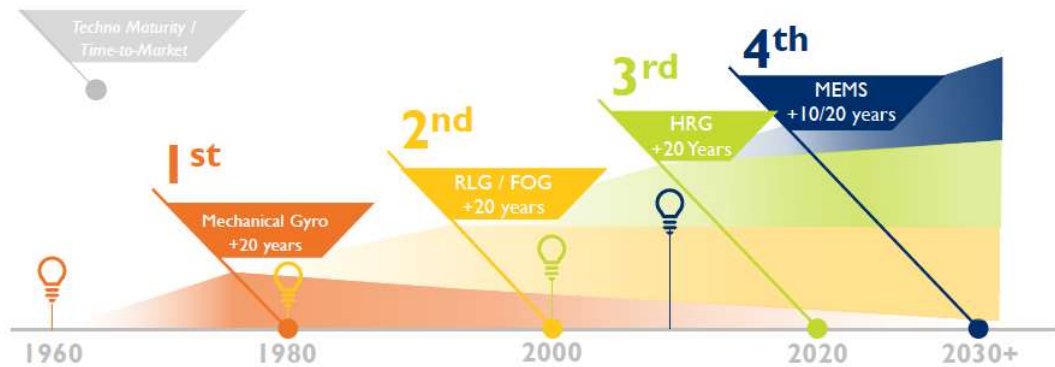


Figure 2.16 Development of gyro technology over the years (Damiano & Girardin, 2020)

According to Figure 2.16 gyro measurement technology starts with mechanical gyros. Mechanical gyros provide accurate angular rate measurements. However, they are expensive, not producible in high volumes and need maintenance. Therefore, RLG and FOGs replaces mechanical gyro. After FOG and RLG, HRGs, which are compact, low-noise, high-performance angular velocity or rotation sensors, came to the fore. After FOG and RLG, HRGs, which are compact, low-noise, high-performance angular velocity or rotation sensors, came to the fore. However, due to manufacturability, price advantage, and increased performance, MEMS will dominate the sensor industry.

At the beginning, MEMS sensors were used on automotive and military applications. Development of design and production phases of MEMS sensors yield to new application areas such as consumer electronics, mobile applications, and medical care. As a result of that popularity, researchers not only look for ways to develop low-cost MEMS sensors, but also studied to increase the performance. To do so, performance improvement designs were developed. This study is one example of that performance improvement designs.

Figure 2.17 compares the performance and cost of sensor technologies. Because of the developments on production methods and performance upgrade methods, MEMS

sensors is expected to perform as well as FOG and RLG sensors in upcoming years. With its cost advantage, it will dominate the market on tactic and navigation applications.

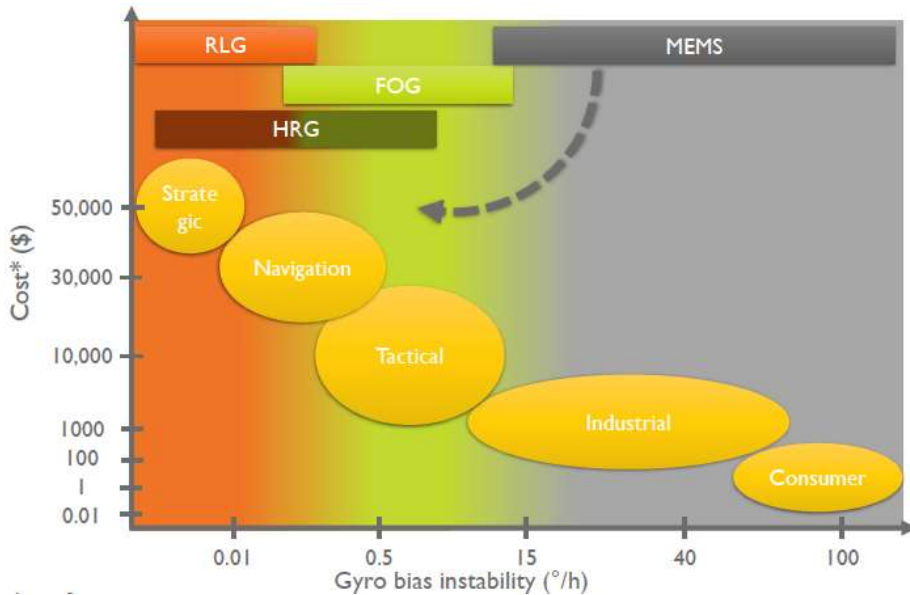


Figure 2.17. Gyro Performance vs Cost Technology Classification (Damiano & Girardin, 2020)

Increasing demand on wearable devices results in an increasing demand on MEMS sensors which led to the need of small, low power, high performance MEMS sensors. In addition to that, usage of those sensors as data source on AI applications increased the need of high performance.

As a result, technological development and needs of industry is the main motivation of developments on MEMS technology. This situation has increased demand on MEMS industry, despite global economy is not that good over the world.

Figure 2.18 presents the near future of gyro design and production technology. In later times, it is predicted that MEMS sensors will replace FOG and RLG gyroscopes, which offer tactical level solutions. On the other hand, quartz-MEMS technology is expected to dominate the tactical grade sensor market.

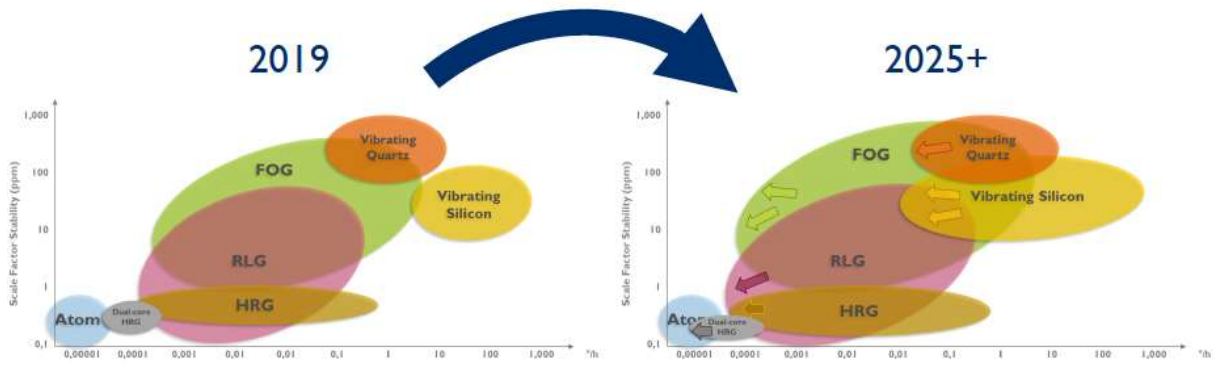


Figure 2.18. The future of gyro technology (Damiano & Girardin, 2020)

CHAPTER 3

MEMS GYROSCOPE DRIVE AXIS CONTROL TECHNIQUES

In this thesis study, it is aimed to improve the performance of a MEMS gyroscope by controlling the movement of the drive axis. For this, many methods are suggested in the literature. However, the proposed methods are either not applicable in practice or insufficient to meet today's performance requirements. For example, even 1 deg/h improvement is very important for a missile's range extension. For this reason, methods that will both improve performance and be applicable have been proposed. Proxy-based sliding mode controller – an extension of PID controller and sliding mode controller- and weighted feedforward controller are proposed within the scope of this thesis.

This chapter begins with the introduction of the closed loop control loop which is constructed within the scope of this thesis and continue with an overview of sliding mode controller and proxy-based sliding mode controller. Besides, feedforward and weighted feedforward controller architectures for the drive axis control are provided in this chapter. Also, controller derivations for our control problem is explained in the scope of this chapter.

3.1 Closed Loop Control Structure

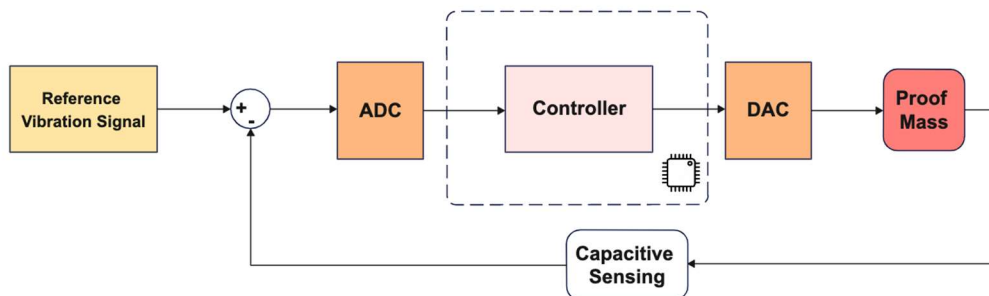


Figure 3.1 Gyro Drive Axis Control Loop

The generic control loop architecture for gyro drive axis control is given in Figure 3.1. Two conversion processes are shown in the figure. Since the controller is implemented on a microcontroller, it needs digital input. Therefore, the reference vibration signal and proof mass motion signal which is sensed by capacitive sensing mechanism are sampled by ADC (Analog to Digital Converter). Since the proof mass operates with analog input, the controller output is converted back to an analog signal to be applied to the proof mass. Therefore, noises and sensitivity losses caused by sampling can also be counted among the parameters that affect system performance.

The control problem comprises of the challenge to maintain the proof mass m oscillating in the x -direction at a given desired motion trajectory with the desired frequency and amplitude even though the motions in the x and y directions are coupled and the angular velocity Ω is unknown.

The desired motion trajectory, presented as reference vibration signal in Figure 3.1, for proof mass on the drive axis is given below:

$$x_d = A \sin w_n t \quad (3.1)$$

The controller parameters must be determined according to the gyro's parameters and performance requirements. The first requirement is minimum steady-state error achieving high performance. Additionally, we need a fast settling time for minimum response time. Since, settling time directly affects the gyro start-up time. If the designer has a limitation for start-up time requirement according to the operational concepts (Ex. Missile firing sequence, camera stabilization time, etc.), controller parameters should be determined according to the limitations.

On the other hand, the displacement margin of the proof mass on the drive axis is the critical limit for the overshoot of the controller. Overshoot should not exceed the displacement range of the drive axis. In case of an overshoot that will cause displacement above the mechanical limits, the sensor will be structurally damaged and will not be able to perform its normal operation.

Our control approaches are located in the controller block of the Figure 3.1 and they are implemented on a microcontroller.

Since PBSMC, one of the controllers proposed in this thesis work, is an SMC-based controller, background on SMC will be given in the continuation of this section, and then it will be continued with PBSMC. Details of sliding mode controller implementation is provided in Section 3.2 and adaptation of PBSMC (Proxy-Based Sliding Mode Controller) for drive axis control is given in Section 3.3.

After the PBSMC, it will be given in detail how the other recommended method, weighted feedforward, is applied to the related problem.

3.2 Sliding Mode Control: A Background Overview

The variable structure control and associated sliding modes were first proposed and developed by Stanislav Emelyanov and Vadim Utkin in the early 1950s in the Soviet Union. (Emelyanov, 1957; Utkin, 2002)

Sliding mode controller is a particular type of variable structure control. During the control process, the system model change structure/parameters according to a discriminant function called a sliding surface between classes of subsystems. For this reason, the method is named as variable structure systems. (Edwards & Spurgeon, 1998)

The most relevant feature of the sliding mode control is its ability to generate robust control algorithms that are invariant under certain conditions. The concept of invariance indicates that the system remains completely insensitive to certain types of disturbances and uncertainties such as measurement errors, modeling errors and parameter tolerances. (Draženović, 1969)

The mismatch between actual plant and mathematical plant model developed for controller is the most obvious uncertainty on the system. And sources of the mismatch can be listed as unmodelled dynamics (choice of simplified representation

of the system dynamics), variation in system parameters and noise effects. (Edwards & Spurgeon, 1998; J.-J. Slotine & Li, 1991)

Sliding mode controllers consist of an appropriate feedback control and a decision rule (switching function) based on a discriminant function switching between classes of control action. The decision rule generates a signal from instantaneous values of the system state variables. The feedback controller tries to control of the system with the help of this signal which is produced by decision rule. Thus, a variable structure system is obtained, which is the combination of various subsystems, each with a specific control structure, defined for certain regions of the system behavior.(Yazıcı, 2008)

The sliding mode controller design process has two steps:

Step 1 : Determining the sliding surface equation which decides the behavior of the system during sliding mode

Step 2: Designing a continuous control rule to make the switching surface an eigenmode for the system dynamics and determination of the discrete rule that will keep the system status reaching the switching function and keep it here.

It is much easier to control 1^{st} order systems than to control n^{th} order systems. Therefore, sliding mode control defines a 1^{st} order behavior in the n^{th} order system. It means that, n^{th} order problems to be replaced by equivalent 1^{st} order problems. The system dynamics are determined by the sliding surface during the sliding mode. Thus, it becomes independent of system parameters. For this reason, the order of the system dynamics becomes lower than the original system. Details and derivations about the problem simplification and reformulation are provided in Section 3.2.1 and 3.2.2.

In the reaching phase/mode, tracking error cannot be directly controlled and system performance is sensitive to uncertainties and noise in the system parameters. Therefore, it is desired that the system variables reach the sliding surface quickly, the reaching phase is as short as possible. The reaching phase can be shortened by

the large amplitude control signal. However, the control signal that can be applied to the system is limited.

Key words for the sliding mode control are sliding surface (sliding manifold or hypersurface), sliding mode/phase, reaching mode/phase. Details about these parameters are provided in the following sections:

3.2.1 Sliding Surface

The sliding surface is the discriminant function that characterizes the operation of the discontinuous nonlinear control input.

To understand the theory behind the sliding surface some derivations are given in the following part which is mainly tailored from (Slotine & Li, 1991) :

Consider the single-input dynamic system

$$x^{(n)} = f(x) + b(x)u \quad (3.2)$$

where the scalar x is the state vector, $x^{(n)}$ is the n^{th} derivative, the scalar u is the control input and

$$x = [x \quad \dot{x} \quad \dots \quad x^{n-1}]^T \quad (3.3)$$

is the state vector.

- $f(x)$ and the control gain $b(x)$ are not exactly known.
- The extent of the imprecision on $f(x)$ is upper bounded by a known continuous function of x , $|f(x) - \tilde{f}(x)| \leq F(x)$
- The control gain $b(x)$ is not exactly known, but is of known sign and is bounded by known, continuous functions of x , $\frac{1}{\beta(x)} \leq \frac{b(x)}{\tilde{b}(x)} \leq \beta(x)$

Where ,

$$F(x) = \max\{f_{max}(x) - \tilde{f}(x), \tilde{f}(x) - f_{min}(x)\}$$

$$\beta(x) = \max \left\{ \frac{b_{max}(x)}{\tilde{b}(x)}, \frac{\tilde{b}(x)}{b_{min}(x)} \right\} \text{ and } \beta(x) \geq 1$$

The control problem is to get the state x to track a specific time-varying state x_d (desired state) in the presence of model mismatches.

$$x_d = [x_d \quad \dot{x}_d \quad \dots \quad x_d^{n-1}]^T \quad (3.4)$$

To achieve the desired state with a finite control u , the initial desired state $x_d(0)$ must be such that:

$$x_d(0) = x(0)$$

And

$$e = x - x_d \quad (3.5)$$

be the tracking error and the tracking error vector is the difference between desired state and real state:

$$e = x - x_d = [e \quad \dot{e} \quad \dots \quad e^{(n-1)}]^T$$

Besides, define a time-varying surface $S(t)$ in the state space R^n by the scalar equation $s(x;t)=0$,

$$S(t) = \{x: s(x; t) = 0\} \quad (3.6)$$

$$s(x; t) = \left(\frac{d}{dt} + \lambda\right)^{(n-1)} e \quad (3.7)$$

and λ is a strictly positive constant and $\lambda_i s$ are the eigenvalues of $s(x;t)$, and n is the order of system dynamics.

For instance, the sliding surface scalar equation for second order system is given in Eq.(3.8):

$$s = \dot{e} + \lambda e \quad (3.8)$$

λ is a positive constant and it is a tuning parameter that defines the slope of the sliding surface in two-dimension. λ directly affects the system dynamics.

The problem of tracking $x = x_d$ is equivalent to that of remaining on the surface $S(t)$ for all $t > 0$ with given initial condition. It means that, $s = 0$ represents a linear differential equation whose unique solution is $e = 0$. (For $s = 0$ case, \dot{e} is equal to $-\lambda e$, since λ is a positive constant and we have a root on the left half plane and the system is asymptotically stable) Thus, the problem tracking in the n-dimensional vector x_d can be reduced to that of keeping the scalar quantity s at zero. As a summary, since the n-dimensional tracking problem is replaced by 1st order stabilization problem in s .

Additionally, bounds on the s directly defines the bounds on the tracking error e . Relationship between bounds on s and e is given in Eq. (3.9).

$$|s| \leq \phi \Rightarrow |e| \leq \varepsilon = \phi / \lambda^{n-1} \quad (3.9)$$

Fast convergence can be achieved with high λ . It means that the reaching phase can be shortened by the large amplitude control signal. However, the control signal that can be applied to the system is limited (limited signal sources, processor limits) and high λ causes an overshoot in system output.

Phase plane is the time domain-based analysis tool, and it is used to analyze second-order systems and does not need linearization for nonlinear systems. This method is also a very useful method for analyzing the sliding surface and observing the transition between reaching and sliding modes. An example phase plane for a second order system is given in Figure 3.2.

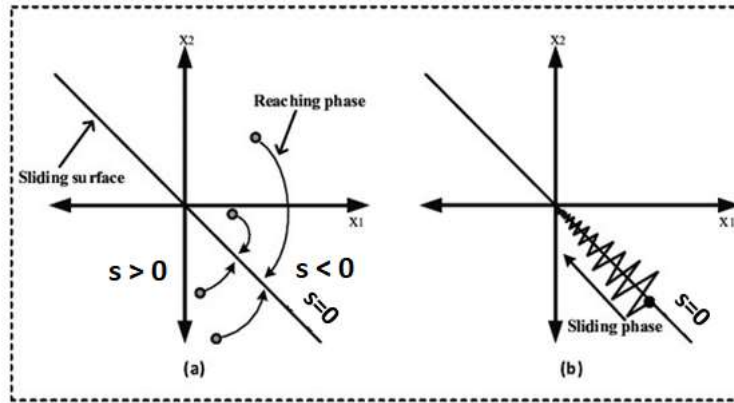


Figure 3.2 Phase Plane (adopted from Yasin et al., 2018)

After the determination of the sliding surfaces in the sliding controller design process, the second step is designing the control rule that satisfies the sliding condition.

$$\frac{1}{2} \frac{d}{dt} s^2 \leq -\eta |s| \quad (3.10)$$

Where η is strictly positive constant.

Eq. (3.10) gives the sliding condition which states that distance to the surface, decreases along all system trajectories. Thus, it constrains trajectories to point towards the sliding surface $S(t)$. In particular, once on the surface, the system trajectories remain on the surface. In other words, satisfying sliding condition makes the surface an invariant set. Additionally, sliding condition implies that some disturbances or dynamic uncertainties can be tolerated while still keeping the surface an invariant set.

3.2.2 Controller Rule

Controller design needs to enforce the system state to sliding surface and keep it on the sliding surface. If the system state can be kept on the sliding surface, the sliding mode dynamics can guarantee the convergence of the tracking error to be zero.

Lyapunov “direct” method, the basis of sliding condition, is generally used for designing such a stable control rule.

Conventional SMC control signal is provided in Eq.(3.10) and the structure of the SMC is shown in Figure 3.3.

$$u_{SMC} = u_{eq} + u_{sw} \quad (3.11)$$

The control signal has two parts. The first part, u_{eq} , equivalent control is valid only on the sliding surface to make it known to the system dynamics as an eigenmode. The second part, u_{sw} , switching control enforces the state trajectories to converge toward the sliding surface. In other words, the control signal is able to steer the $s(x; t)$ to zero in finite time using both control parts.

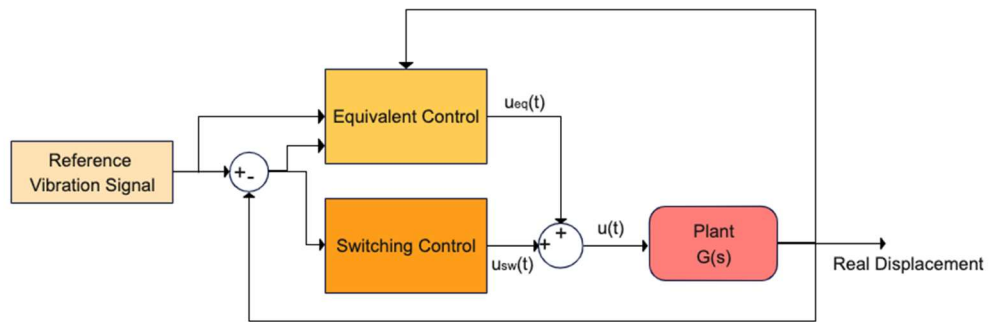


Figure 3.3 Sliding Mode Controller Structure

The equivalent control generates a continuous control signal that directs the system towards the equilibrium, where $\dot{s} = 0$ (Edwards & Spurgeon, 1998). And derived by equating the derivative of sliding surface to 0 and this equivalent controller is a continuous controller to make the sliding surface an eigenmode for the system using the system dynamical estimation, as well as control gain estimation as well as disturbance estimation.

An example for derivation of u_{eq} is given below:

$$\ddot{x} = f(x, \dot{x}) + b(x)u$$

$$F(x) = \max\{f_{max}(x) - \tilde{f}(x), \tilde{f}(x) - f_{min}(x)\}$$

$$\beta(x) = \max \left\{ \frac{b_{max}(x)}{\tilde{b}(x)}, \frac{\tilde{b}(x)}{b_{min}(x)} \right\} \text{ and } \beta(x) \geq 1$$

$$s = \dot{e} + \lambda e, \quad \dot{s} = \ddot{e} + \lambda \dot{e}, \quad \ddot{e} = \ddot{x} - \ddot{x}_d$$

$$\dot{s} = \ddot{x} - \ddot{x}_d + \lambda \dot{e} = 0$$

$$\dot{s} = \tilde{f}(x, \dot{x}) + \tilde{b}(x)u - \ddot{x}_d + \lambda \dot{e} = 0$$

$$u_{eq} = \tilde{b}(x)^{-1} (-\tilde{f}(x, \dot{x}) + \ddot{x}_d - \lambda \dot{e})$$

The switching control signal is produced according to the sliding conditions or reaching rules. Many methods are proposed for the reaching rules in the literature. These rules are derived by using Lyapunov “direct” method and the reaching rule approach directly determines the dynamics of the switching function.

For instance, switching function defined as :

$$\dot{s} = -Q \text{sgn}(s) + Kf(s) \quad (3.12)$$

Where Q and K are positive-definite diagonal matrix.

$$\text{sgn}(s) = [\text{sgn}(s_1) \text{sgn}(s_2) \dots \text{sgn}(s_m)]^T$$

$$f(s) = [f_1(s_1) f_2(s_2) \dots f_m(s_m)]^T$$

$$s_i f_i(s_i) > 0 \quad s_i \neq 0 \text{ and } i = 1, 2, 3 \dots, m$$

f_i is a scalar function, Q should be large enough to suppress all uncertainties and $\text{sgn}(s)$ is sign vector \vec{s}

$$\text{where } \text{sgn}(s) = \begin{cases} -1 & \text{if } s < 0 \\ 0 & \text{if } s = 0 \\ 1 & \text{if } s > 0 \end{cases}$$

Reaching rules are produced according to values of Q and K . And the basic rules are listed below:

Constant rate reaching rule:

$$u_{sw} = -Qsgn(s) \quad (3.13)$$

Constant plus proportional rate reaching rule:

$$u_{sw} = -Qsgn(s) - Ks \quad (3.14)$$

Power rate reaching rule:

$$u_{sw} = -Q|s|^a - sgn(s) \quad (3.15)$$

In this thesis work, constant rate reaching rule is preferred and control signal.

The final controller rule for the second order system is given below:

$$u_{SMC} = u_{eq} + u_{sw}$$

$$u_{SMC} = \tilde{b}(x)^{-1}(-\tilde{f}(x, \dot{x}) + \ddot{x}_d - \lambda\dot{e}) - Qsgn(s)$$

And this controller rule should satisfy the sliding condition Eq. (3.10) :

$$Q \geq \beta(x)(F(x) + \eta) + (\beta(x) - 1)|-\tilde{f}(x, \dot{x}) + \ddot{x}_d - \lambda\dot{e}|$$

Q and η are controller design parameters. If there is a high degree of uncertainty in the system, the gain should be chosen as high as the system allows. Mechanical and electrical limits play an important role in determining Q .

Since sliding mode control is discontinuous in nature and the continuous control is under dynamics . As a result, if the system may can go beyond the sliding surface after the system states reach the sliding surface. Since the control class switches for $s < 0$ and $s > 0$ the switching control signal is generated with a opposing sign and the states are brought back onto the surface. In such a control, the system changes direction too much in a short time to keep the systems states on the sliding surface. The rapid change of the direction with unlimited frequency is called “chattering”.

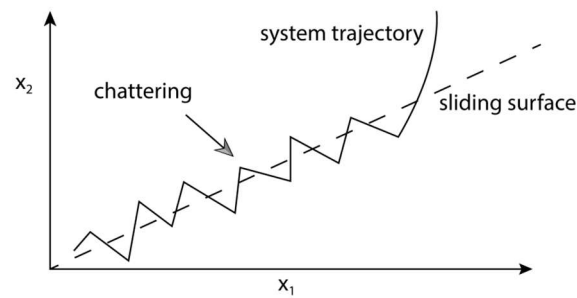


Figure 3.4 Representation of Chattering on the Sliding Surface (Adopted from (Tanakitkorn et al., 2018))

Chattering is a harmful phenomenon since the control effort has high frequency that may trigger nonlinear modes of the system it leading to degradation of tracking control accuracy. This phenomenon can damage the mechanics of the systems and cause heating, etc. due to excited nonlinearities. (V. Utkin & Lee, 2006). Therefore, SMC is not recommended for high dynamic systems. In the literature, two different reasons are presented as the cause of chattering:

- The first reason is the neglected fast dynamics in the ideal model (Unmodeled dynamics with small-time constants)
- The second reason is the utilization of digital controllers with finite sampling time (Theoretically, the ideal sliding mode implies infinite switching frequency, after the discretization, switching frequency can not exceed the sampling frequency.)

Various methods have been proposed by the researchers in order to overcome this disadvantage of the sliding mode control.

3.2.3 Our Proposed SMC Design for the Gyro Drive Axis Control Problem

Sliding mode controller is insensitive to parameter variations and it has complete disturbance rejection. Therefore, it is suitable for gyro proof mass control. It provides robustness against to environmental effects (temperature, vibration, etc.), noise variations such as mechanical noise, electronic noise and measurement inaccuracies (Ex. Analog to digital and digital to analog conversions)

Sliding mode controller as drive axis controller is given in Figure 3.5. The set-point is the desired/reference proof mass drive axis displacement. Additionally, the difference between desired trajectory and real proof mass trajectory defines the tracking error. Equivalent control and switching control actions satisfies the sliding condition.

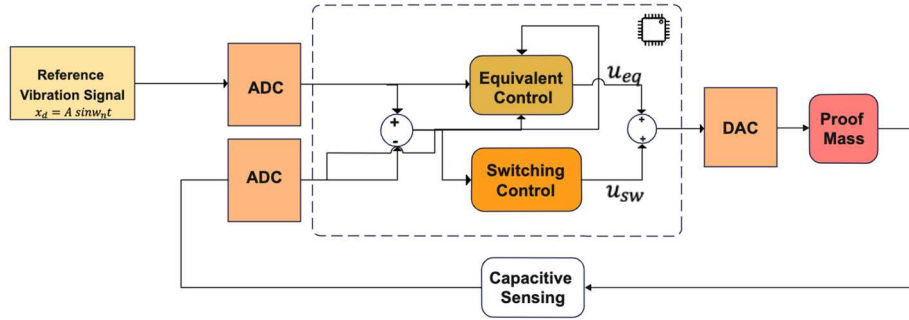


Figure 3.5 Sliding Mode Controller for Gyro Drive Axis Control Problem

For gyro control application we generate the sliding mode based on the drive axis dynamic model which is provided in Chapter 2 with Eq.(2.14).

The control action derivation starts with the derivation of equivalent control.

Firstly, we try to get $\ddot{x} = f(x, \dot{x}) + bu$ form:

$$\ddot{x} + 2\zeta_x w_{nx} \dot{x} + w_{nx}^2 x + 2\zeta_{xy} w_{nxy} \dot{y} + w_{nxy}^2 y = \frac{u_x}{m} + 2\Omega \dot{y} \quad (3.16)$$

$$\ddot{x} = \frac{u_x}{m} + 2\Omega \dot{y} - 2\zeta_x w_{nx} \dot{x} - w_{nx}^2 x - 2\zeta_{xy} w_{nxy} \dot{y} - w_{nxy}^2 y$$

x : drive axis displacement

x_d : drive axis reference displacement

y : sense axis output

$\ddot{x} = f(x, \dot{x}) + bu$ form of the dynamic equation is given in Eq. (3.17):

$$\begin{aligned} f(x, \dot{x}) &= 2\Omega\dot{y} - 2\zeta_x w_{nx}\dot{x} - w_{nx}^2 x - 2\zeta_{xy} w_{nxy}\dot{y} - w_{nxy}^2 y \\ b &= 1/m \end{aligned} \quad (3.17)$$

$$s = \dot{e} + \lambda e, \quad \dot{s} = \ddot{e} + \lambda \dot{e},$$

$$\dot{s} = (\ddot{x} - \ddot{x}_d) + \lambda(\dot{x} - \dot{x}_d)$$

$\dot{s} = 0$ on the sliding surface and we try to find equivalent control:

$$(\ddot{x} - \ddot{x}_d) = -\lambda(\dot{x} - \dot{x}_d)$$

$$\ddot{x} = \ddot{x}_d - \lambda(\dot{x} - \dot{x}_d)$$

$$f(x, \dot{x}) + bu = \ddot{x}_d - \lambda(\dot{x} - \dot{x}_d)$$

$$\begin{aligned} \frac{u_{eq}}{m} + 2\Omega\dot{y} - 2\zeta_x w_{nx}\dot{x} - w_{nx}^2 x - 2\zeta_{xy} w_{nxy}\dot{y} - w_{nxy}^2 y \\ = \ddot{x}_d - \lambda(\dot{x} - \dot{x}_d) \end{aligned}$$

$$\begin{aligned} \frac{u_{eq}}{m} = \ddot{x}_d - \lambda(\dot{x} - \dot{x}_d) - 2\Omega\dot{y} + 2\zeta_x w_{nx}\dot{x} + w_{nx}^2 x + 2\zeta_{xy} w_{nxy}\dot{y} + \\ w_{nxy}^2 y \end{aligned}$$

$$\begin{aligned} \frac{u_{eq}}{m} = \ddot{x}_d + \lambda\dot{x}_d + (2\zeta_x w_{nx} - \lambda)\dot{x} - 2\Omega\dot{y} + w_{nx}^2 x + 2\zeta_{xy} w_{nxy}\dot{y} + \\ w_{nxy}^2 y \end{aligned}$$

$$u_{eq} = m (\ddot{x}_d + \lambda\dot{x}_d + (2\zeta_x w_{nx} - \lambda)\dot{x} - 2\Omega\dot{y} + w_{nx}^2 x + 2\zeta_{xy} w_{nxy}\dot{y} + w_{nxy}^2 y)$$

$$u_{sw} = -Qsgn(s)$$

$$u_x = u_{eq} + u_{sw}$$

$$\begin{aligned} u_x = m (\ddot{x}_d + \lambda\dot{x}_d + (2\zeta_x w_{nx} - \lambda)\dot{x} - 2\Omega\dot{y} + w_{nx}^2 x + 2\zeta_{xy} w_{nxy}\dot{y} + \\ w_{nxy}^2 y) - Qsgn(s) \end{aligned} \quad (3.18)$$

Where, $e = e = x_d - x, \dot{e} = \dot{x}_d - \dot{x}, \ddot{e} = \ddot{x}_d - \ddot{x}, \frac{w_{nx}}{q_x} = 2\zeta_x w_{nx}$

In the scope of this thesis work, sliding mode controller for a Coriolis MEMS gyro drive axis is implemented according to Eq. (3.18). Simulation studies and experimental results are given in Chapter 4. Ideal sensor parameters are used for controller signal calculation. On the other hand, uncertainties and disturbances are added to system to observe the robustness of the controller and controller gain Q is determined according to level of uncertainty to satisfy sliding condition.

3.2.4 Chattering Minimization by Fat-Boundary Layer Sliding Mode Controller

In order to eliminate the chattering on the control signal boundary layer approach is proposed in the literature (Erbatur & Çallı, 2009; Tanakitkorn et al., 2018).

The boundary layer approach is the most simple and popular solution for the chattering problem. And depends on the application of a high gain feedback when the motion of the system reaches ϕ vicinity of a sliding manifold. (J. J. Slotine & Sastry, 1983)

The parameter ϕ defines the thickness of the boundary layer as shown in Figure 3.6.

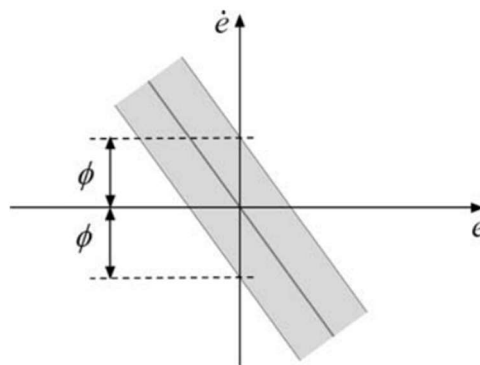


Figure 3.6 Representation of Boundary Layer on the Sliding Surface (Adopted from (Erbatur & Çallı, 2009))

The classical SMC behavior is valid outside the boundary layer. Basically, this approach provides an efficient solution by replacing the sign function with the saturation function.

The modified version of control signal is provided in Eq. (3.19).

$$u_{sw} = -Qsat(s / \phi) \quad (3.19)$$

$$u_x = u_{eq} + u_{sw}$$

$$sat(s) = \begin{cases} -1 & \text{if } s < -\phi \\ s / \phi & \text{if } -\phi \leq s \leq \phi \\ 1 & \text{if } s > \phi \end{cases}$$

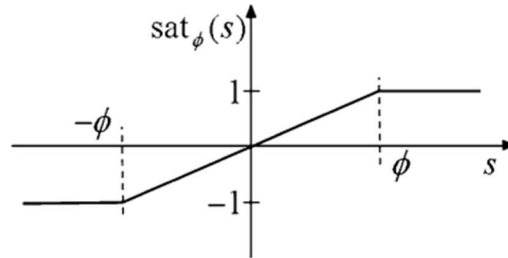


Figure 3.7 Representation of Saturation Function (Adopted from (Erbatur & Çallı, 2009))

In this method, determining an appropriate value for the boundary layer thickness (ϕ) is crucial; it directly affects tracking and robustness performance. This method reduces the effects of chattering, but compromises excellent tracking. For instance, a thin boundary layer cannot solve the chattering problem. On the other hand, a too wide boundary layer selection causes degradation in tracking performance and robustness. (Erbatur & Çallı, 2009; Mizov, 2015). Generally, amplitude of chattering is measured to determine the boundary layer thickness. This is followed by increasing or decreasing the thickness to find the optimum performance.

This method is also implemented in the scope of this thesis work to compare the results with the other proposed methods. Both simulation studies and experimental studies are implemented.

3.3 Proxy-Based Sliding Mode Control: A Background Overview

Although the sliding mode controller is robust and easy to implement, it also causes a decrease in performance due to the chattering problem. One of the most common methods used to overcome this problem is proxy-based sliding mode control method.

Proxy-based sliding mode control is an extension of PID and SMC. This method combines PID control and SMC algebraically to reduce chattering effect. PID controller defines low/local dynamics and SMC specifies high/global dynamics of the system. Finally, PBSMC system provides overdamped response without sacrificing tracking accuracy.

A proxy (virtual object) is placed between the desired position and the real position to implement proxy-based sliding mode controller to reduce to chattering phenomenon caused by the sign function. The proxy is a virtual object that does not exist in reality and used for pooling control signals. On the other hand, PID controller added between controlled system and proxy. PID controller and SMC are coupled through proxy.

The physical representation of PBSMC is given in Figure 3.8, and Figure 3.9 shows how the PID controller output and PBSMC output are pooled through the proxy.

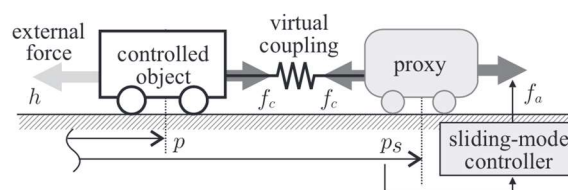


Figure 3.8 Physical Interpretation of Proxy Based Sliding Mode Control (Kikuuwe & Fujimoto, 2006)

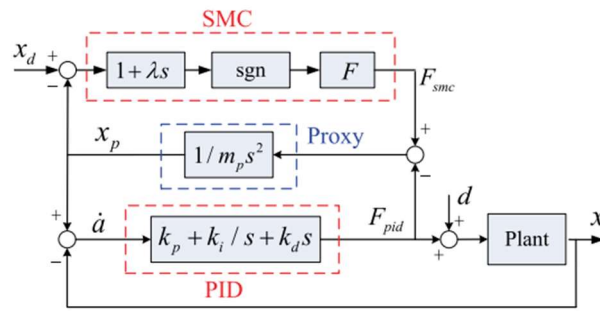


Figure 3.9 Block Diagram of Control Loop with PBSMC (Gu et al., 2015)

3.3.1 Our Proposed of PBSMC Design to Gyro Drive Axis Control Problem

Although PBSMC is widely used in robotic applications, it has not been used for sensor applications before. The most important property of PBSMC is that using PID controller small position errors can be eliminated and using SMC large position errors are eliminated. Therefore, even a small change can be eliminated and performance of gyro can be increased. In this study, as a novel implementation to gyro control, PBSMC will provide smooth and overdamped solutions under environmental effects (temperature changes, vibration, package stress, etc.) and noise variations such as mechanical noise, electronic noise.

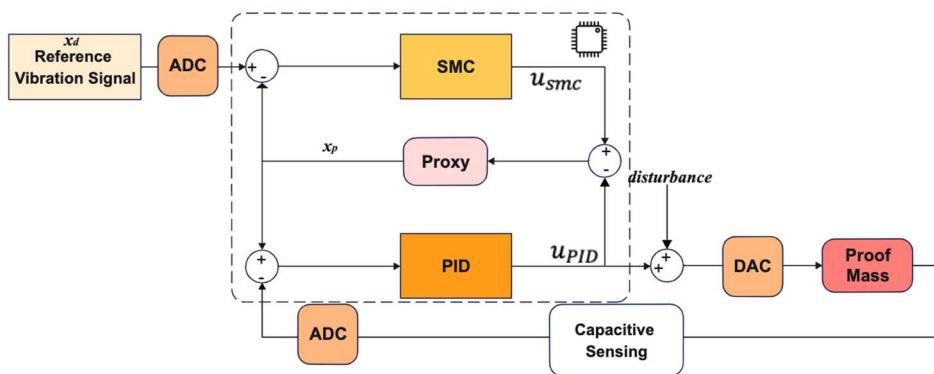


Figure 3.10 Proxy-Based Sliding Mode Controller Working Principle

PBSMC implementation is for gyro drive axis control problem is depicted in Figure 3.10. For our gyro control application, we want to control the displacement of proof mass on drive axis. Therefore, motion of the proof mass on the drive axis is our plant. The PID controller, thus, causes an interaction signal u_{PID} between the plant and proxy. At the same time, the proxy is also controlled by a SMC, which applies u_{smc} , to track the desired reference vibration signal. Small position errors are compensated by PID controller and large position errors are eliminated by sliding mode controller. Since a proxy has been added to the system, all equations must be updated according to this new architecture. Updated derivations are given in the following section. Additionally, how the PID controller output and the SMC output are combined is also given in this section.

Starting with the rearranging the sliding surface in Eq. (3.8) according to the proxy application. In the new version sliding surface x_d is our desired drive axis displacement and x_p is the proxy displacement.

$$s = (x_d - x_p) + \lambda(x_d - \dot{x}_p) \quad (3.20)$$

Eq. (3.20) gives the updated version of scalar sliding surface equation.

$$u_{PID} = K_P(x_p - x) + K_I \int (x_p - x)dt + K_D(\dot{x}_p - \dot{x}) \quad (3.21)$$

Eq. (3.21) provides the PID control signal.

Rearranging the sliding surface Eq (3.8) to merge the PID controller and SMC control signals yields our proxy based sliding mode control. x is the real displacement of proof mass on the drive axis:

$$s = (x_d - x) + \lambda(\dot{x}_d - \dot{x}) - (x_p - x) - \lambda(\dot{x}_p - \dot{x}) \quad (3.22)$$

For notational simplification Eq. (3.22) is reformulated:

$$s = \sigma - \dot{a} - \lambda\ddot{a} \quad (3.23)$$

where $\sigma = (x_d - x) + \lambda(\dot{x}_d - \dot{x})$ and $a = \int (x_p - x)dt$

Control signal becomes:

$$u_{smc} = Qsgn(\sigma - \dot{a} - \lambda\ddot{a}) \quad (3.24)$$

$$u_{PID} = K_P\dot{a} + K_I a + K_D\ddot{a} \quad (3.25)$$

Considering the proxy, the displacement equation can be derived as (m_p is the proxy mass):

$$m_p \ddot{x}_p = u_{smc} - u_{PID} \quad (3.26)$$

In practice, proxy mass in Eq.(3.26) is set to be zero to get final version of controller signal. Then, $u = u_{smc} = u_{PID}$ is satisfied. Finally, the PBSMC law is obtained by

$$u = Qsgn(\sigma - \dot{a} - \lambda\ddot{a}) \quad (3.27)$$

$$u = K_P\dot{a} + K_I a + K_D\ddot{a} \quad (3.28)$$

$$\ddot{a} = \frac{1}{K_D} (u - K_I a - K_P\dot{a}) \quad (3.29)$$

To overcome chattering problem the discontinuous signum function is replaced with saturation function with mathematical approximations:

$$u = Qsgn(\sigma - \dot{a} - \lambda \left(\frac{1}{K_D} (u - K_I a - K_P\dot{a}) \right)) \quad (3.30)$$

$$u = Qsgn\left(\frac{\lambda}{K_D} \left(\frac{K_D}{\lambda} (\sigma - \dot{a}) + K_I a + K_P\dot{a} - u \right)\right) \quad (3.31)$$

$$Y = Asgn[B(Z - Y)] \Leftrightarrow Y = A \text{ sat} \left(\frac{Z}{A} \right) \quad (3.32)$$

Eq. (3.32) is used to reformulate Eq. (3.31)

$$\text{Where, } A = Q, \quad B = \frac{\lambda}{K_D}, \quad Z = \frac{K_D}{\lambda} (\sigma - \dot{a}) + K_I a + K_P\dot{a}, Y = u$$

$$\text{sat}(\zeta) = \begin{cases} \text{sgn}(\zeta), & \text{if } |\zeta| > 1 \\ \zeta, & \text{if } |\zeta| \leq 1 \end{cases}$$

We can get Eq. (3.33)

$$u = Q \text{sat} \left(\frac{1}{Q} \left(\frac{K_D}{\lambda} (\sigma - \dot{a}) + K_I a + K_P\dot{a} \right) \right) \quad (3.33)$$

Eq. (3.31) and Eq. (3.33) are algebraically equivalent.

Final and implementable version of PBSMC is illustrated in Figure 3.11. This model is used in our gyro drive axis control application.

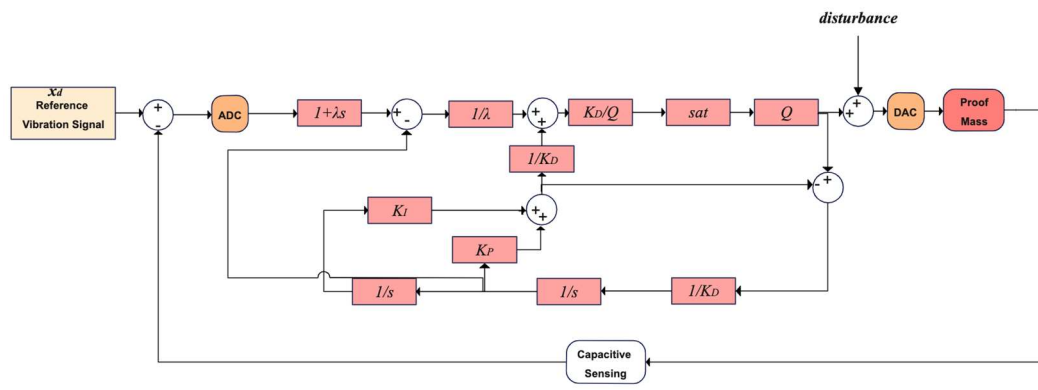


Figure 3.11 Proxy-Based Sliding Mode Controller Design for Gyro Drive Axis

Derived PBSM controller for our problem is implemented according to the Figure 3.11. Disturbance term is added to simulate the model uncertainty and environmental effects on the parameters.

According to parameter setting (K_p , K_d , K_i , λ) PBSMC controller can be act as a sliding mode controller or PID controller. Situations are summarized in Table 3.1.

Table 3.1 PBSMC Behaviors According to Parameters

Parameter Values	Result
$K_D \rightarrow \infty$	Sliding Mode Controller
$\lambda = K_D/K_P, K_I = 0$	PID Controller

By setting $K_p \rightarrow \infty$ the PBSMC behaves like conventional SMC with the form of $u = Q \text{sgn}(x_d - x + \lambda(\dot{x}_d - \dot{x}))$ and for the second case ($\lambda = K_D/K_P, K_I = 0$) PBSMC converges to traditional PID controller.

Simulation implementations and experimental studies about the PBSMC application for gyro drive axis control problem are provided in Chapter 4. Performance results and comparisons with the other control methods are also provided in Chapter 4.

3.4 Feedforward Controller: A Background Overview

The primary purpose of feedback is to compensate for external disturbances and model uncertainties. In the feedback controller, no corrective action is taken until a deviation in the controlled variable occurs. Thus, the controller performance is strongly affected by disturbance and/or setpoint changes. On the other hand, a predictive control action can be applied to the system to compensate for the effects of known/measurable disturbances. However, feedback controllers do not provide this feature. In addition to that, feedback control becomes unsatisfactory in systems that have high uncertainty and rapid parameter changes. For example, processes that have long time delays and/or significant and frequent disturbance. Various methods are suggested in the literature to overcome feedback control deficiencies. One of these methods is the feedforward controller or compensator.

When a sufficiently accurate process model is available, control performance can generally be improved by conveniently employing an additional feedforward control law (Visioli, 2006). To the best of our knowledge, the feedforward control method has not been applied as a gyro drive axis controller before. It is applied, and superiorities over the conventional methods are presented in this study.

Feedforward control can be used to improve system tracking performance. It means that feedforward reduces the error faster and keeps the error smaller relying on the feedback algorithm alone.

Feedforward control theory presents two different methodologies: disturbance feedforward method and command/setpoint feedforward method.

The disturbance feedforward controller method is based on the measurement of the disturbance and feeding to the feedforward control mechanism. Therefore, the

controller suppresses the effect of disturbance before it occurs on plant output. However, using additional sensors to measure the disturbance of each source is compelling and not possible on a gyro system. The disturbance feedforward control method is given in Figure 3.12.

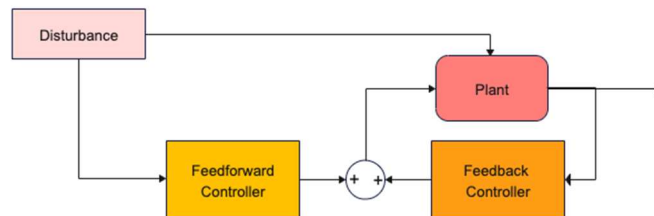


Figure 3.12 Disturbance Feedforward Controller

In the second method, the setpoint feedforward method, setpoint change acts as a disturbance in the feedback loop. Therefore, this method does not need additional measurements. Setpoint feedforward controllers can be defined as two degrees of freedom control systems, and Figure 3.13 shows the setpoint/ 2- DOF feedforward controller.

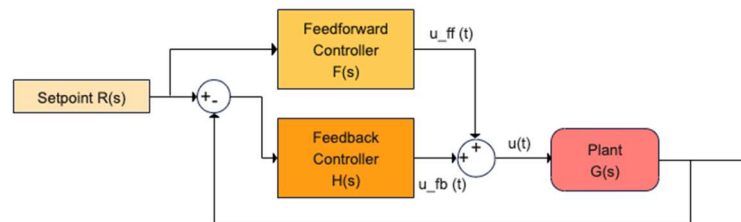


Figure 3.13 Setpoint/2-DOF Feedforward Controller

The feedforward controller/compensator is defined by Eq.(3.34) as the inverse of the plant model.

$$F(s) = \frac{1}{G(s)} \quad (3.34)$$

Hence, accuracy of the plant model is directly effects the control loop performance

$$u_{ff}(s) = R(s) \frac{1}{G(s)} \quad (3.35)$$

Total control signal is equal to sum of feedback control output and feedforward control signal as defined by Eq. (3.36)

$$u(t) = u_{fb}(t) + u_{ff}(t) \quad (3.36)$$

The advantages of feedforward controller are listed below (Marlin, 2000):

1. The feedforward controller compensates for a disturbance before the process output is affected.
2. The feedforward controller does not affect the stability of the control system.

On the other hand, disadvantages of feedforward control are summarized below:

1. Steady-state offset cannot be eliminated.
2. Feedforward controller needs additional sensor for disturbance measurement.

Finally, feedforward controller design rules are given below:

1. The process must be linear or linearized.
2. The disturbance variable must indicate the occurrence of an important disturbance.
3. The disturbance dynamics must not be significantly faster than the feedback controller output variable dynamics.

For our gyro drive axis control problem desired motion trajectory of gyro proof mass can be defined as setpoint when the setpoint method is applied to the gyro drive axis control problem. Additionally, the dynamic model of gyro presents the plant in the control loop, and system output is modeled as proof mass displacement.

3.4.1 Our Proposed of Weighted Feedforward Controller Design to Gyro Drive Axis Control Problem

Weighted feedforward method is implemented in the scope of this thesis work. This method is based on optimizing the total controller signal by weighting the controller signals. Modified version of the total controller signal is given in Eq.(3.37).

$$u(t) = K_1 u_{fb}(t) + K_2 u_{ff}(t) \quad (3.37)$$

K_1 and K_2 is equal to 1 for classical feedforward controller. The aim of classical feedforward controller is to make closed loop transfer function 1. To accomplish this, exact plant transfer function must be known. However, this is not possible for every plant. For instance some applications which can not be accurately get the plant model or has a nonlinear plant model use linearized plant model, estimated plant model or simplified model. (Ex. The simplified gyro dynamic model which is given in Eq. (2.10) is used for W-FF implementation) Thus, mismatch between real plant model and estimated plant model occurs. Since there is no exact plant transfer function, expected feedforward controller performance cannot be obtained. In order to overcome this problem weighted feedforward method is suggested. The weights are used to reduce the effect of mismatch between exact plant model and estimated plant model. Location of the overall system poles and zeros can be adjusted by changing the values of K_1 and K_2 in Eq.(3.38).

$$\frac{Y(s)}{R(s)} = \frac{K_2 + K_1 G(s)H(s)}{1 + K_1 G(s)H(s)} \quad (3.38)$$

To get the best result the weight of the feedback controller must be higher than the feedforward controller. For $K_2 > K_1$ case whole system becomes unstable. On the other hand, system zeros come closer to $j\omega$ axis and this accelerates the system response.

An example is given to understand the effect of feedforward and weighted feedforward controllers. Control loops with PID controller, FF controller, and W- FF controller are shown in Figure 3.14. Transfer function of the plant is given in Eq.(3.39):

$$G(s) = \frac{s^2 + 4.8s + 16}{s^2} \quad (3.39)$$

Firstly, root locus analysis for feedback controller, weighted feedforward controller and weighted feedforward controller $K_2 > K_1$ case are presented in Figure 3.15 ,

Figure 3.16 and Figure 3.17. Moreover, responses to step input are presented in Figure 3.17. As expected, the tracking and overshoot performance of W-FF is better than the other controllers. In summary, the superiority of W-FF is clearly observed.

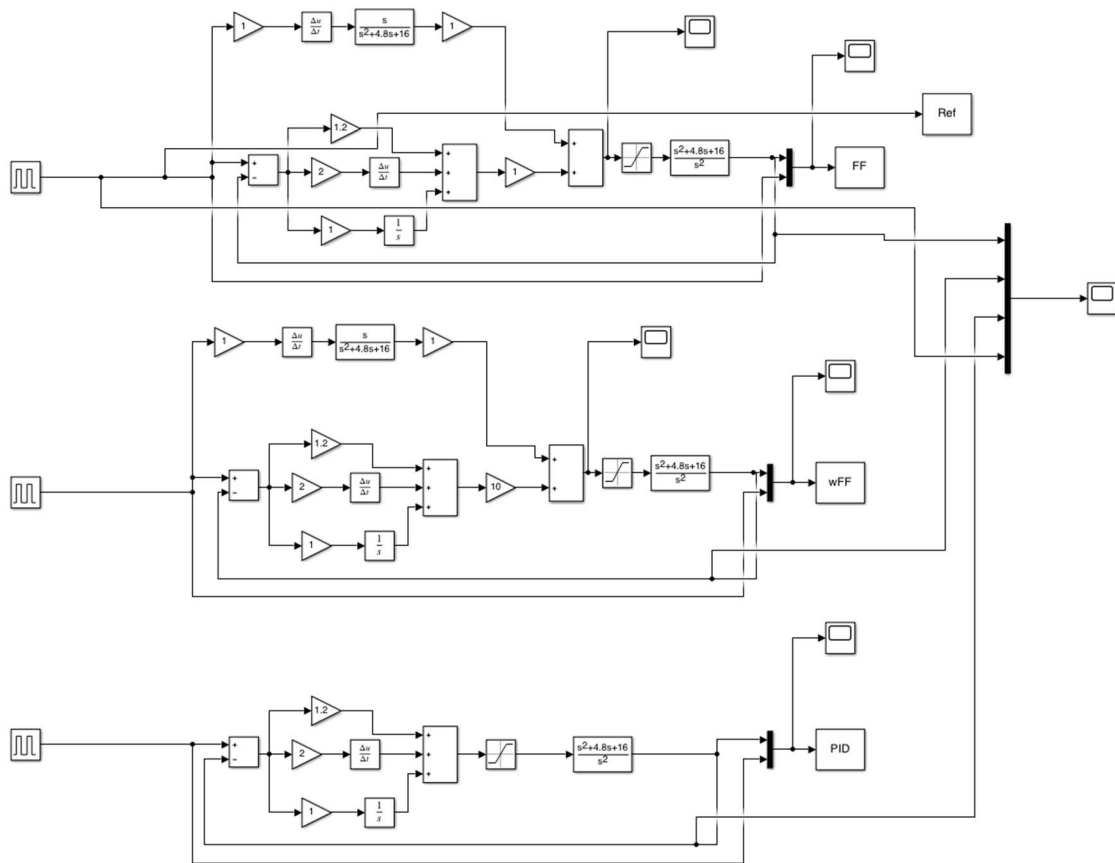


Figure 3.14 Example application for feedforward and W-FF controller

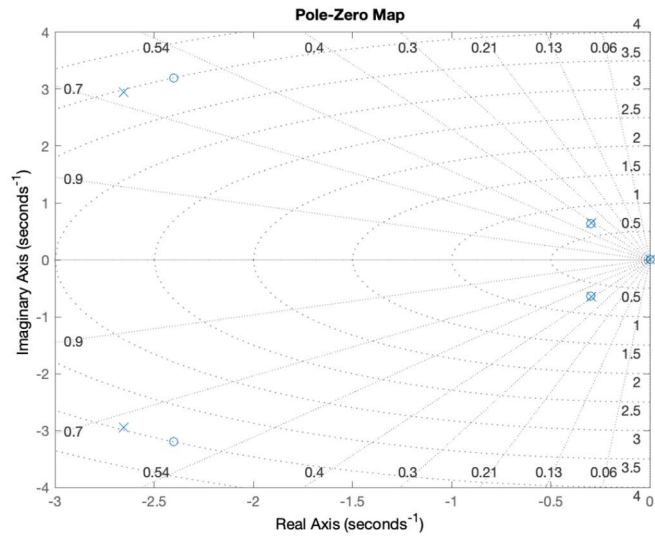


Figure 3.15 Pole-Zero Analysis for feedback control with PID controller

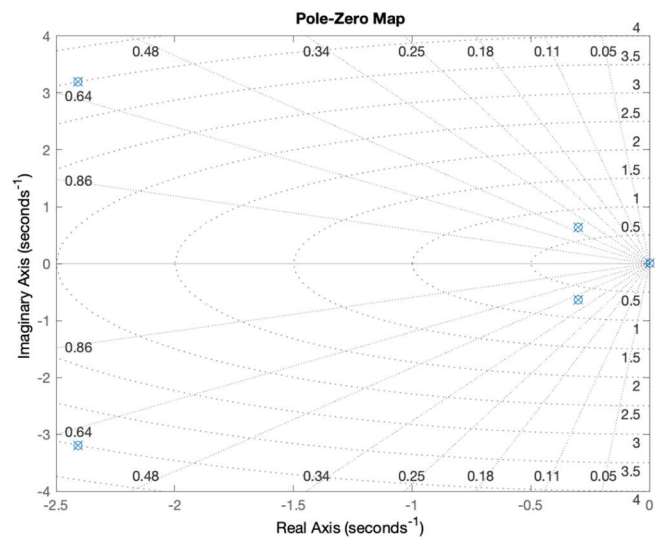


Figure 3.16 Pole-Zero Analysis for feedforward control, $K_1 > K_2$

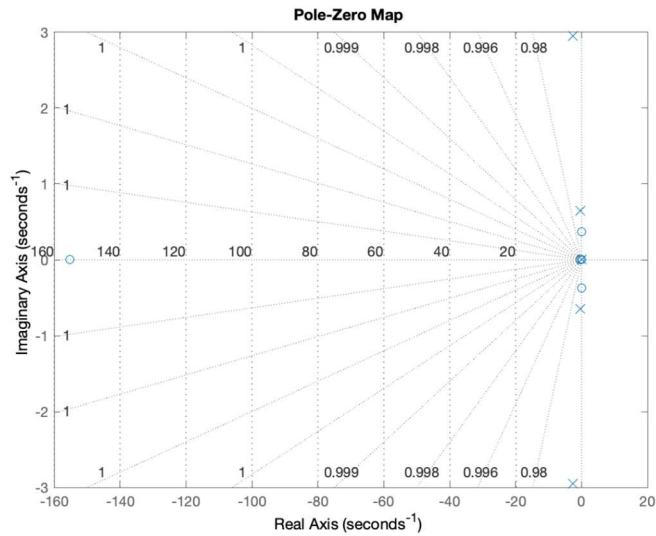


Figure 3.17 Pole-Zero Map Analysis for feedforward control, $K_2 > K_1$

When $K_2 > K_1$ poles of the closed loop system approach the $j\omega$ -axis and the system converges to unstable state.

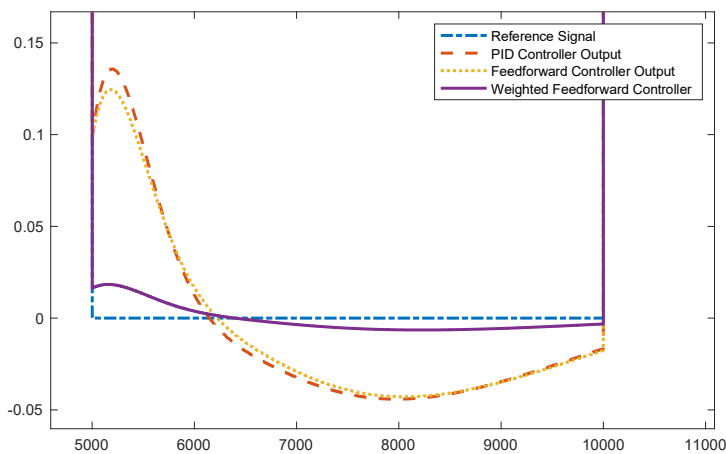


Figure 3.18 Step responses for PID, FF and W-FF

The accuracy of the estimated process model directly changes the effectiveness of a feedforward control. Therefore, the dynamic model of gyro drive axis is estimated or modeled accurately.

During the design phase of a gyro, step forces $u_x(t)$, $u_y(t)$ in the x and y directions are applied and step responses of the gyroscope drive and sense axis are generated according to Eq.(2.8) and Eq.(2.9). From these step responses, unknown coefficients are estimated by using second-order transfer function models. These transfer function models are used in feedforward controller design. $G(s)$ in Eq.(3.34) represents the transfer function of the gyro drive axis dynamic model. $1/G(s)$ gives the transfer function of the feedforward controller. The reference displacement which is given in Eq. (3.34) shows the reference input for the control loop. Real displacement of proof mass is measured as a system output. Architecture of the weighted feedforward control for gyro drive axis control problem is shown in Figure 3.19.

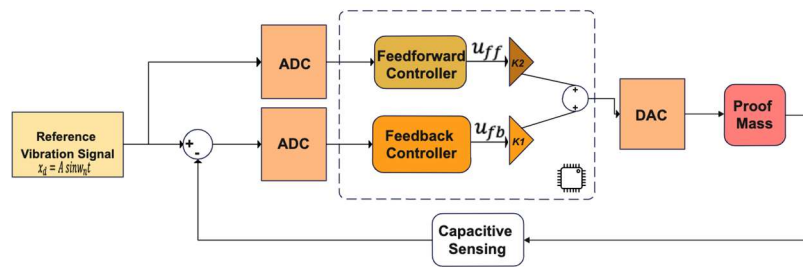


Figure 3.19. Weighted Feedforward Controller for Drive-Axis Control

In this study, feedback part of feedforward controller is designed as a PID controller. In addition to feedforward controller design, simulations are implemented to observe individual performance of PID controller.

At the beginning, the controller parameters are determined by simulation studies. After that, they are tuned according to the experimental data to get the best performance. Details of the simulation and experimental studies of PID controller, weighted feedforward controller, SMC and PBSMC are provided in Chapter 4.

CHAPTER 4

SIMULATION AND EXPERIMENTAL RESULTS

This chapter explains the results of simulation and experimental studies which are implemented based on the proposed methods.; PBSMC, SMC, SMC-BL and weighted feedforward controller.

The chapter starts with MEMS gyro dynamic model implementation. After that, simulation architectures and simulation properties, inputs and outputs are provided. Furthermore, this chapter explains the experimental measurement setup, sensor prototype used in the experimental implementation of the our approaches.

Finally, experimental results, observations and comments about the results are provided. Additionally, comparisons between simulation outputs and experimental outputs are presented.

4.1 Gyro Dynamic Model

As mentioned in Chapter 2, sensor design parameters determine the dynamic behavior of the drive axis and sense axis of the gyro. In this thesis, a single axis and single mass Coriolis vibratory MEMS gyro prototype is used for the controller implementation.

Firstly, the gyro prototype is simulated in MATLAB/Simulink environment. Eq. (2.14) and Eq. (2.15) are generated with design parameters which are given in Table 4.1. Both drive and sense axis outputs are obtained. And angular rate estimation is carried out by demodulation stage.

A single-axis and single mass Coriolis vibratory MEMS gyro is used in both simulation and experimental studies.

Table 4.1. MEMS Gyro Parameters

Parameter	Value
Mass (m)	0.57×10^{-8} kg
k_{xx}	235.8 N/m
d_{xx}	0.429×10^{-6} N s/m
k_{yy}	240.3 N/m
d_{yy}	0.687×10^{-3} N s/m
k_{xy}	5 N/m
d_{xy}	0.429×10^{-6} N s/m
Reference Vibration Signal Amplitude	600 mV
Reference Vibration Signal Frequency	17000 Hz

When subjected to rotation around the gyro measurement axis, the proof mass vibrates along the drive axis, and the applied angular rate modulates the vibration amplitude caused by self oscillation. This modulated sensing signal is detected by the sensing circuit, which provides the sense axis output, and is demodulated using the reference vibration signal from the drive circuit. (Wheeler & Digonnet, 2021)

Figure 4.1 shows the signal processing loop which is implemented to estimate the angular rate output from the sense axis output. DSBDC (double sideband suppressed carrier modulation) demodulator is used for demodulation of sense axis output.

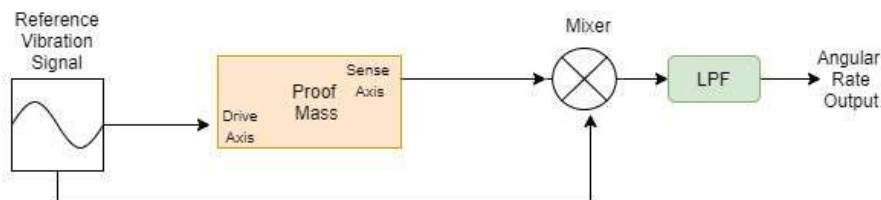


Figure 4.1 Signal Processing Loop for Angular Rate Estimation

4.2 Simulation Results

After the gyro implementation, proposed controllers SMC, SMC-BL, PBSMC and W-FF controller are built by Simulink software. PID controller is also implemented to compare the performance parameters with classical controllers.

Simulation parameters are given in Table 4.2.

Table 4.2 Simulation Parameters

Parameter	Value
Input Angular Rate	0.1745 rad/s (10 deg/s)
Sampling Period	1×10^{-8} sn
Disturbance Noise Power	0.3

Simulation scenarios are designed according to our hardware modeling given in Chapter 2. A desired reference vibration signal is applied as drive axis input in the simulation. Additionally, disturbance noise is applied to sensing axis input to simulate the effects of mechanical-thermal noise and packaging stress. Disturbance noise is modeled as band limited white noise.

4.2.1 PID Controller Results

Simulink PID controller block simulates the controller against a plant model, and that block is used to control the dynamic gyro model. General representation of PID controller is provided in Eq. (4.1) and Controller parameters are given in Table 4.3. MATLAB/Simulink PID controller block is used in this section. Parameters of the controller tuned by transfer function based tuning method.

$$u(t) = K_p e(t) + K_i \int e(t) dt + K_d \frac{de}{dt} \quad (4.1)$$

Table 4.3 PID Controller Parameters

Parameter	Value
K _i	5878
K _p	2.0789
K _d	1.6038×10^{-4}

Figure 4.2 shows the drive axis reference vibration signal and controlled displacement of the drive axis and Figure 4.3 presents the controller error. It can be observed from Figure 4.2 and Figure 4.3 that there is a difference between the reference signal and the PID controlled displacement output. The PID controller provides tracking capability but can not zeroize the error. But, it is easily implementable. This controller can be selected according to the target gyro performance.

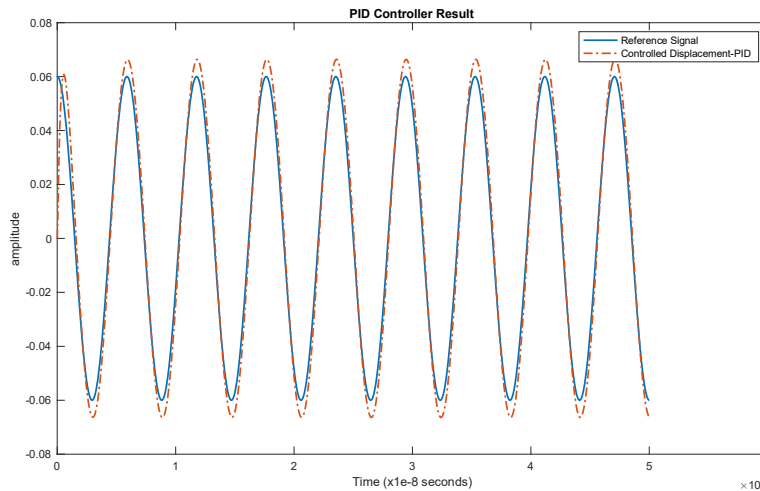


Figure 4.2. PID Controller Tracking Performance for Drive Axis Control

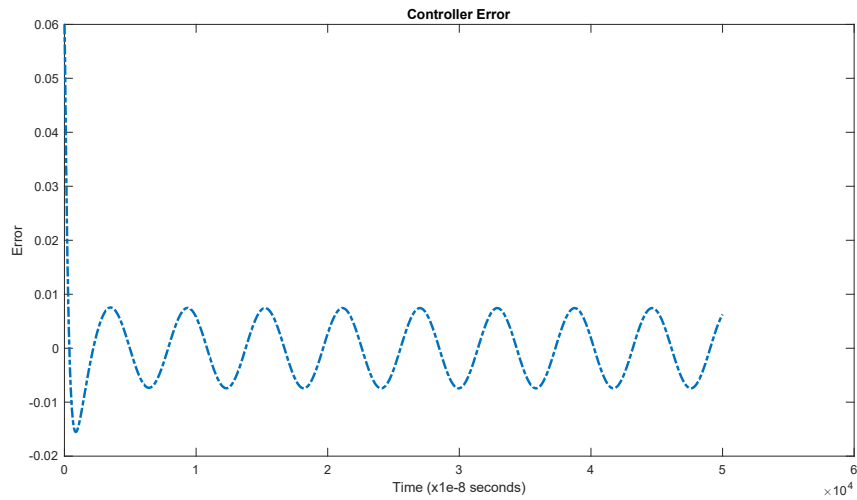


Figure 4.3. Controller Tracking Error Performance PID

Angular rate measurement of the gyroscope, whose sliding axis control is made by the PID controller, is given in Figure 4.4. It oscillates around input rate 10 deg/s (0.1745 rad/s). The maximum error of the measurement is 68.4166 deg/h, which directly affects the platform's orientation calculation performance.

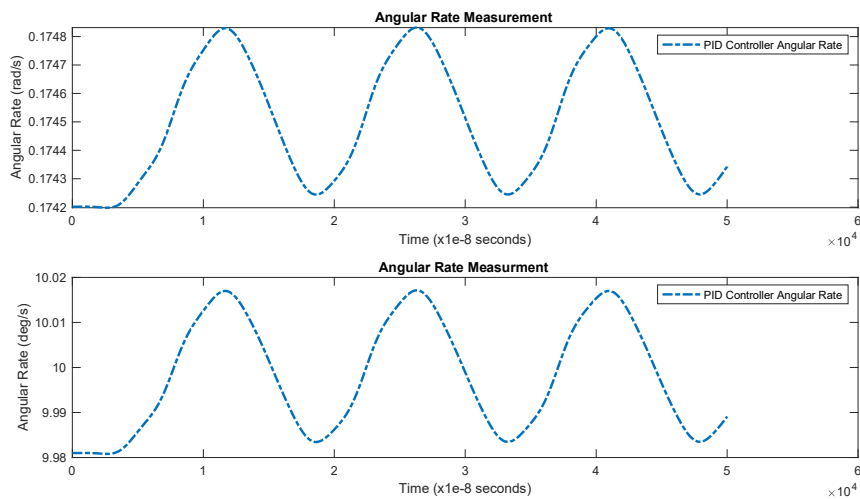


Figure 4.4. Angular Rate Measurement with PID Controller (for 10 deg/s)

4.2.2 Sliding Mode Controller and Sliding Mode Controller with Boundary Layer Results

After the PID controller implementation, the performance of SMC and SMC-BL are observed. The values of the design parameters for the controllers Q , λ and ϕ are given in Table 4.4. As mentioned in Chapter 3, performance and chattering reduction vary with the boundary layer's thickness (ϕ). The easiest way to determine the thickness is to measure chattering amplitude, which is used in this thesis work.

Table 4.4 SMC and SMC-BL Parameters

Parameter	Value
Q	900
λ	100
ϕ	0.23

Q is determined according to the overshoot requirements. Additionally, value of λ is obtained after a few trials, providing the smallest controller error and convergence time. The boundary layer's thickness (ϕ) is also determined by measuring the amplitude of the chattering.

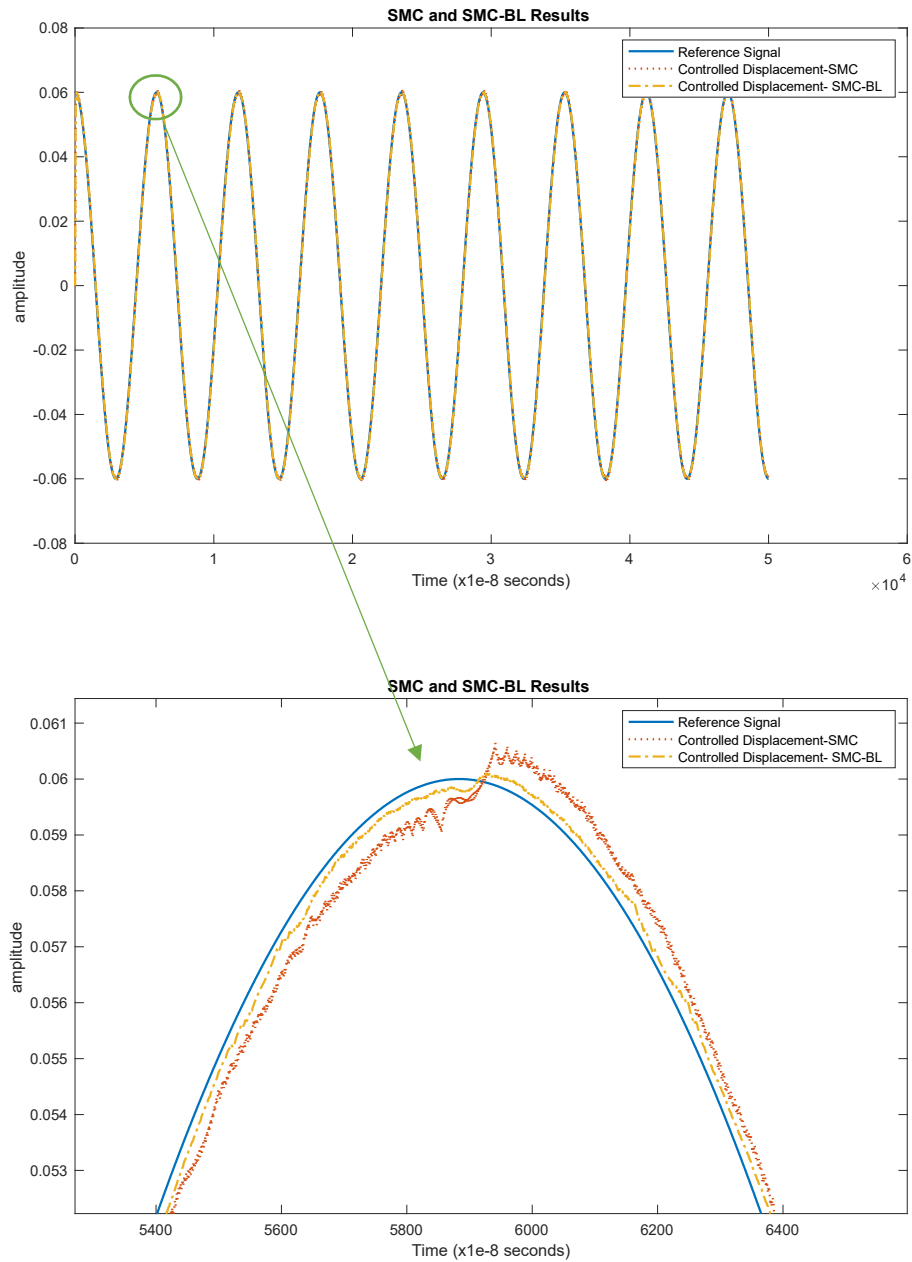


Figure 4.5. SMC and SMC-BL Tracking Performance for Drive Axis Control

Figure 4.5 and Figure 4.6 show that the tracking performances of SMC and SMC-BL are better than PID controller as expected. The drive axis displacement has approached the reference vibration signal. The effect of the boundary layer method is also clearly seen in Figure 4.5. Chattering is reduced, and the difference between the reference signal and the controlled displacement has become smaller.

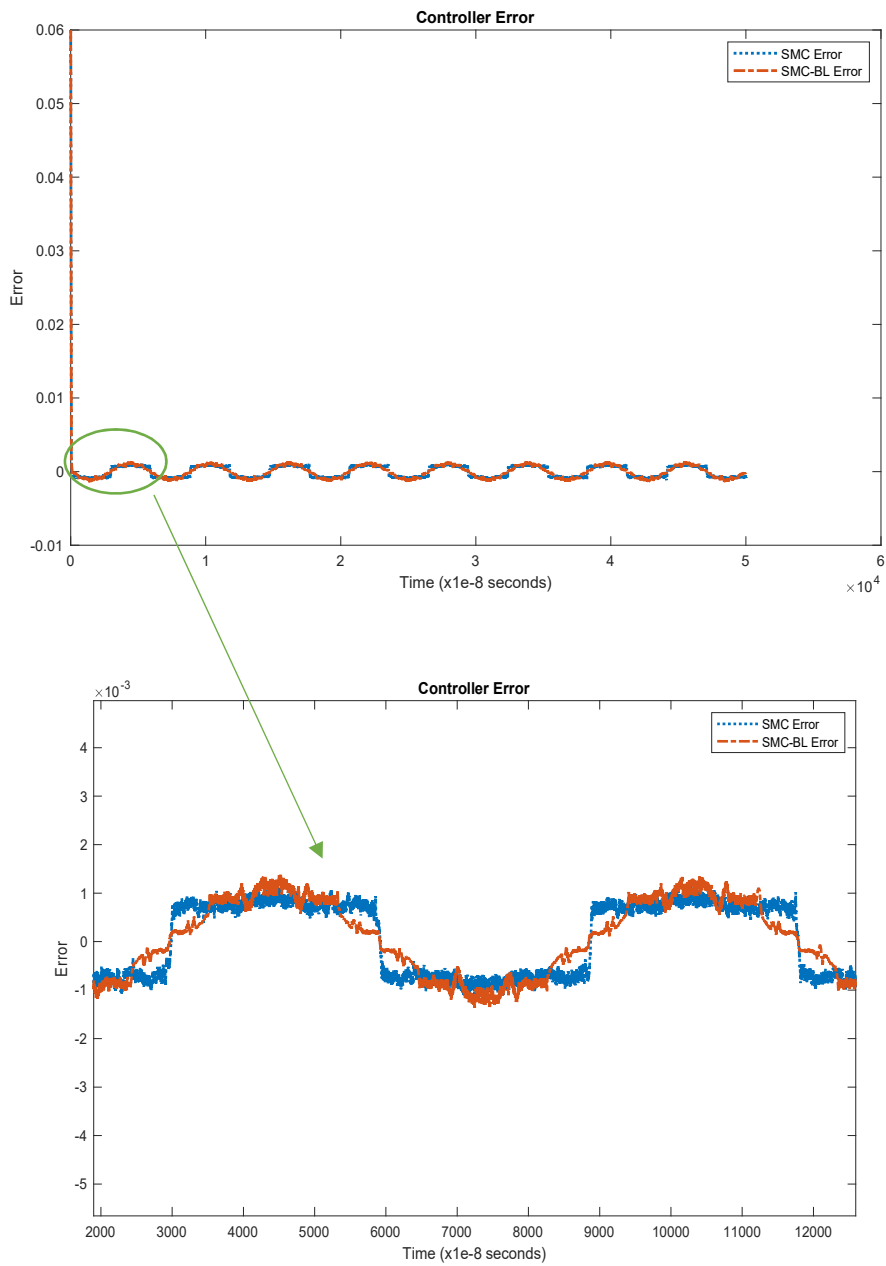


Figure 4.6. SMC and SMC-BL Controller Tracking Error Performance

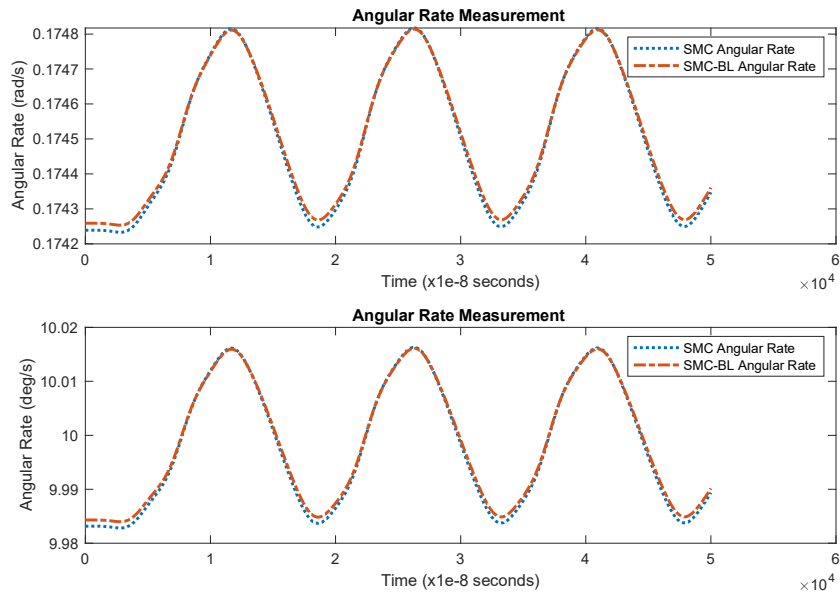


Figure 4.7. Angular Rate Measurement with SMC and SMC-BL (for 10 deg/s)

Angular rate measurements of the gyroscope, whose sliding axis control is made by the SMC and SMC-BL controller are given in Figure 4.7. Similar to PID, oscillation is observed around at the input rate of 10 deg/s (0.1745 rad/s). But the maximum error of the measurements are 65.4812 deg/h and 64.7974 deg/h, which are better than PID controller measurement accuracy.

4.2.3 Proxy-Based Sliding Mode Controller Results

Proxy-Based Sliding Mode Controller has been proposed and applied for the first time for closed loop gyro design applications.

PBSMC is designed with the PID controller and SMC parameters given in Table 4.2 and Table 4.3. Also, PBSMC is implemented according to Figure 3.10 by using the Simulink graphical environment. Code generation feature of Simulink is handy for research and development applications. Therefore, Simulink is used for simulation and code generation studies in this thesis study.

The controller performance parameters and angular rate measurements with PBSMC are presented in the following figures.

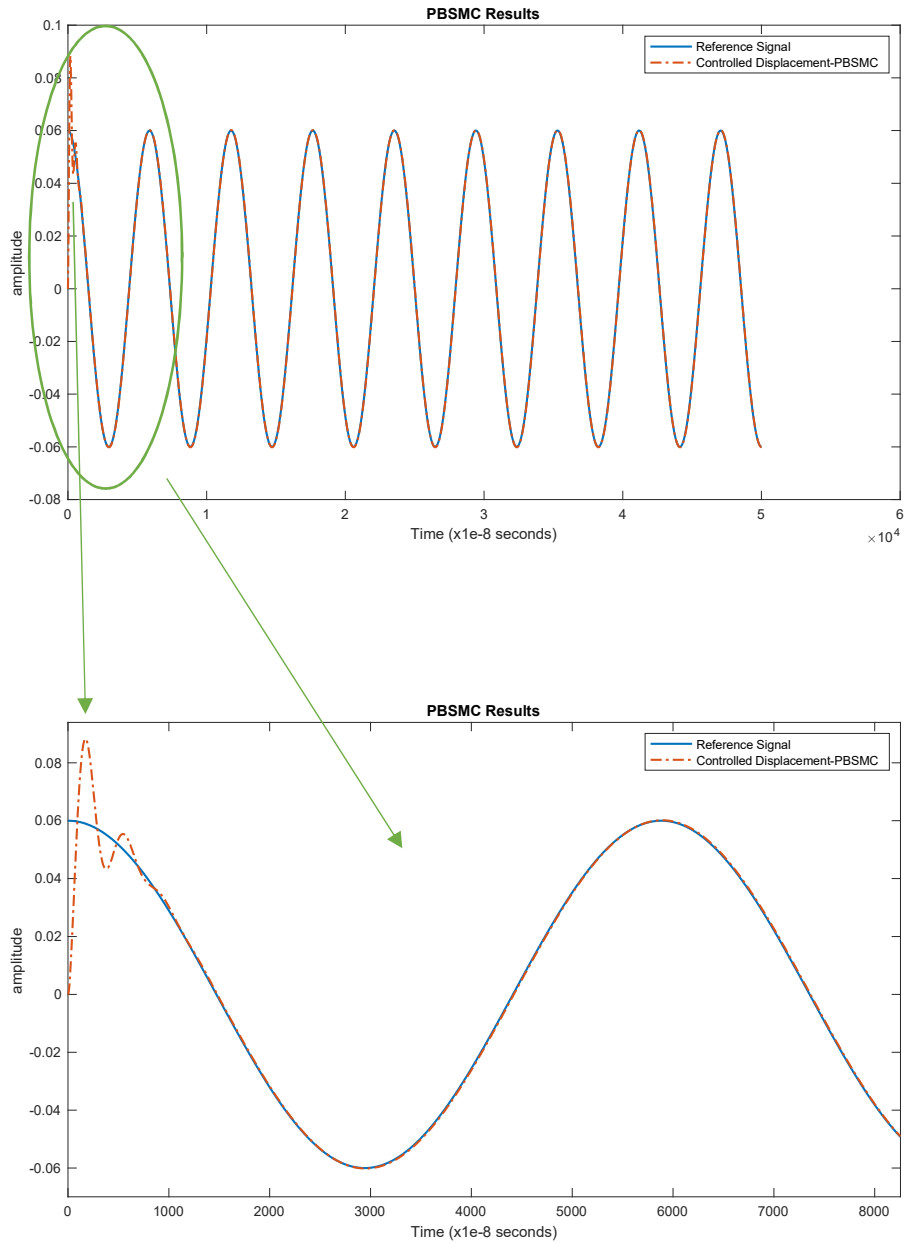


Figure 4.8. PBSMC Tracking Performance for Drive Axis Control

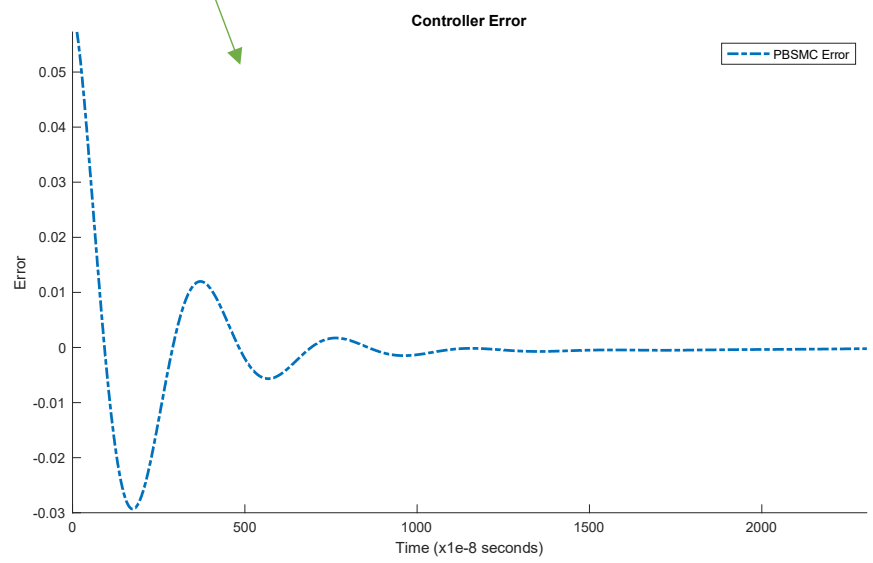
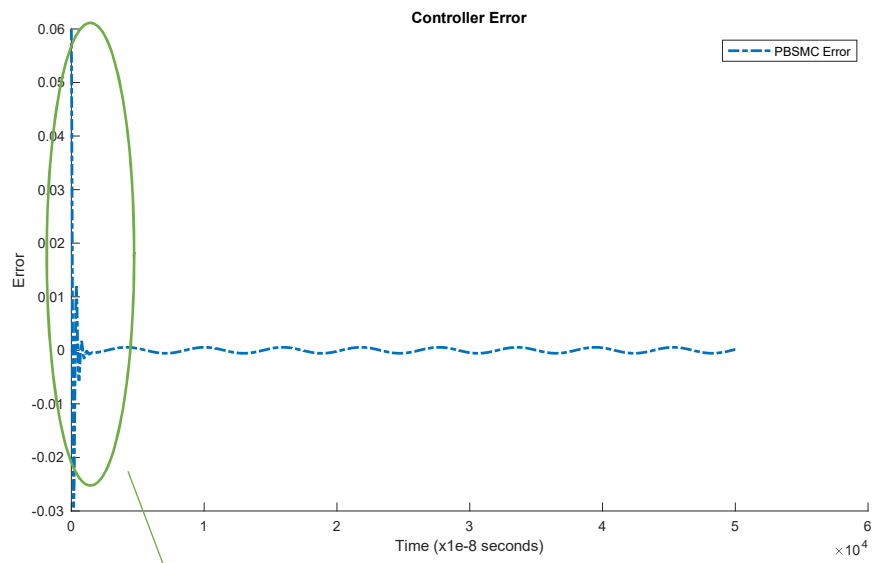


Figure 4.9. PBSMC Tracking Error Performance

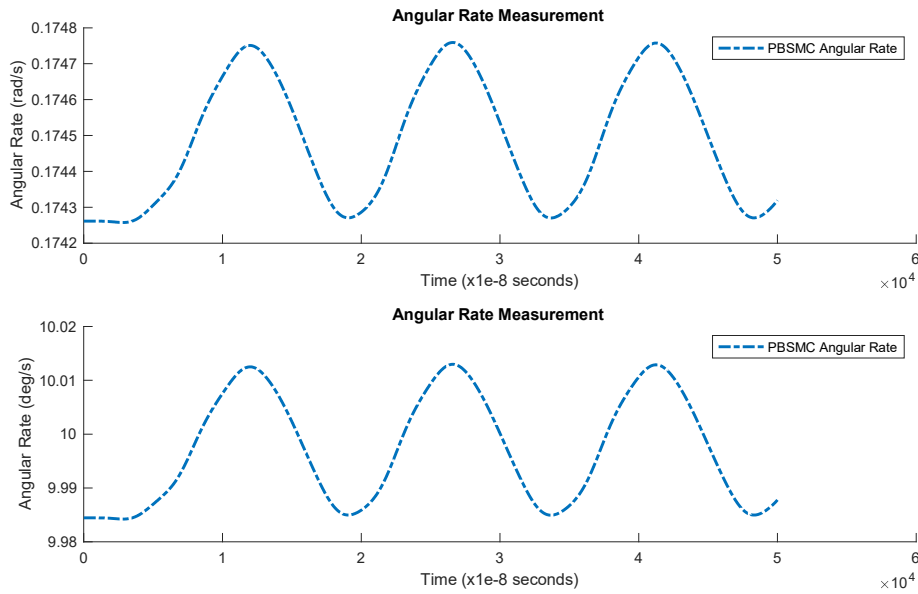


Figure 4.10. Angular Rate Measurement with PBSMC (for 10 deg/s)

Figure 4.8 shows that the proof mass easily tracks the reference vibration signal on the drive axis. On the other hand, unlike PID controller and SMC, the oscillation was observed during the initialization phase. But, the duration and amplitude of the oscillation don't affect the overall sensor performance.

The effect of oscillation in the PBSMC solution can also be observed from the controller error figure. It can be observed from Figure 4.9 that controller error converges to zero after the oscillation.

As a result of the increase in controller performance, an increase in sensor measurement accuracy has also been observed. Maximum sensor error is measured as 53.4687 deg/h.

4.2.4 Weighted Feedforward Controller Results

Weighted Feedforward Controller has been proposed and applied for the first time for closed loop gyro design applications.

W-FF is designed with the PID controller, feedforward controller and weighting coefficients. These parameters are given in Table 4.5. Also, W-FF is implemented according to Figure 3.9 and Eq. (3.38) by using the Simulink graphical environment. And the transfer function of the plant (gyro drive axis) is given in Eq (4.2)

$$G(s) = \frac{1}{ms^2 + d_{xx}s + k_{xx}} \quad (4.2)$$

Table 4.5 W-FF Controller Parameters (PID Controller Parameters and Weighting Coefficients)

Parameter	Value
Ki	5878
Kp	2.0789
Kd	1.6038×10^{-4}
K1	30
K2	0.1

The controller performance parameters and angular rate measurements with W-FF are presented in Figure 4.11, Figure 4.12 and Figure 4.13.

According to the simulation results W-FF provides the best proof mass drive axis tracking performance. Similar to the PBSMC, there is an oscillation in the initialization phase. The duration and amplitude of the oscillation don't affect the overall sensor performance. It just causes delay the convergence time of the system.

The effect of oscillation in the W-FF solution can also be observed from the controller from Figure 4.12. And Figure 4.12 shows that controller error converges to zero after the oscillation.

The angular rate measurement is given in Figure 4.13 and it shows that measurement oscillates around input angular rate 10 deg/s with 46.7289 deg/h maximum error.

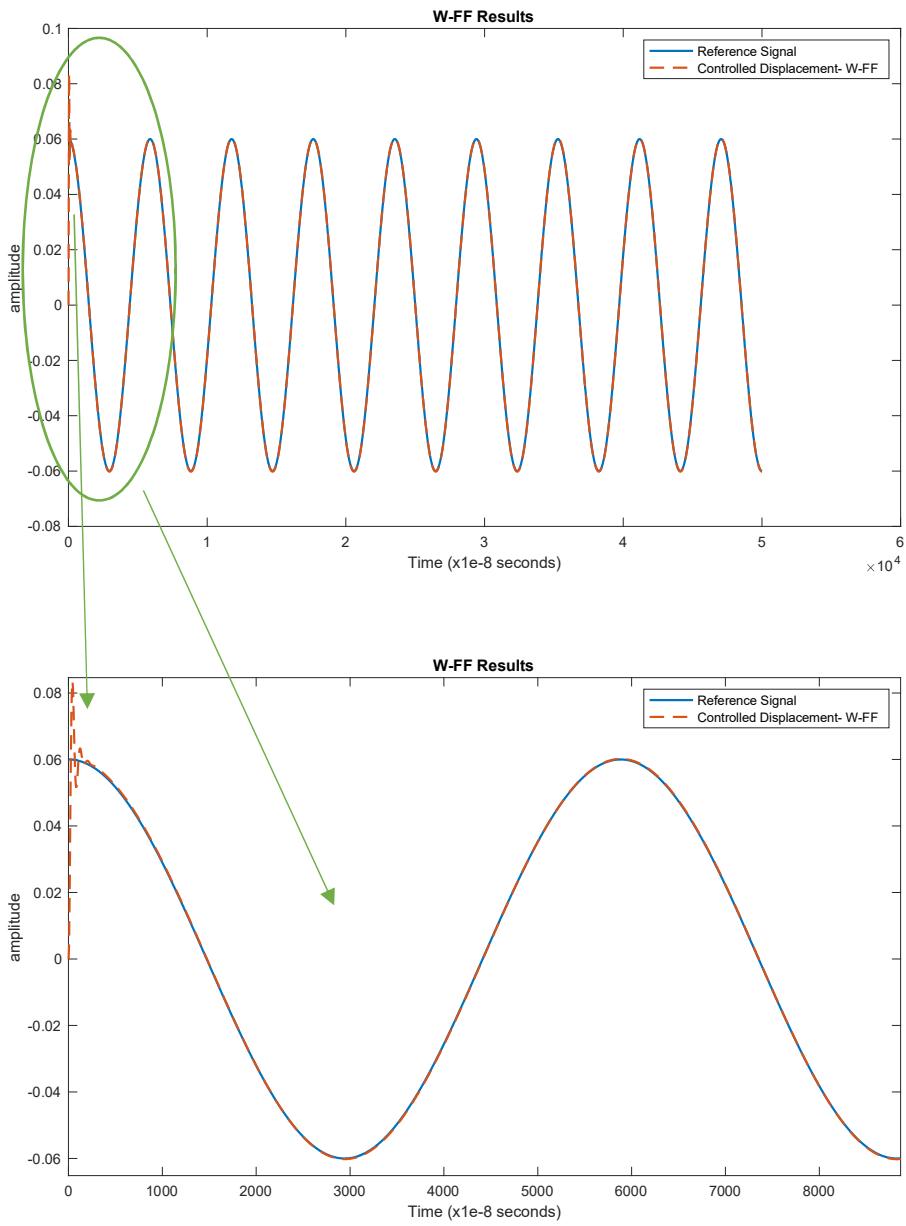


Figure 4.11.W-FF Tracking Performance for Drive Axis Control

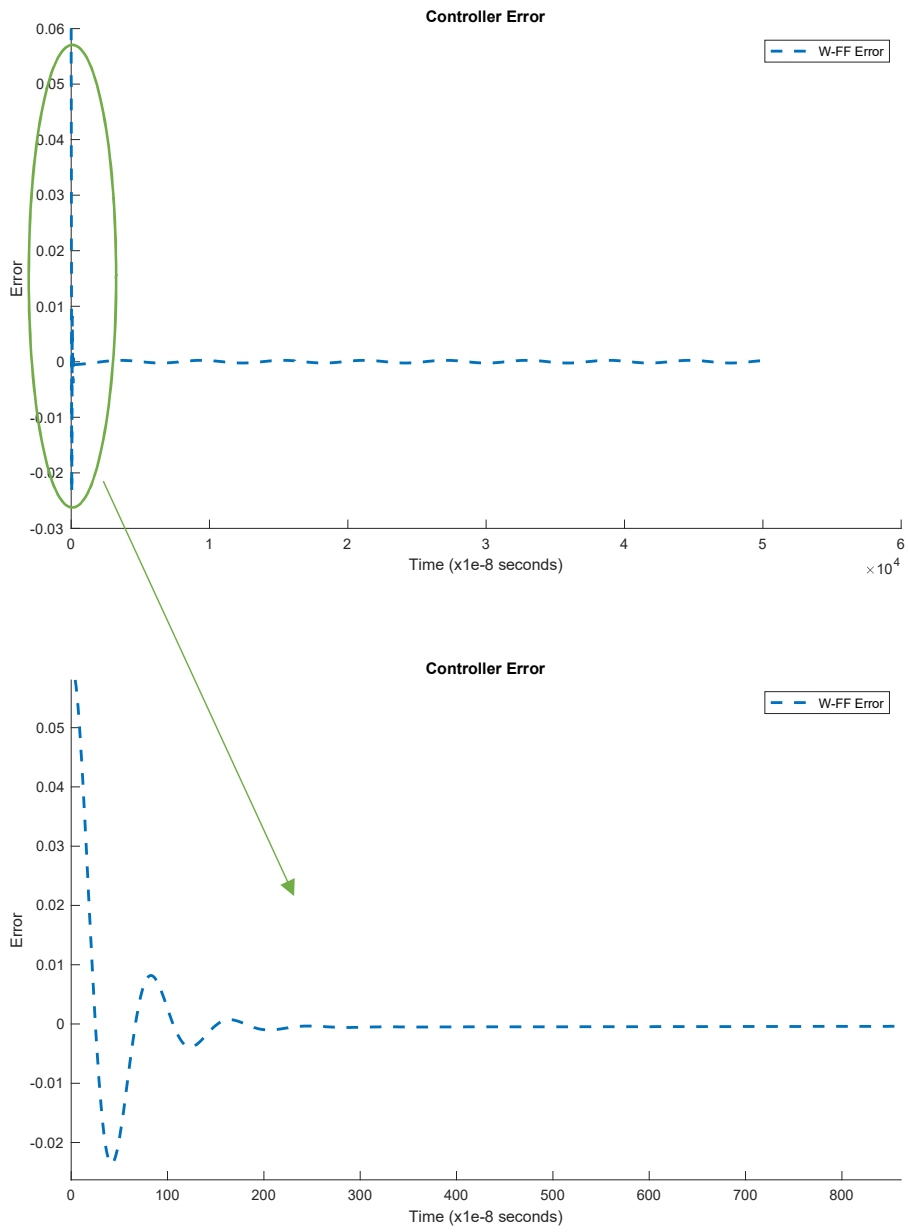


Figure 4.12. W-FF Controller Tracking Error Performance

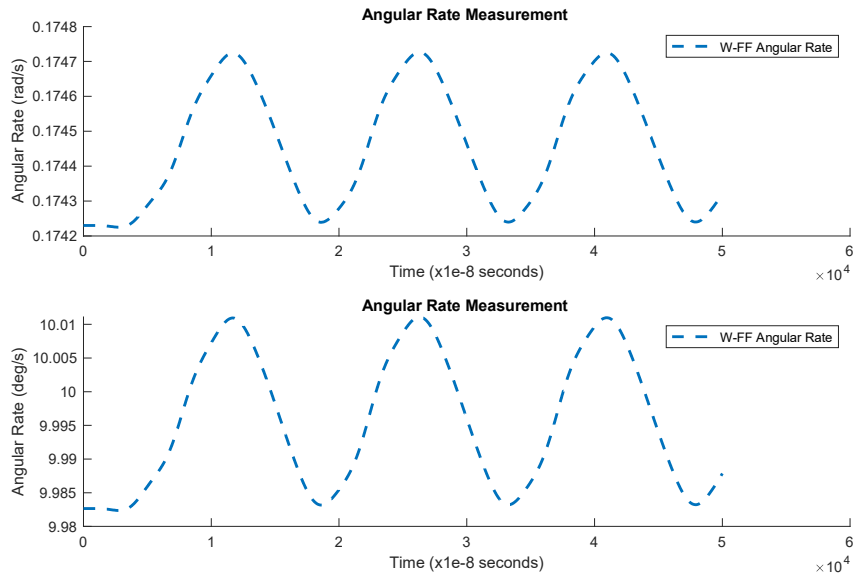


Figure 4.13. Angular Rate Measurement with W-FF (for 10 deg/s)

4.2.5 Simulation Result Comparison of Controller Performances

To better understand the difference between controller performances, the results are compared with each other and presented in Figure 4.14, Figure 4.15, Figure 4.16, Figure 4.17, and Figure 4.18.

When all simulation results are evaluated, W-FF provides the best performance and PBSMC provides the closest results to W-FF. This can be observed both from the Figures 4.14 to 4.17, Table 4.6 and Table 4.7.

Although W-FF results are superior to PBSMC results, this situation will change when distortions and model uncertainties are more significant. Because, simulation studies are carried out under the assumption that the sensor model parameters are known precisely, however, in practical applications, this is not possible.

SMC provided the fastest convergence, although the main drawback of SMC is chattering.

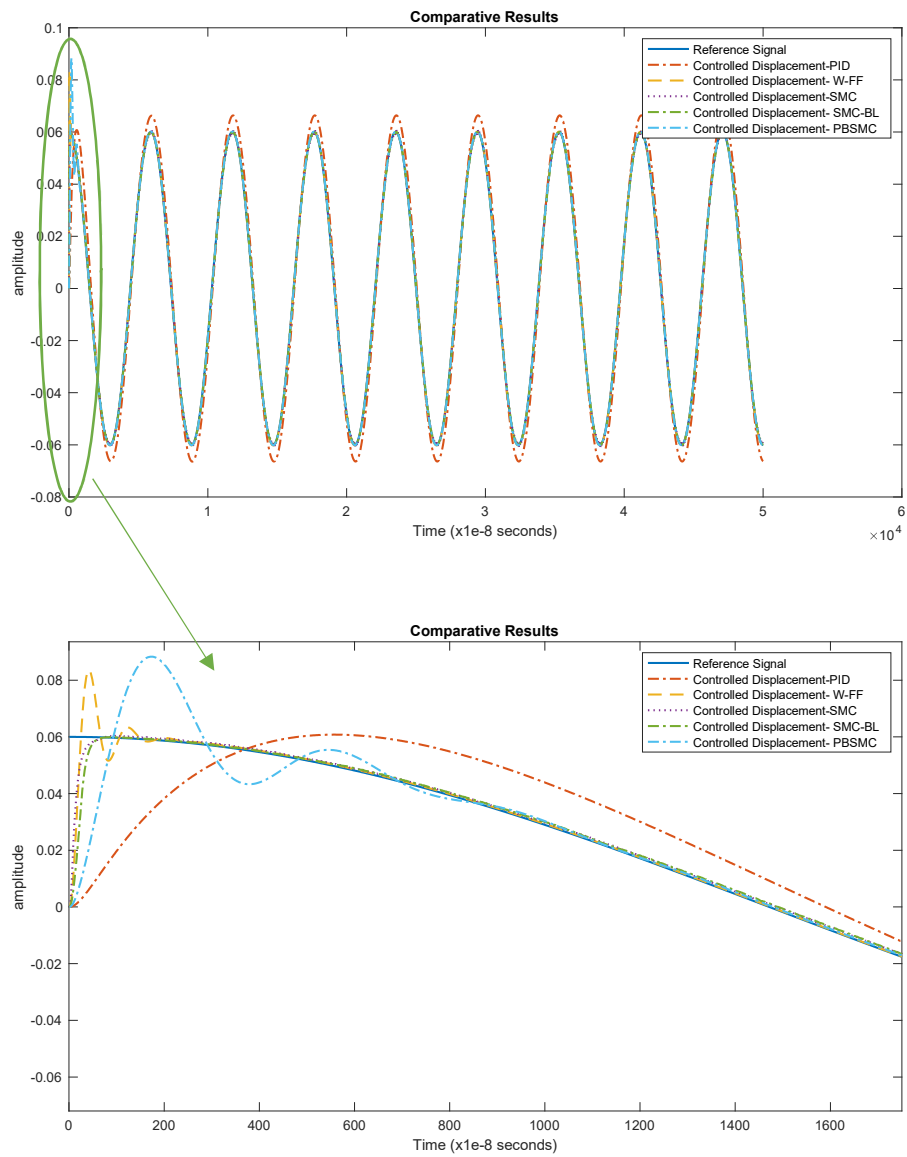


Figure 4.14. Controller Tracking Performance for Drive Axis Control (Initial Phase)

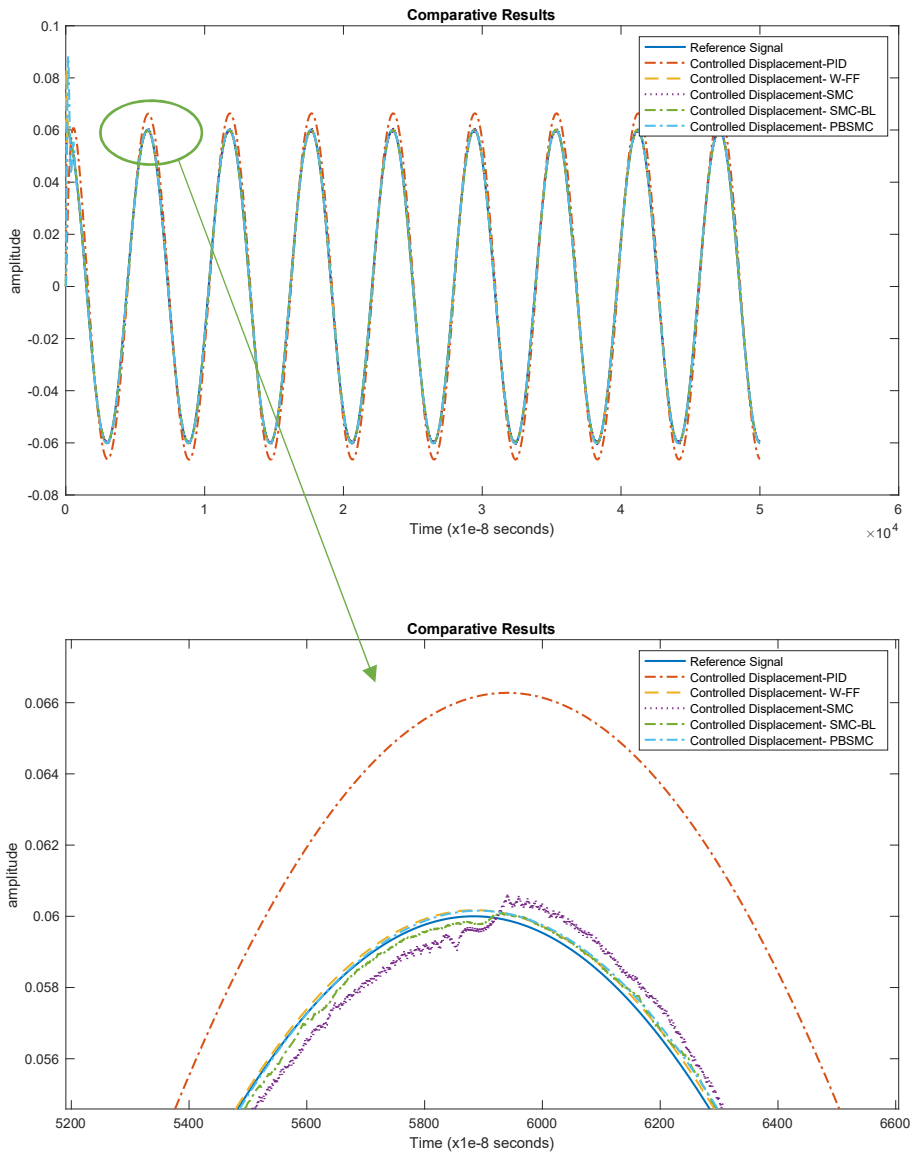


Figure 4.15. Controller Tracking Performance for Drive Axis Control (Steady State Phase)

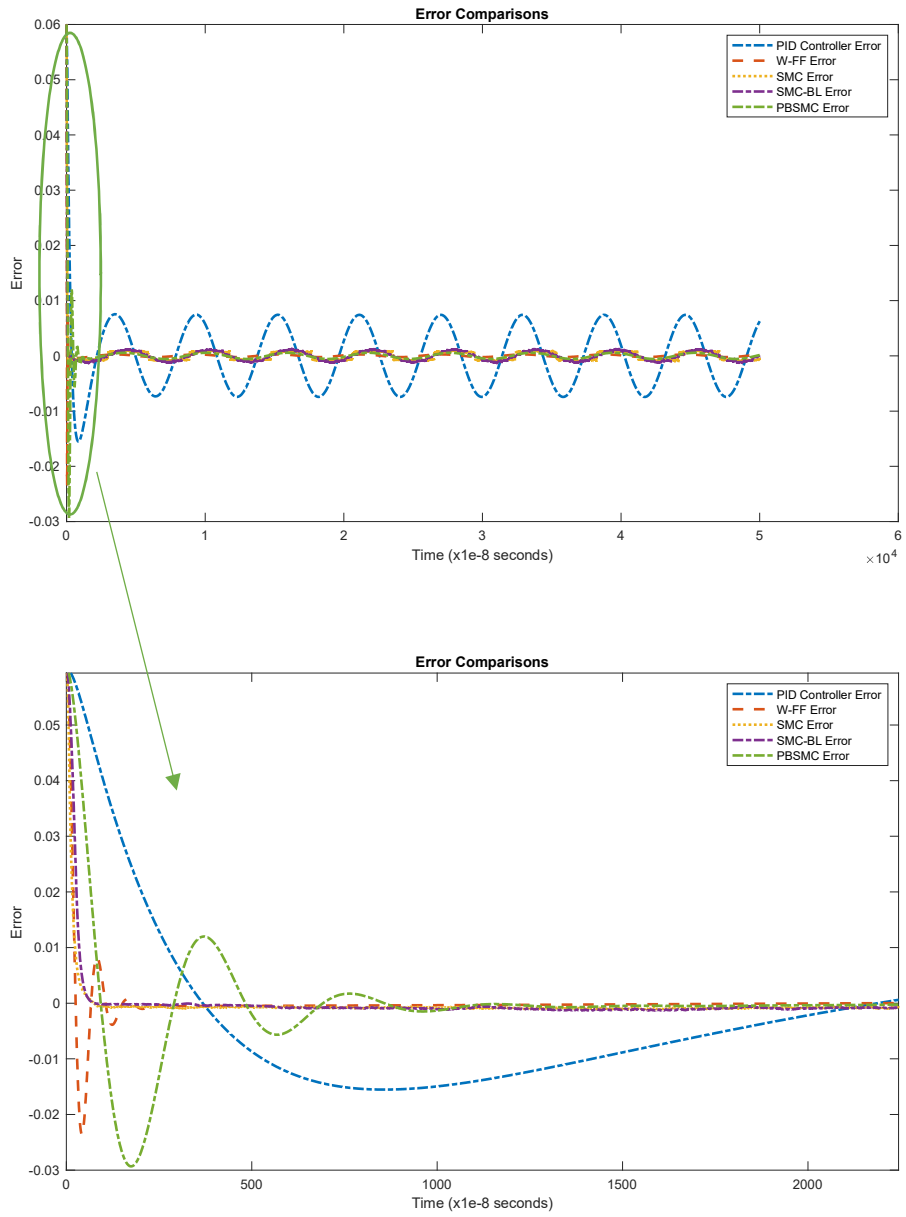


Figure 4.16. Controller Error Comparison (Initial Phase)

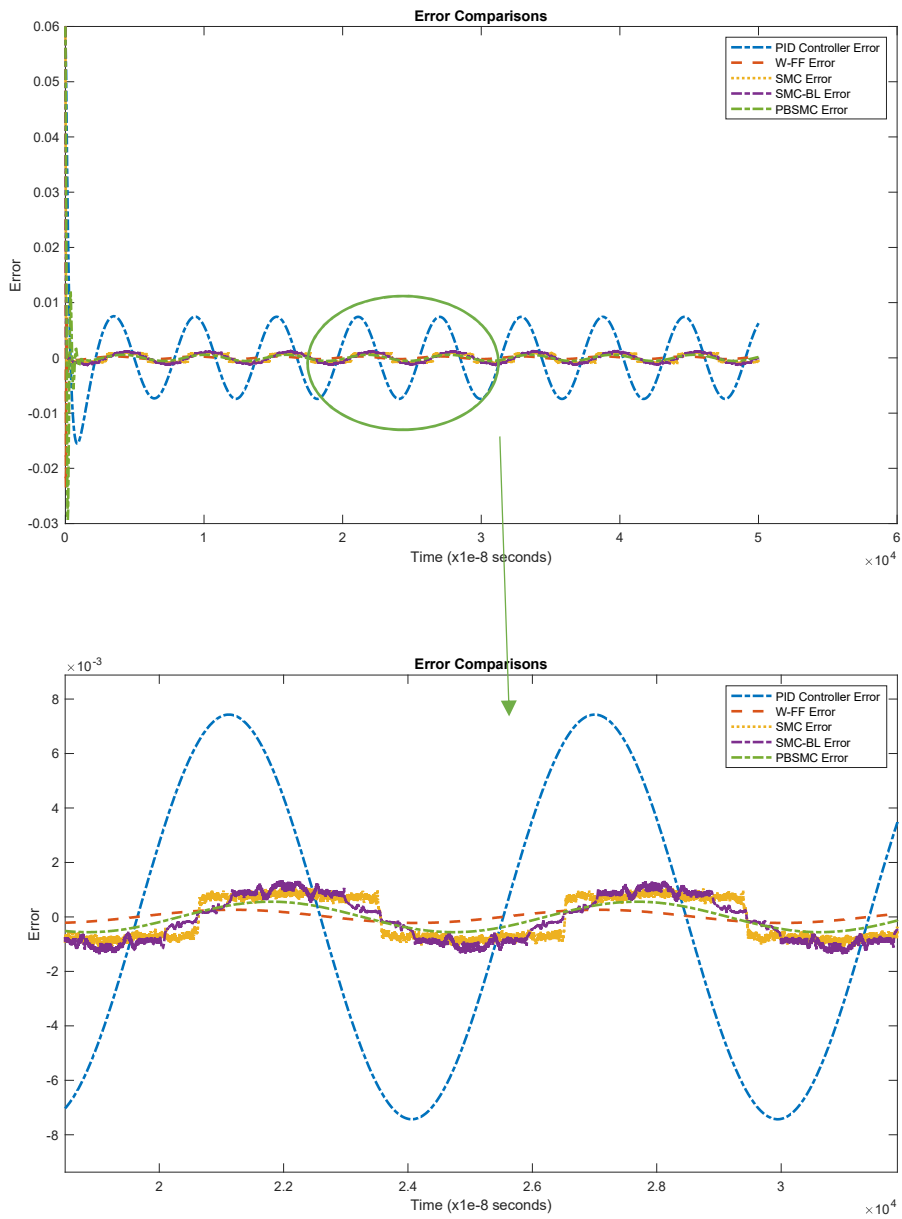


Figure 4.17. Controller Error Comparison (Steady State Phase)

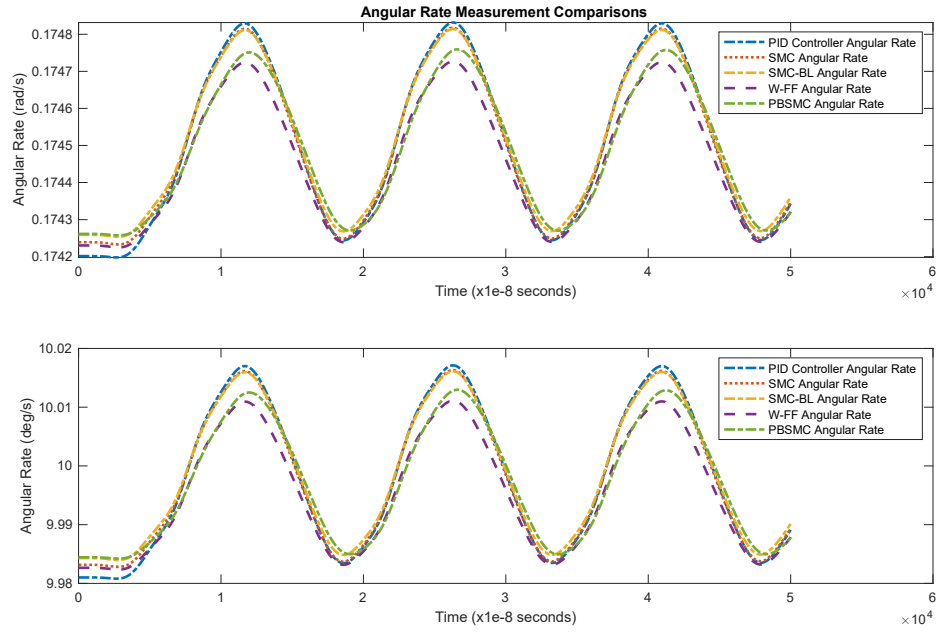


Figure 4.18 Angular Rate Measurement Comparisons (for 10 deg/s)

Table 4.6 also shows superiority of W-FF numerically. As expected, steady state RMS error and tracking delay performance is better than the other controllers. There is an oscillation on the initialization of PBSMC and W-FF. Therefore, RMS error of PBSMC and W-FF are greater than the PID, SMC and SMC-BL. The amplitude of this oscillations can be reduced by adjusting the PID controller coefficients for more sensitive applications. Error convergence times are provided for comparison.

Table 4.6 Error Performance and Convergence Time for Controllers

Parameter	<i>PID</i>	<i>SMC</i>	<i>SMC-BL</i>	<i>PBSMC</i>	<i>W-FF</i>
RMS Error	0.0061	0.0011	0.0013	0.0022	0.0011
Steady State RMS Error	0.0052	7.8583×10^{-4}	7.9064×10^{-4}	3.9427×10^{-4}	1.6983×10^{-4}
Error Convergence Time (s)	376×10^{-8}	93×10^{-8}	82×10^{-8}	870×10^{-8}	289×10^{-8}

Moreover, high convergence time has no negative effect on angular rate data, that is acquired by using output of sense axis. The reason is that group delay of LPF used for demodulation is bigger than any convergence time. The total group delay and start-up time requirement of the sensor is decisive for adjusting the convergence time.

Table 4.7 Angular Rate Measurement Total Error Comparison

Parameter	<i>PID</i>	<i>SMC</i>	<i>SMC-BL</i>	<i>PBSMC</i>	<i>W-FF</i>
Maximum	-68.4166	-65.4812	-64.7974	-53.4687	-46.7289
Error	deg/h	deg/h	deg/h	deg/h	deg/h

4.3 Experimental Results

In this section, experimental test setup and tests which are performed to verify simulation results and controller performances are summarized. The parameters of the prototype used in the experiment are the same as the simulated gyro parameters.

4.3.1 Experimental Setup

The experimental setup is presented in Figure 4.19 For the test setup, the MEMS prototype is driven by the circuit running on the drive axis. A single axis rate table is used to generate input angular rate. Properties of the rate table are listed in Table 4.8.

Table 4.8 Rate Table Properties

Parameter	<i>Value</i>
Angular Position Inspection	0.001
Resolution	
Rate Accuracy	10^{-5} (360° average)
Rate Range	0.0001-150 deg/s

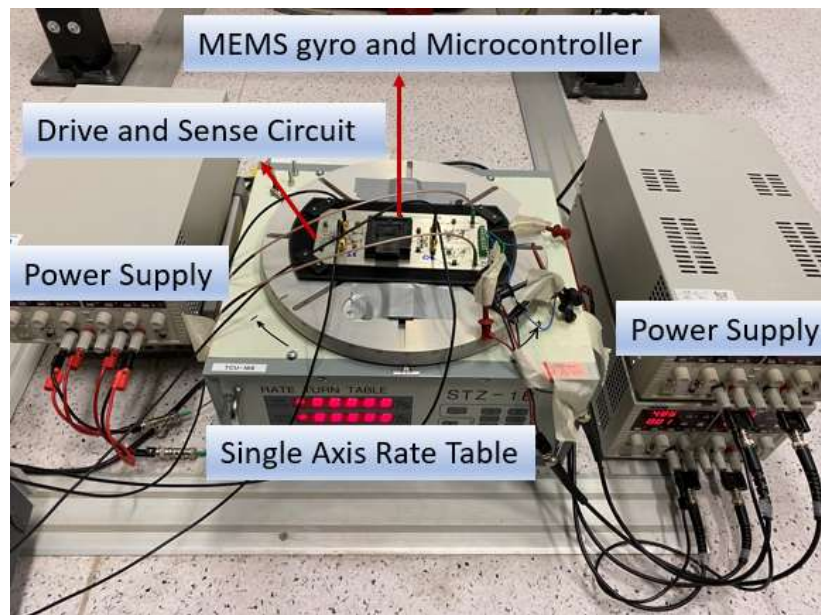


Figure 4.19. Experimental Setup

Developed controllers are programmed over a low-cost microcontroller. Angular rate measurements are gathered by demodulation of the data on the sense axis.

For the tests, the Agilent MSO9254A Mixed Signal Oscilloscope (Analog Signals are sampled with 500 Mhz on oscilloscope probe and stored in the oscilloscope memory) is used with a 50 MHz sampling rate to log the required data.

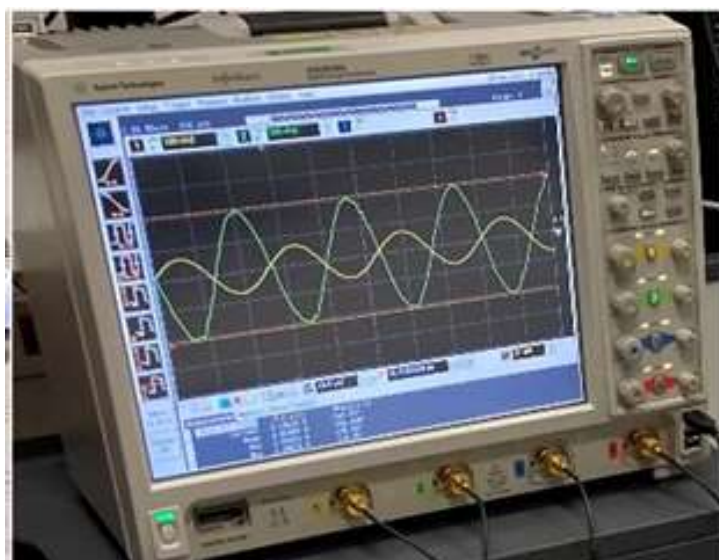


Figure 4.20. Experimental Setup -Data Monitoring and Logging

Tests are implemented at 0.1745 rad/s (10 deg/s) and 0.3490 rad/s (20 deg/s) to understand the angular rate error performance under different angular rates. Details about 0.3490 rad/s (20 deg/s) rate test is provided in Chapter 5 Sensitivity Analysis.

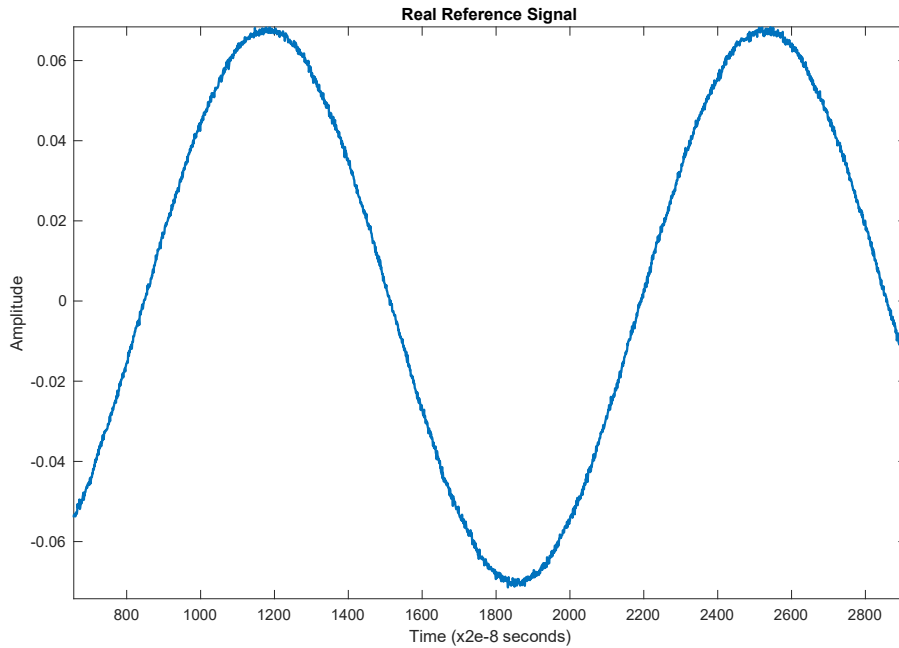


Figure 4.21. Reference Vibration Signal in Real Application

Reference vibration signal, which is generated by electronics on the drive circuit, contains noisy components. This noise can come from electronic noises from components, pathways, switching components, etc. The first observation about the experimental studies can be stated that real applications can not use the ideal reference vibration signal. Therefore, the effect of the noisy reference signal is expected to be eliminated by the controller. Additionally, tests are performed under an uncontrolled temperature environment. Due to their structure, MEMS devices are highly affected by temperature changes. Again, this effect is expected to be reduced by the controller.

4.3.2 PID Controller Results

Since the PID controller is not robust enough, PID solution is affected by noise and the tracking performance is reduced. It can be observed from Figure 4.22, Figure 4.23 and Figure 4.24.

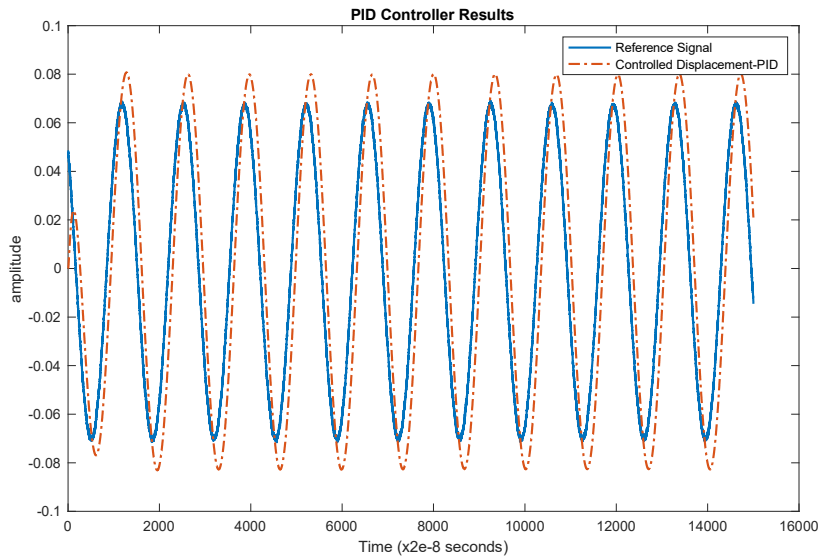


Figure 4.22. PID Tracking Performance for Drive Axis Control-Experimental Data

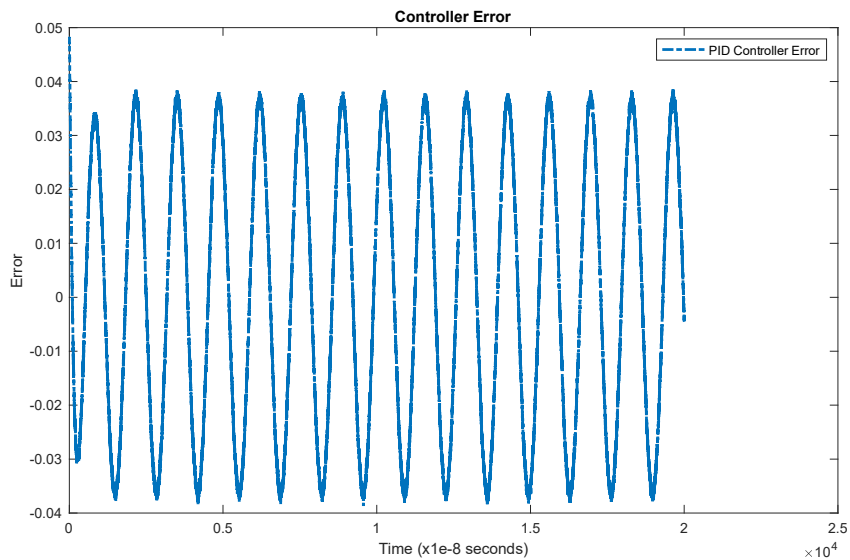


Figure 4.23. PID Controller Tracking Error Performance -Experimental Data

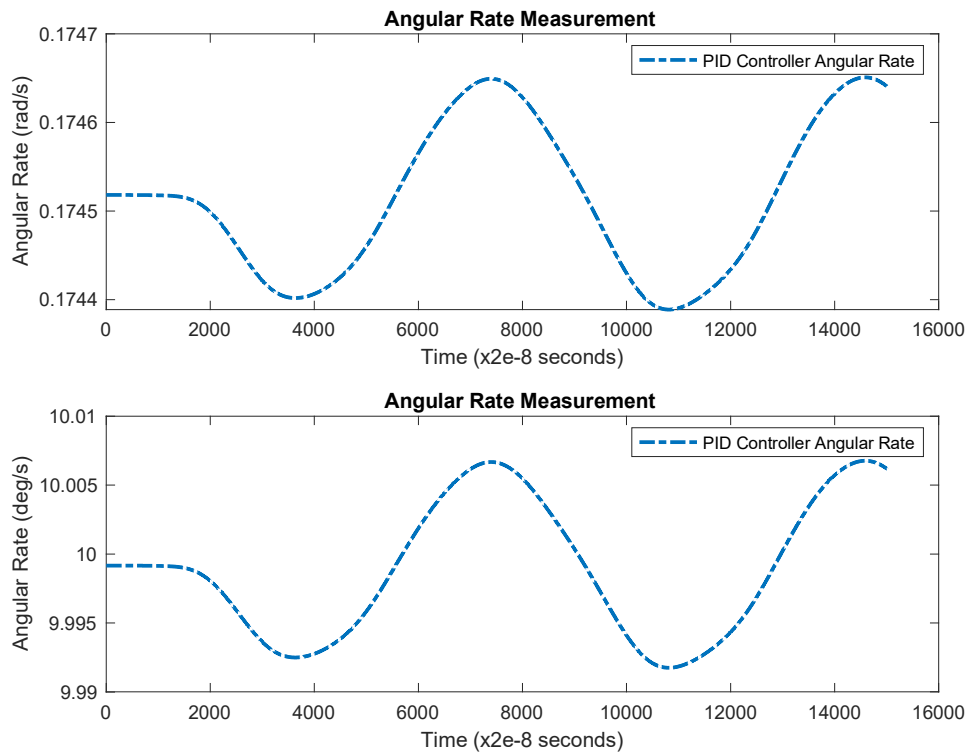


Figure 4.24. Angular Rate Measurement with PID - Experimental Data (for 10 deg/s)

In the experimental studies, a decrease in the reference signal tracking performance of the PID solution is observed. However, convergence was not observed in the controller error and it was determined that the oscillation amplitude in the error also increased. Under these conditions, PID is not suitable for such an application.

4.3.3 Sliding Mode Controller and Sliding Mode Controller with Boundary Layer Results

The results of the experimental tests with SMC are given in Figure 4.25, Figure 4.26 and Figure 4.27. Both SMC and SMC-BL solutions track the reference vibration signal successfully. However, it is determined that the error levels of both controllers are above the simulation data. The errors converge, but their amplitudes increase. The angular rate measurement oscillates around the input angular rate, similar to the

simulation. Error measurements for tracking and angular rate measurements are summarized in Table 4.8 and Table 4.9.

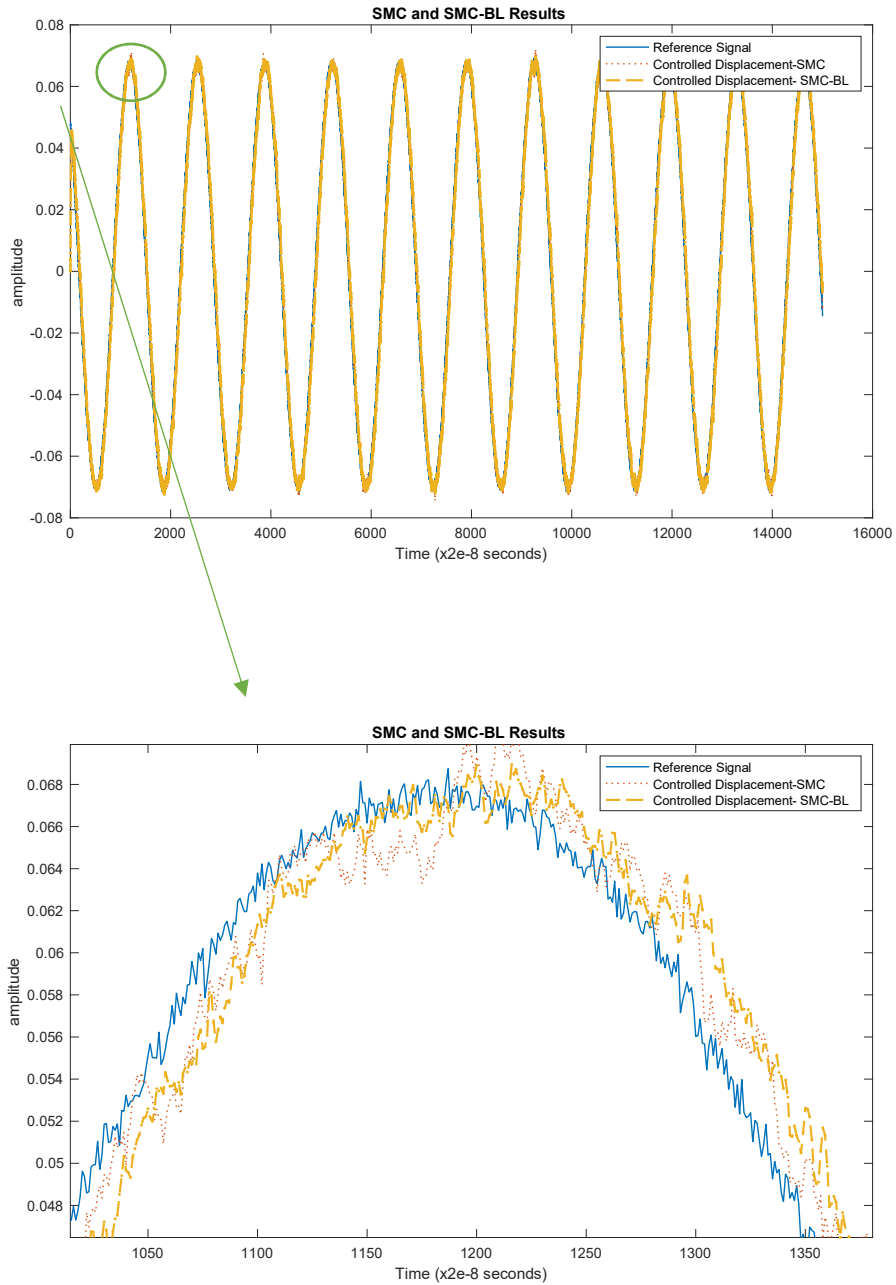


Figure 4.25. SMC and SMC-BL Tracking Performance for Drive Axis Control- Experimental Data

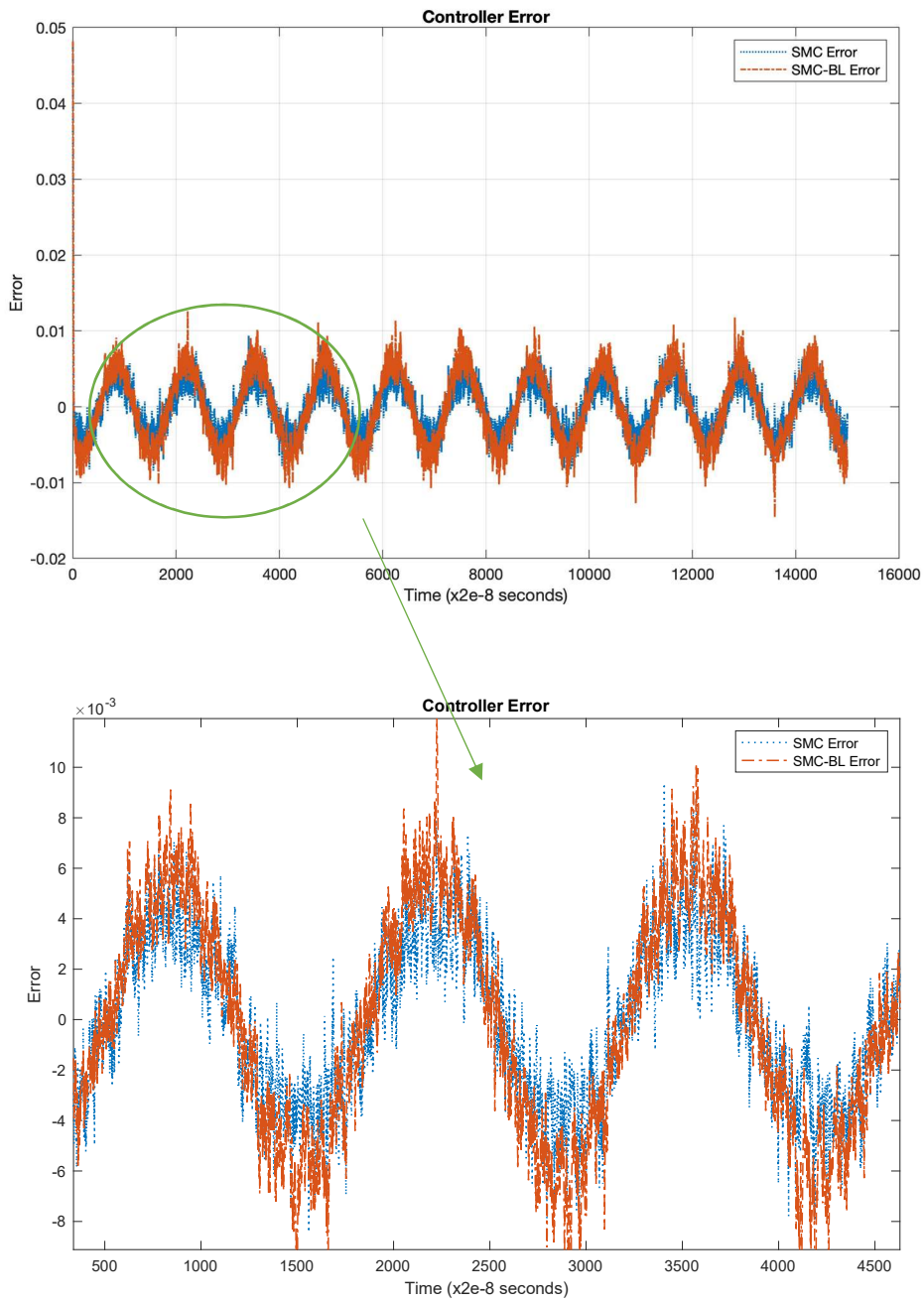


Figure 4.26. SMC and SMC-BL Controller Tracking Error Performance - Experimental Data

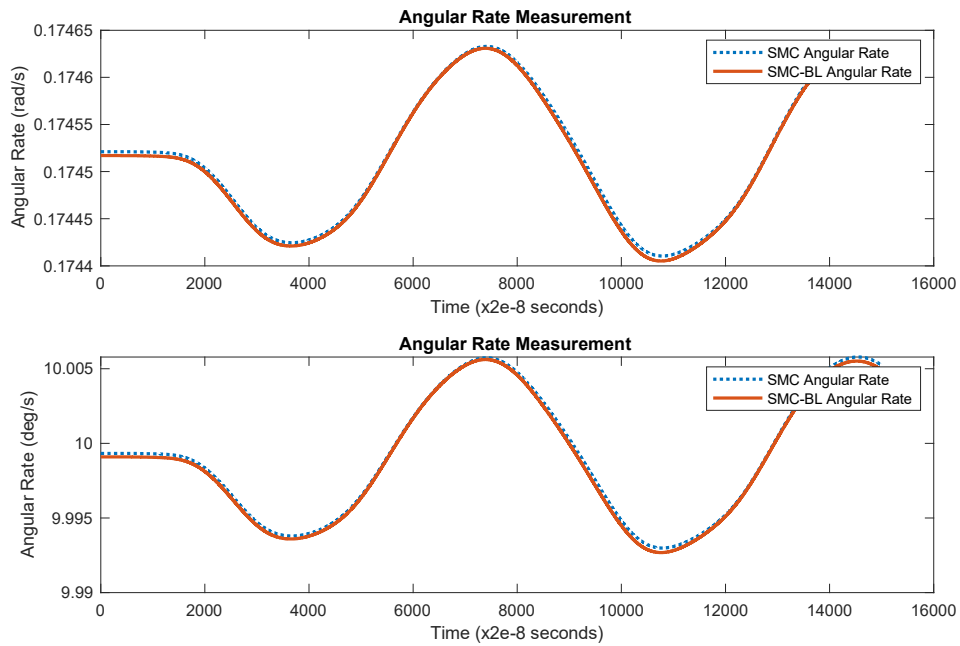


Figure 4.27. Angular Rate Measurement with SMC and SMC-BL - Experimental Data (for 10 deg/s)

4.3.4 Proxy-Based Sliding Mode Controller Results

The results of the experimental tests with PBSMC are given in Figure 4.28, Figure 4.29 and Figure 4.30. PBSMC tracks the reference vibration signal successfully. However, it is observed that the error level is above the simulation data. Because of the noisy reference vibration signal, the error signal becomes noisy. On the other hand, the controller error converges. The angular rate measurement oscillates around the input angular rate, similar to the simulation. Error measurements for tracking and angular rate measurements are summarized in Table 4.8 and Table 4.9.

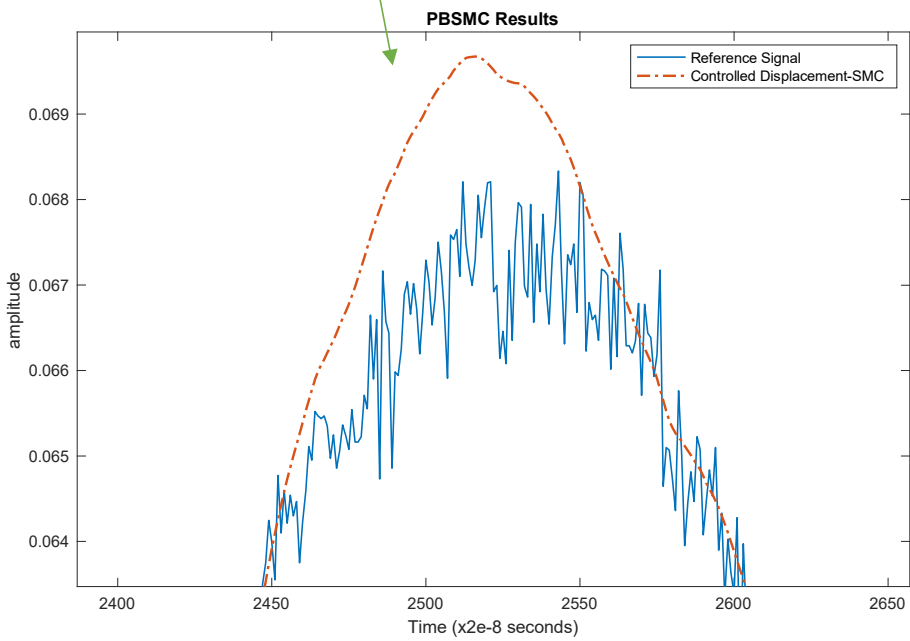
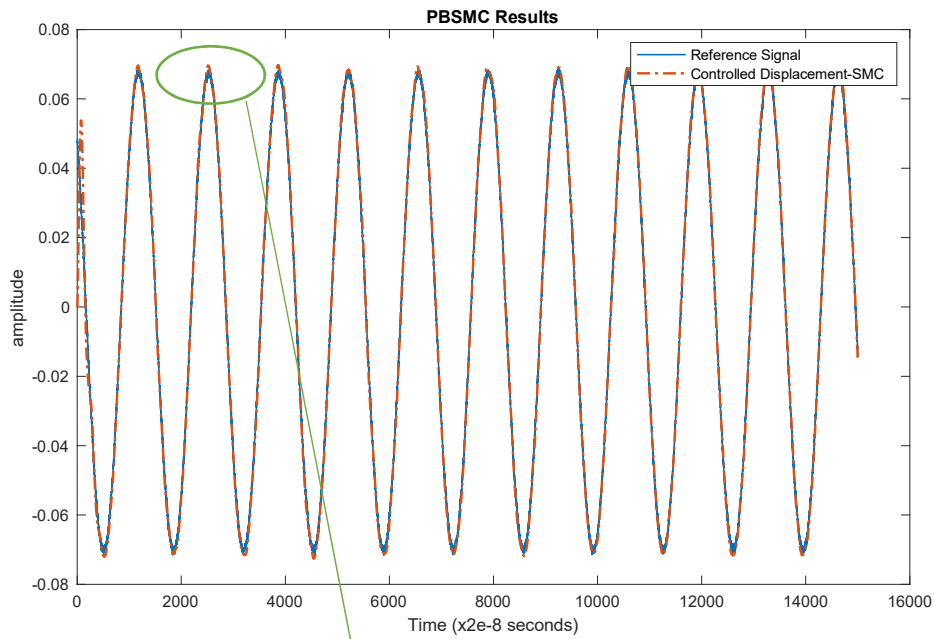


Figure 4.28. PBSMC Tracking Performance for Drive Axis Control-Experimental Data

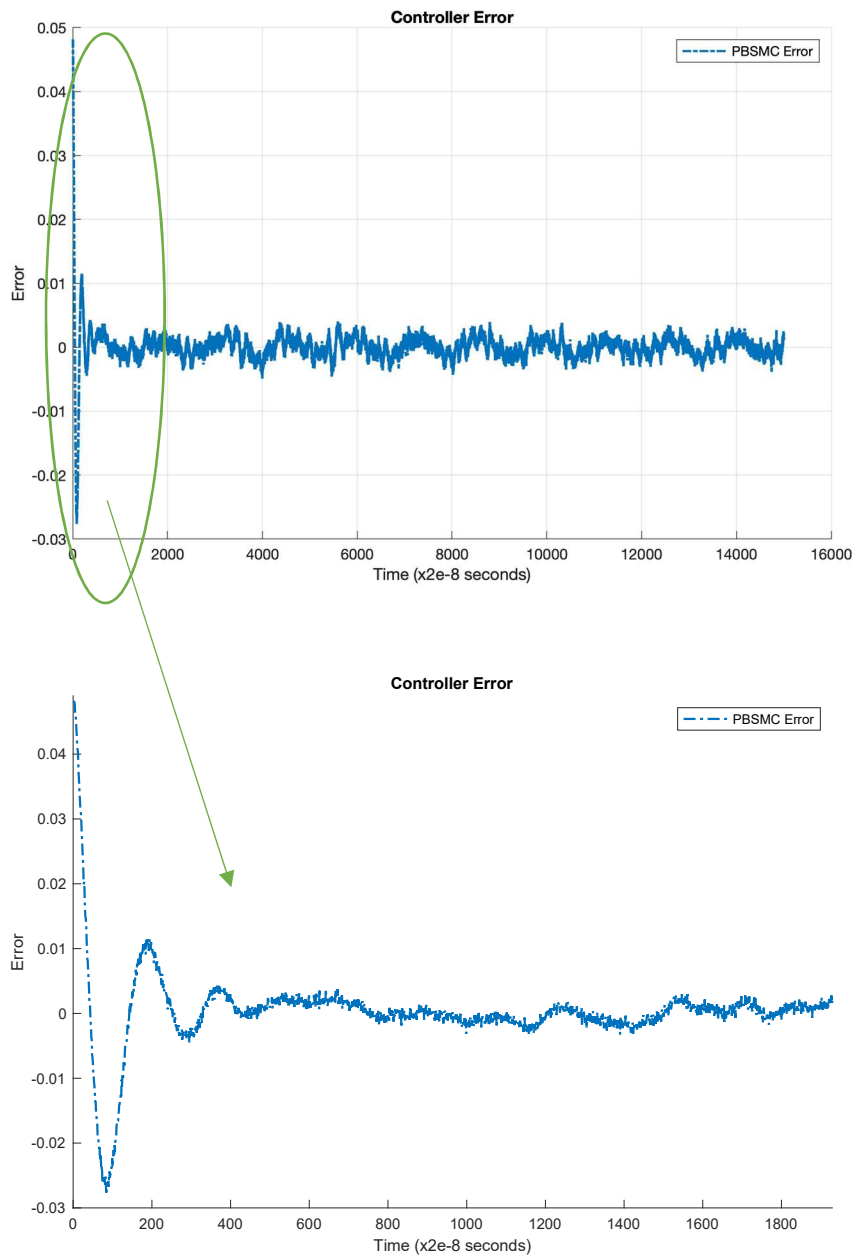


Figure 4.29. PBSMC Tracking Performance for Drive Axis Control-Experimental Data

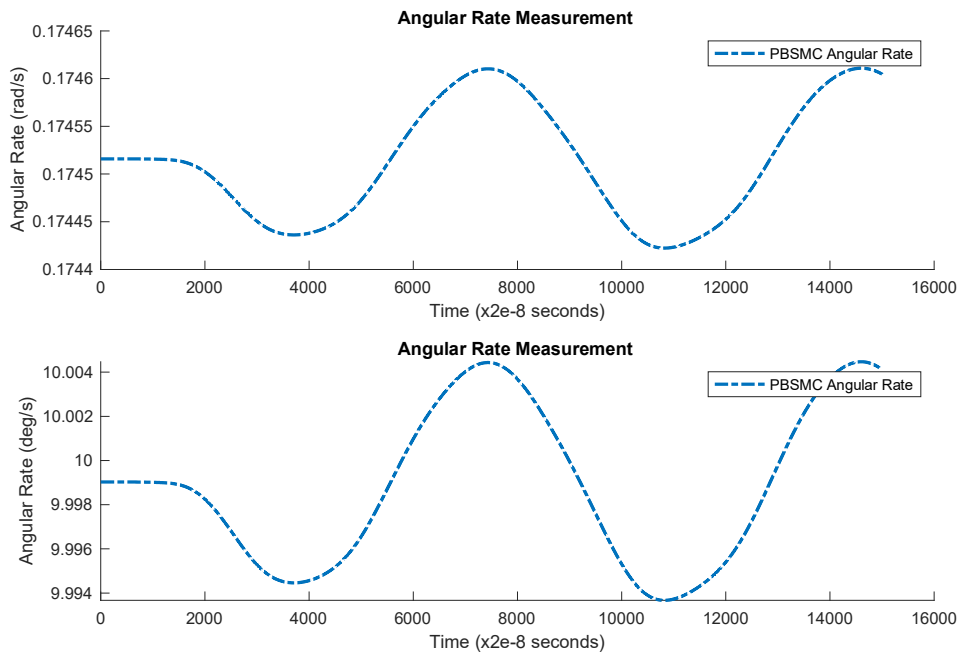


Figure 4.30. Angular Rate Measurement with PBSMC - Experimental Data (for 10 deg/s)

4.3.5 Weighted Feedforward Controller Results

The results of the experimental tests with W-FF are given in Figure 4.31, Figure 4.32 and Figure 4.33. W-FF tracks the reference vibration signal successfully. Similar to the other controllers - the error level is above the simulation data. Additionally, the controller error converges. The angular rate measurement oscillates around the input angular rate, similar to the simulation. Error measurements for tracking and angular rate measurements are summarized in Table 4.6 and Table 4.7.

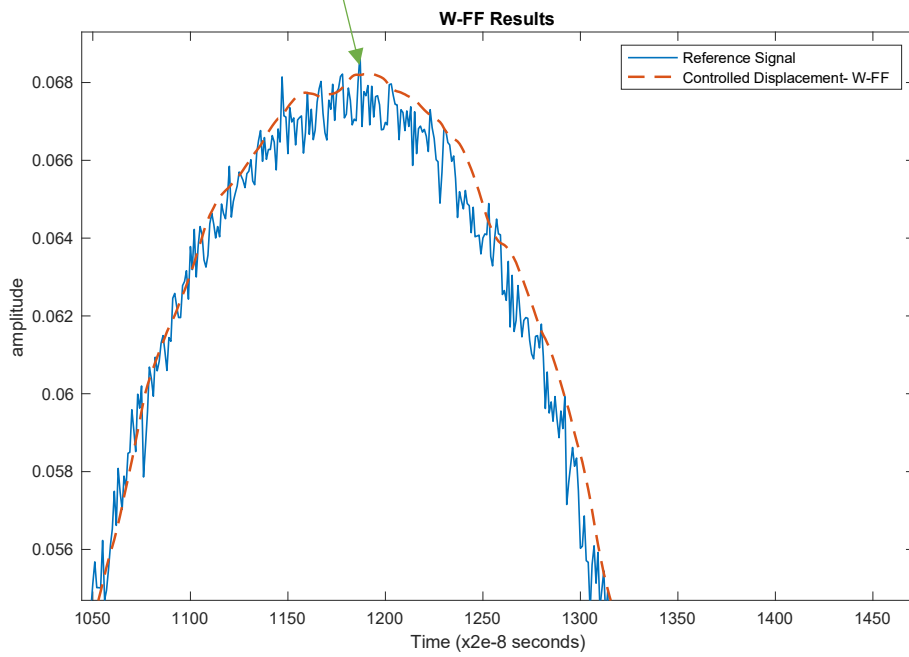
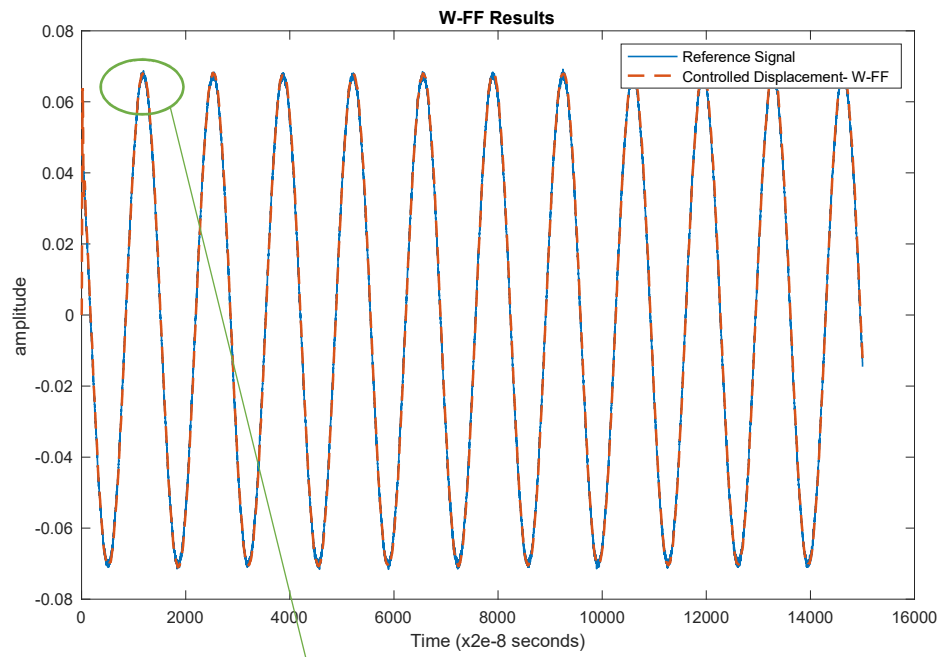


Figure 4.31. W-FF Tracking Performance for Drive Axis Control-Experimental Data

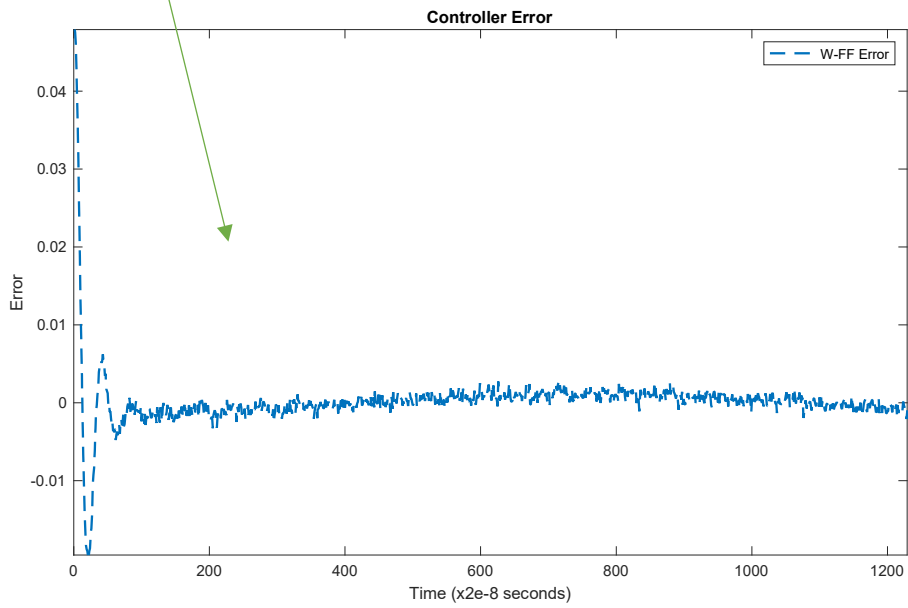
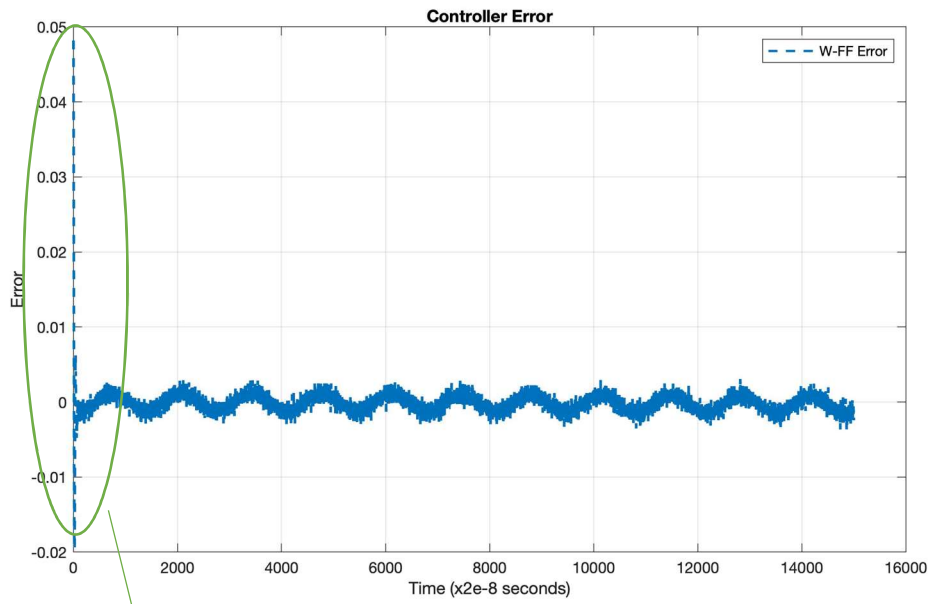


Figure 4.32.W-FF Controller Tracking Error Performance -Experimental Data

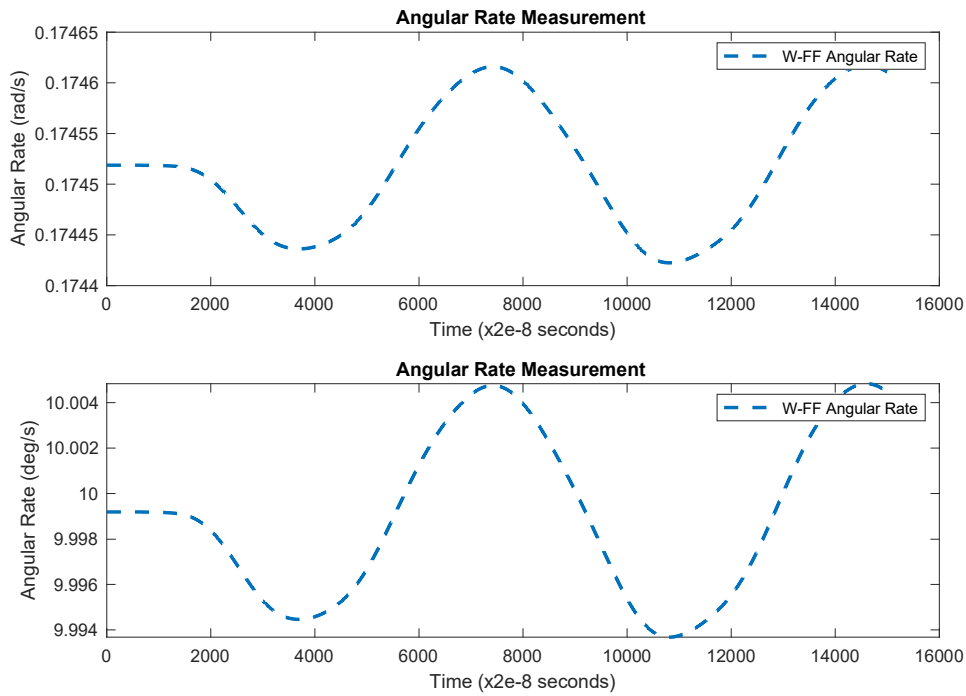


Figure 4.33. Angular Rate Measurement with W-FF - Experimental Data (for 10 deg/s)

4.3.6 Experimental Result Comparison of Controller Performances

To show the difference between controller performances, comparative results are presented in Figure 4.34, Figure 4.35, Figure 4.36, Figure 4.37, and Figure 4.38.

When all simulation results are evaluated, W-FF provides the best performance. And PBSMC provides the closest results to W-FF. This can be observed both from the figures and Table 4.8 and Table 4.9.

The decrease in the performance of the PID controller is better understood with Figure 4.34. Additionally, there are degradations in the performance of SMC, SMC-BL, PBSMC and W-FF but the amount degradation is negligible when compared with PID performance. This proves the robustness of the other methods.

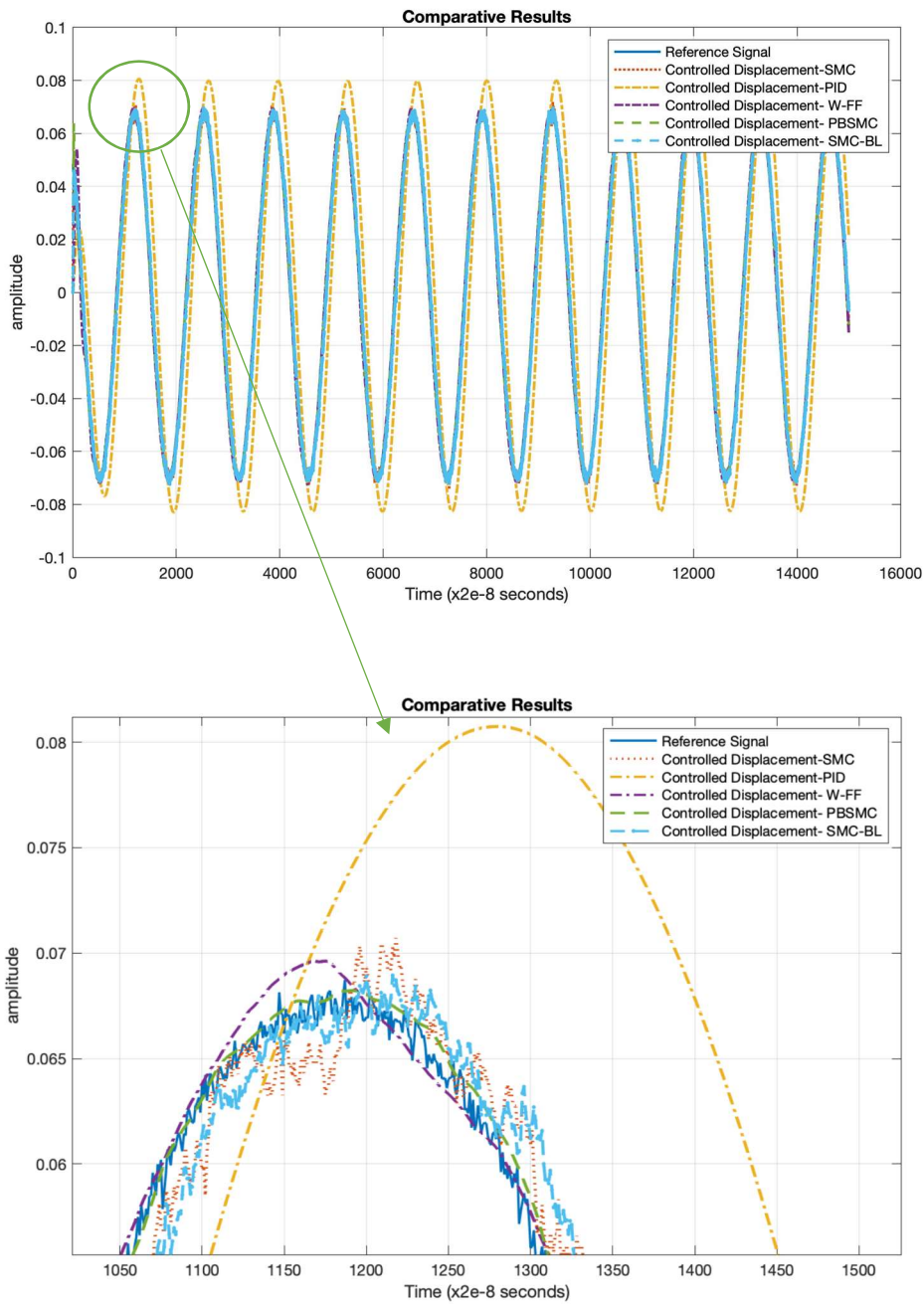


Figure 4.34. Controller Tracking Performance for Drive Axis Control – Experimental Data

Figure 4.34 shows that PBSMC performs better than the other control methods. W-FF performance is very close to PBSMC. The chattering effect on the SMC solution

is clearly observable. On the other hand, the overall performance of the PID controller has not been satisfactory.

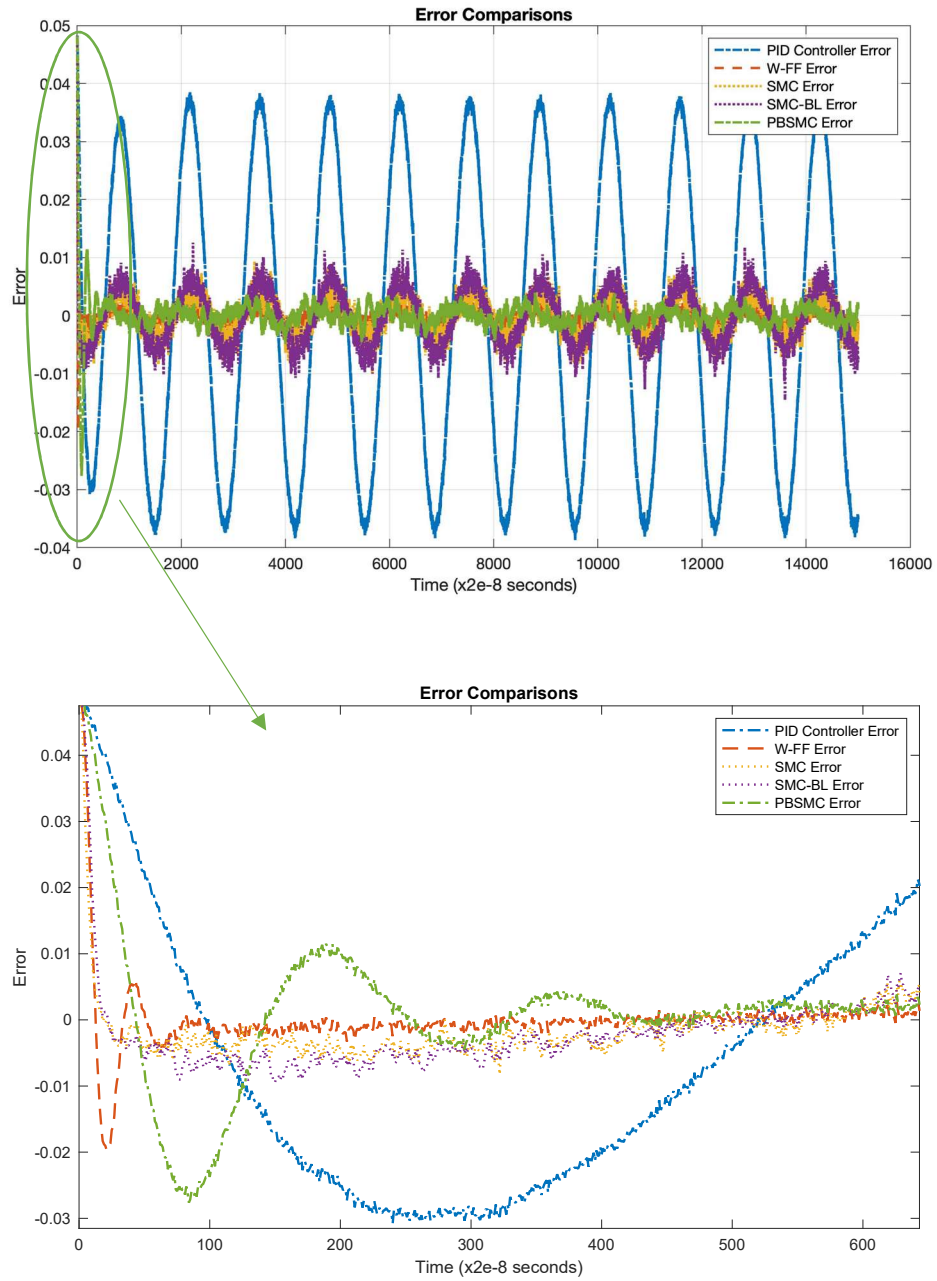


Figure 4.35. Controller Error Comparison (Initial Phase) – Experimental Data

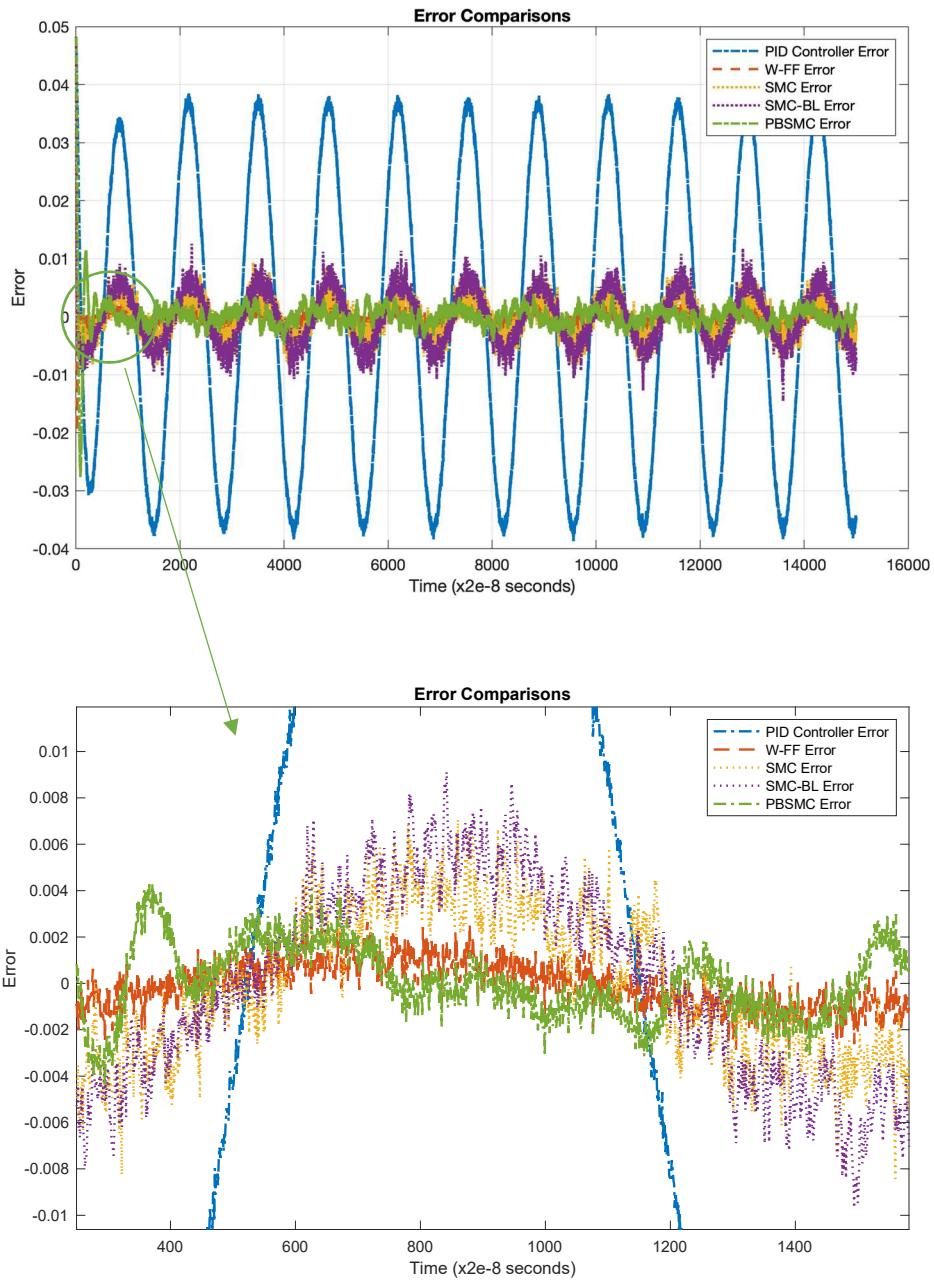


Figure 4.36. Controller Error Comparison (Steady State Phase) – Experimental Data

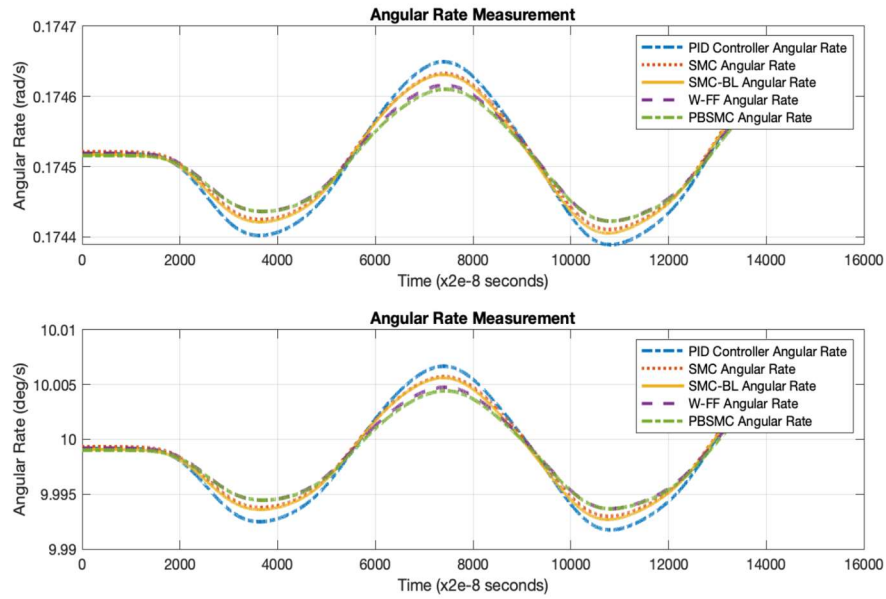


Figure 4.37 Angular Rate Measurement Comparison-Experimental Data

Applications held with experimental data show that PBSMC has the best performance. PID performance shows worse performance than the simulation. This is because of the fact that the input signal is noisier than the simulation data. Moreover, the parameters which cause uncertainty in the system are more effective in the experiment than the simulations.

Table 4.9 Error Performance and Convergence Time for Controllers

Parameter	<i>PID</i>	<i>SMC</i>	<i>SMC-BL</i>	<i>PBSMC</i>	<i>W-FF</i>
RMS Error	0.0257	0.0033	0.0046	0.0024	0.0022
Steady State RMS Error	0.0258	0.0033	0.0045	0.0014	0.0017
Error Convergence Time (s)	NA	38×10^{-8}	112×10^{-8}	593×10^{-8}	125×10^{-8}

Table 4.10 Angular Rate Measurement Total Error Comparison

Parameter	<i>PID</i>	<i>SMC</i>	<i>SMC-BL</i>	<i>PBSMC</i>	<i>W-FF</i>
Maximum Error	-31.1341	-27.5947	-26.9839	-22.8719	-24.1894
	deg/h	deg/h	deg/h	deg/h	deg/h

In conclusion, PID performance is worse than the simulation in the experiment: however, SMC, SMC-BL, PBSMC and W-FF performances are close to the simulations.

Moreover, because of the LPF applied to the demodulated data, the effect of the noise on the angular rate is not seen in the experimental angular rate data.

The experiment results show that the differences can be observed between simulation results and real applications. While W-FF method gives the best results in the simulation environment, PBSMC method gives the best results in experimental data.

Experimental PBSMC and W-FF initial oscillation data for the controlled displacement is slightly different from the simulation. There are no initial oscillations on the controlled displacement signals.

When angular rate measurement is investigated, PBSMC overrides other control methods for angular rate measurement, which oscillates at the approximately applied 10 deg/s rate.

CHAPTER 5

SENSIVITY ANALYSIS

In order to observe the characteristics and robustness of the controllers, sensitivity analysis are performed and the results are presented in this chapter. As mentioned in the previous chapters, noise represents the uncertainties in the system. Therefore, simulation studies are repeated for different noise values to observe the variations on the controller performances. Additionally, performance, noise and chattering characteristics of sliding mode controller is observed by changing the sliding mode controller parameters (Q, λ, ϕ). After that, experimental results which are performed under different input rates to compare the angular rate error performances are summarized.

5.1 Error Performance Comparison for Different Noise Levels

The robustness performance of controllers are simulated by changing the power of the noise. Tracking performance of the PID is drastically decreased by increased noise, whereas both controller error and angular rate measurement error increase. SMC performance is not affected by noise power change. When all of the control methods are compared, PBSMC tracking performance overrides all other methods which is shown in Table 5.1. Performance degradation of the PID controller and the behaviors of other controllers under different noise levels are shown in Figure 5.1, Figure 5.2

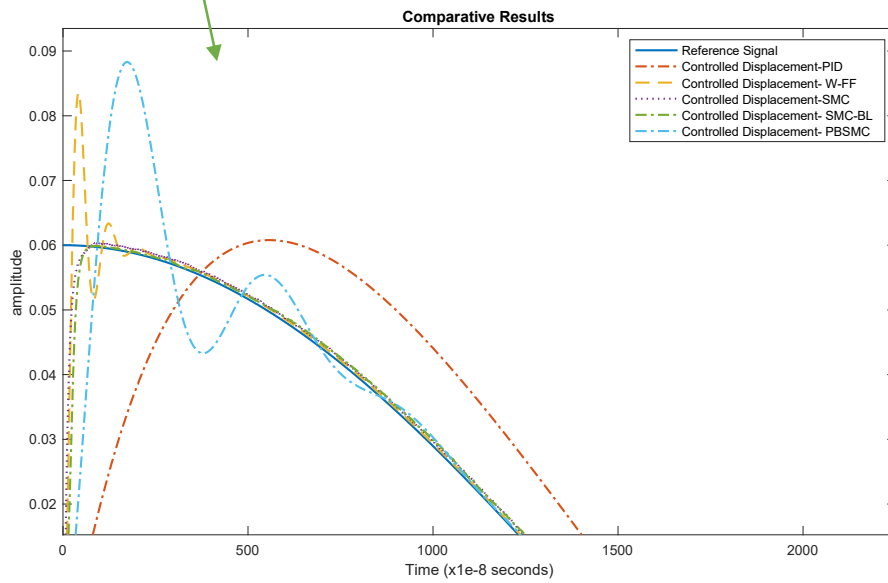
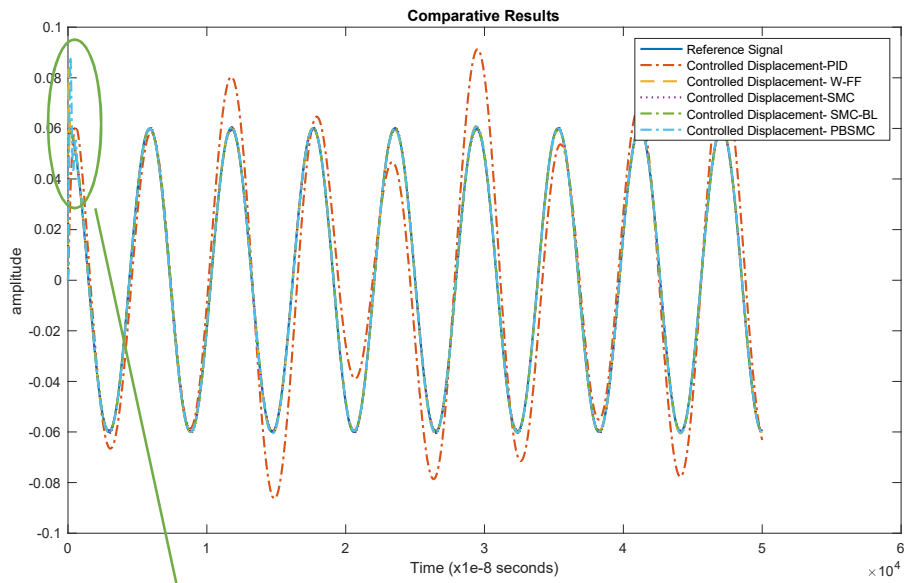


Figure 5.1 Controller Tracking Performance for Drive Axis Control – 0.5 PSD (Initial Phase)

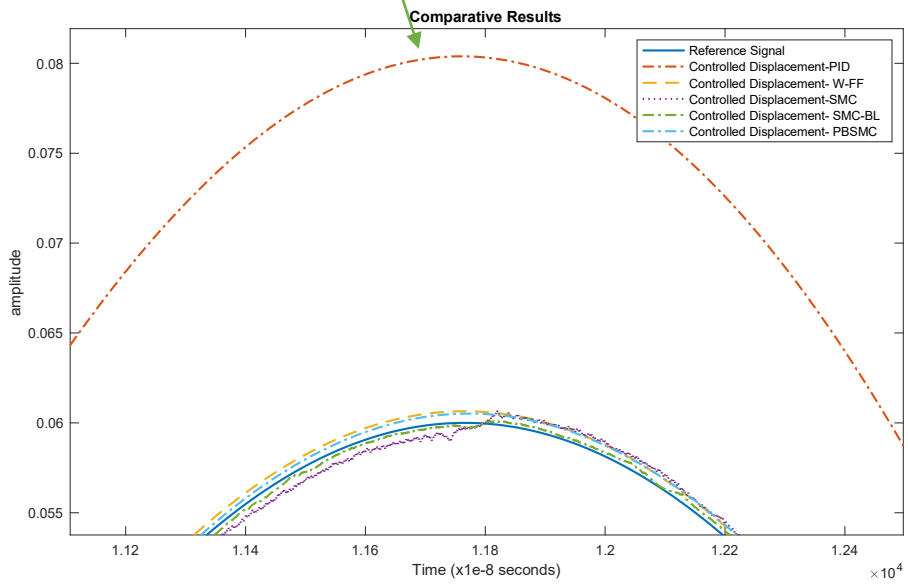
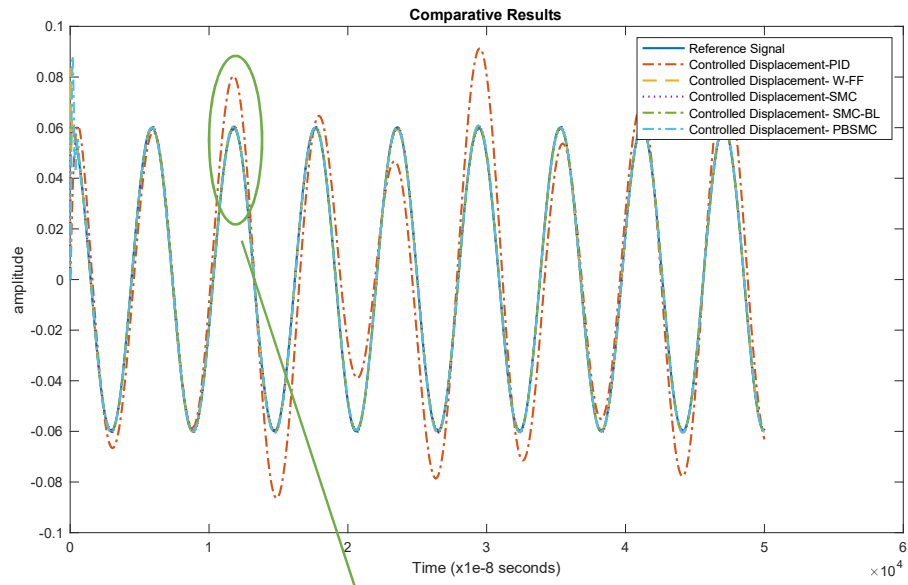


Figure 5.2 Controller Tracking Performance for Drive Axis Control – 0.5 PSD (Steady State Phase)

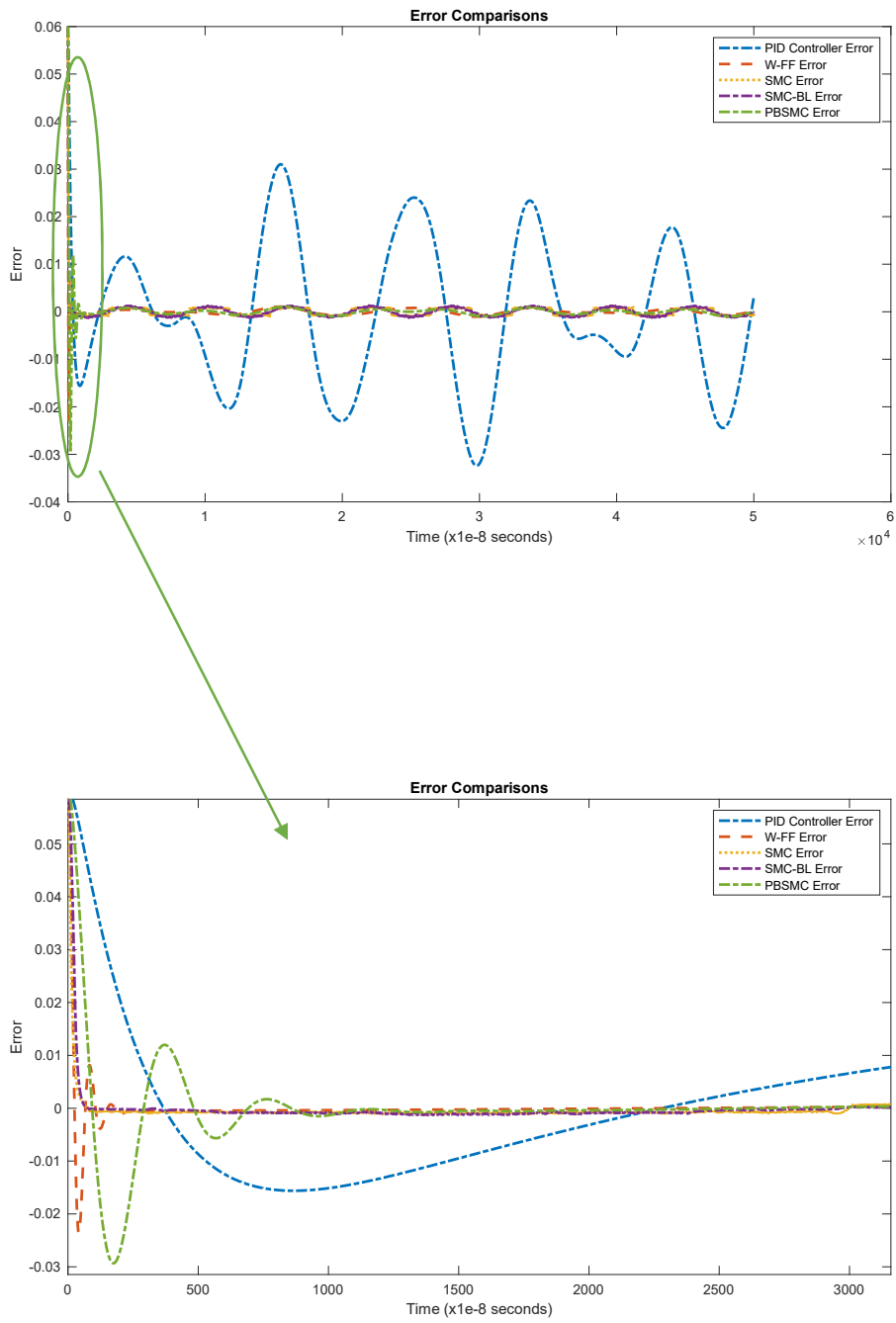


Figure 5.3 Error Comparisons – 0.5 PSD (Initial Phase)

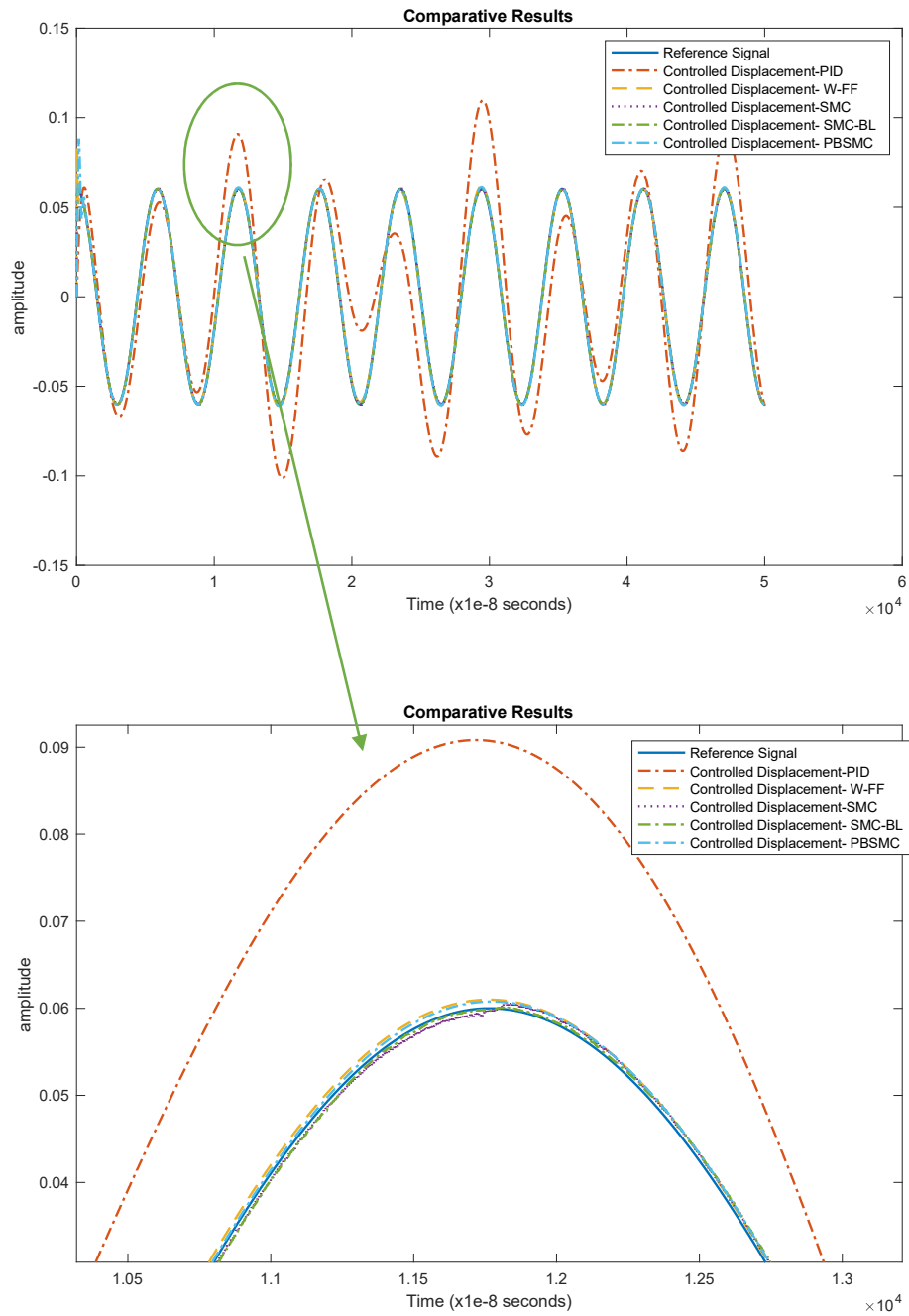


Figure 5.4 Controller Tracking Performance for Drive Axis Control – 1.5 PSD

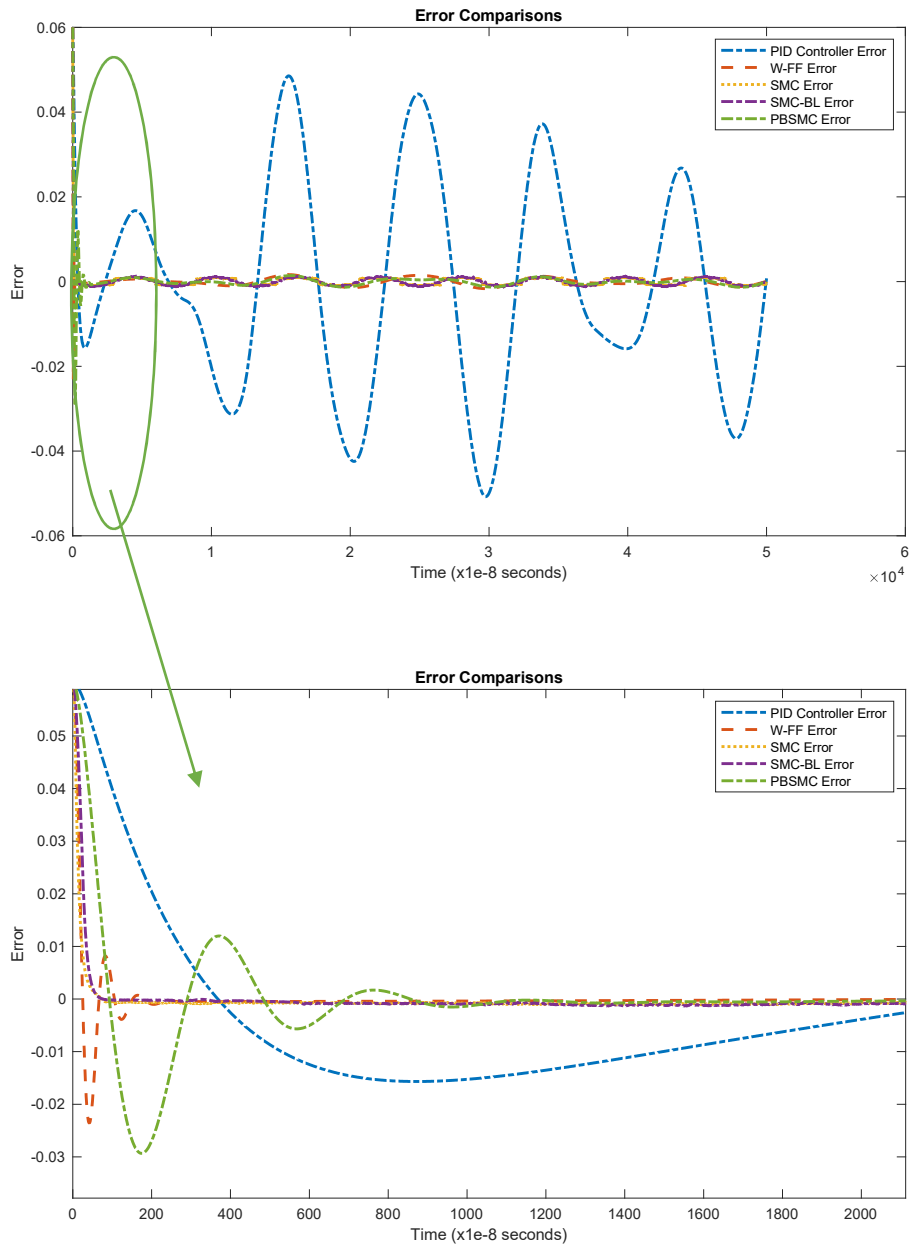


Figure 5.5 Error Comparisons – 1.5 PSD (Initial Phase)

Table 5.1 Error Performance Comparison for Different Noise Power Level

	<i>PID</i>	<i>SMC</i>	<i>SMC -BL</i>	<i>PBSMC</i>	<i>W-FF</i>
SS RMS Error—0.5	0.0156	7.8621×	7.9335×	5.1134×	5.1472×
Noise power		10 ⁻⁴	10 ⁻⁴	10 ⁻⁴	10 ⁻⁴
SS RMS Error—0.8	0.0196	7.8532×	7.9146×	5.6769×	6.3702×
Noise power		10 ⁻⁴	10 ⁻⁴	10 ⁻⁴	10 ⁻⁴
SS RMS Error—1.5	0.0267	7.8707×	7.8707×	6.8035×	8.5678×
Noise power		10 ⁻⁴	10 ⁻⁴	10 ⁻⁴	10 ⁻⁴

After the effect of noise level observation, two additional simulation studies are carried out:

- Reference vibration signal amplitude is increased and decreased. However, it is seen that this parameter does not play a crucial role on control performance.
- Referencevibration signal frequency is changed. While the frequency is decreased, performance of controller is not decreased. However, around 40kHz PID controller does not track the reference signal.

Performance degradation of the PID controller can be observed from Figure 5.6 and Figure 5.7.

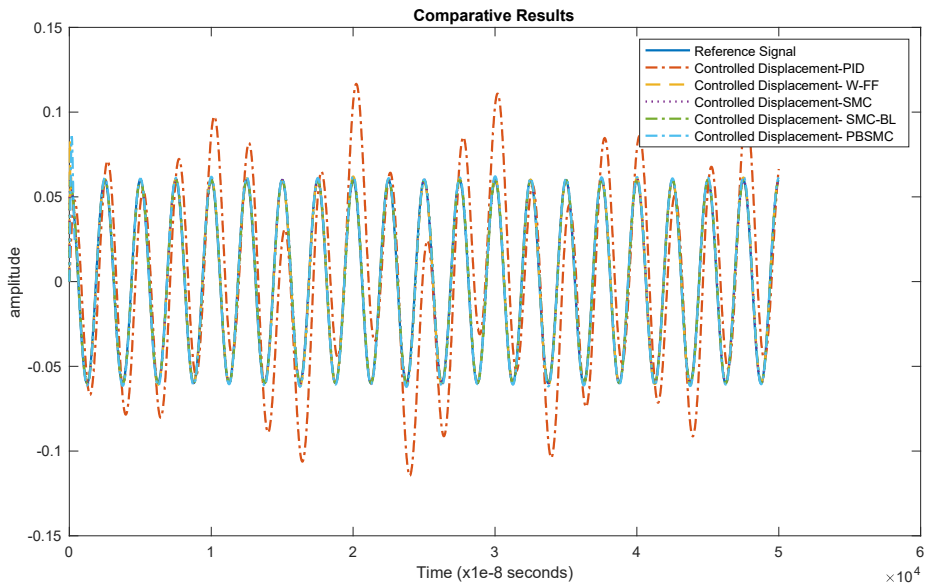


Figure 5.6 Controller Tracking Performance for Drive Axis Control – 40 kHz Reference Vibration Signal Frequency

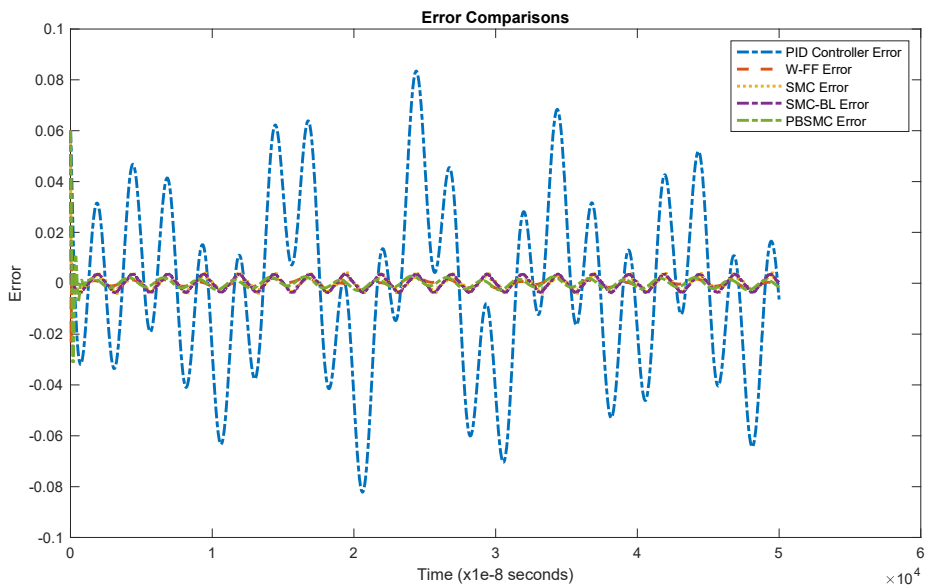


Figure 5.7 Error Comparisons – 40 kHz Reference Vibration Signal Frequency

It can be clearly observed from the figures, while the frequency increases and PID performance decreases, other controllers remain unresponsive. Additionally, Figure 5.7 shows that the PID controller error amplitude increases and becomes irregular.

5.2 Controller Performance Comparison for Different SMC Parameters

To better understand the effects of the SMC design parameters, simulations are implemented with different Q , λ , ϕ values. First of all, value of λ is increased from 100 to 900. Sensitivity analysis results according λ variation are shown in Figure 5.8 and Figure 5.9.

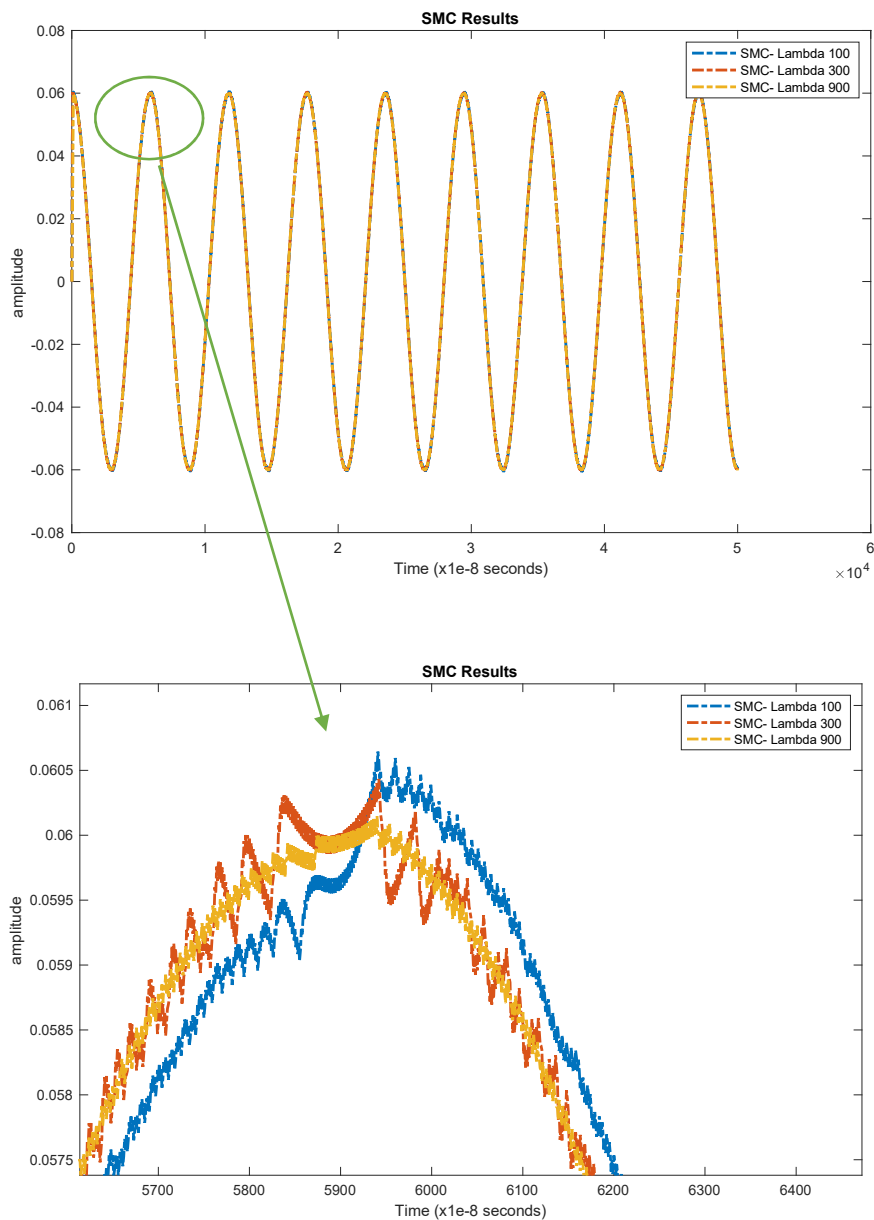


Figure 5.8 Effect of λ on the SMC Tracking Performance

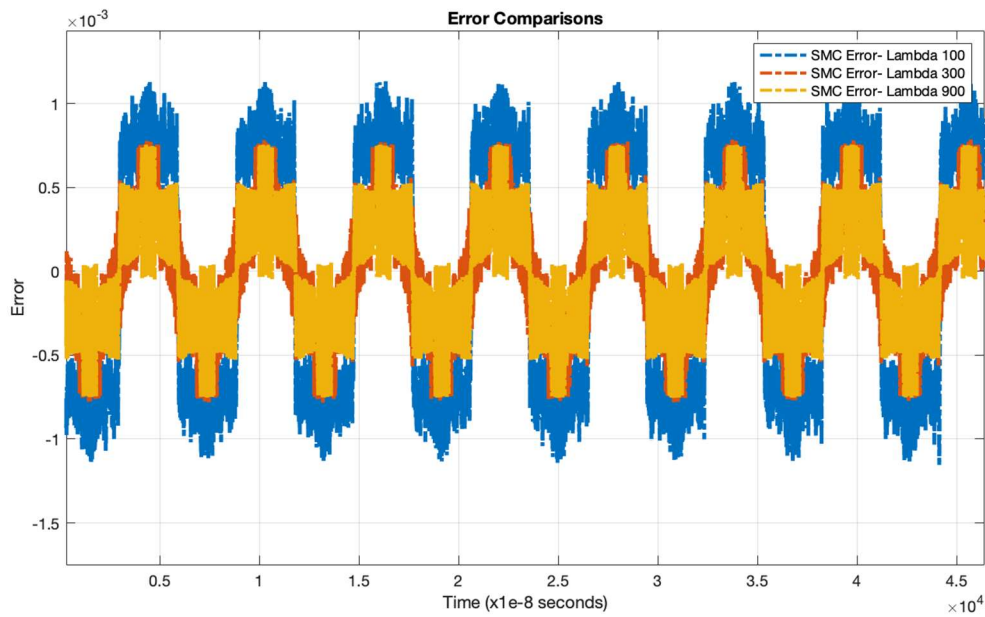


Figure 5.9 Effect of λ on the SMC Error Performance

It can be easily observed from the figures, amplitude of the chattering and error levels are decreased with the increase in the λ . This is an expected result since λ directly affects the system dynamics. Simulation results shows that results but the control signal that can be applied to the system is limited. Therefore, $\lambda = 100$ is an ideal value for our application.

Similarly, the effect of Q , which is the controller gain, was also observed in the simulation environment. Amplitude of the switching signal varies with the value of Q . Therefore, amplitude of chattering is increased with high Q and decreased with small Q . On the other hand, controller shows worse tracking performance when the value of Q is decreased. But according to the physical limitations of the sensor value of Q cannot exceed 900. And there is a trade-off between chattering amplitude and tracking performance. However, $Q=450$ provides the best chattering performance, it cannot provides the best tracking performance. Figure 5.10 and Figure 5.11 shows the effect of Q on the tracking and error performance.

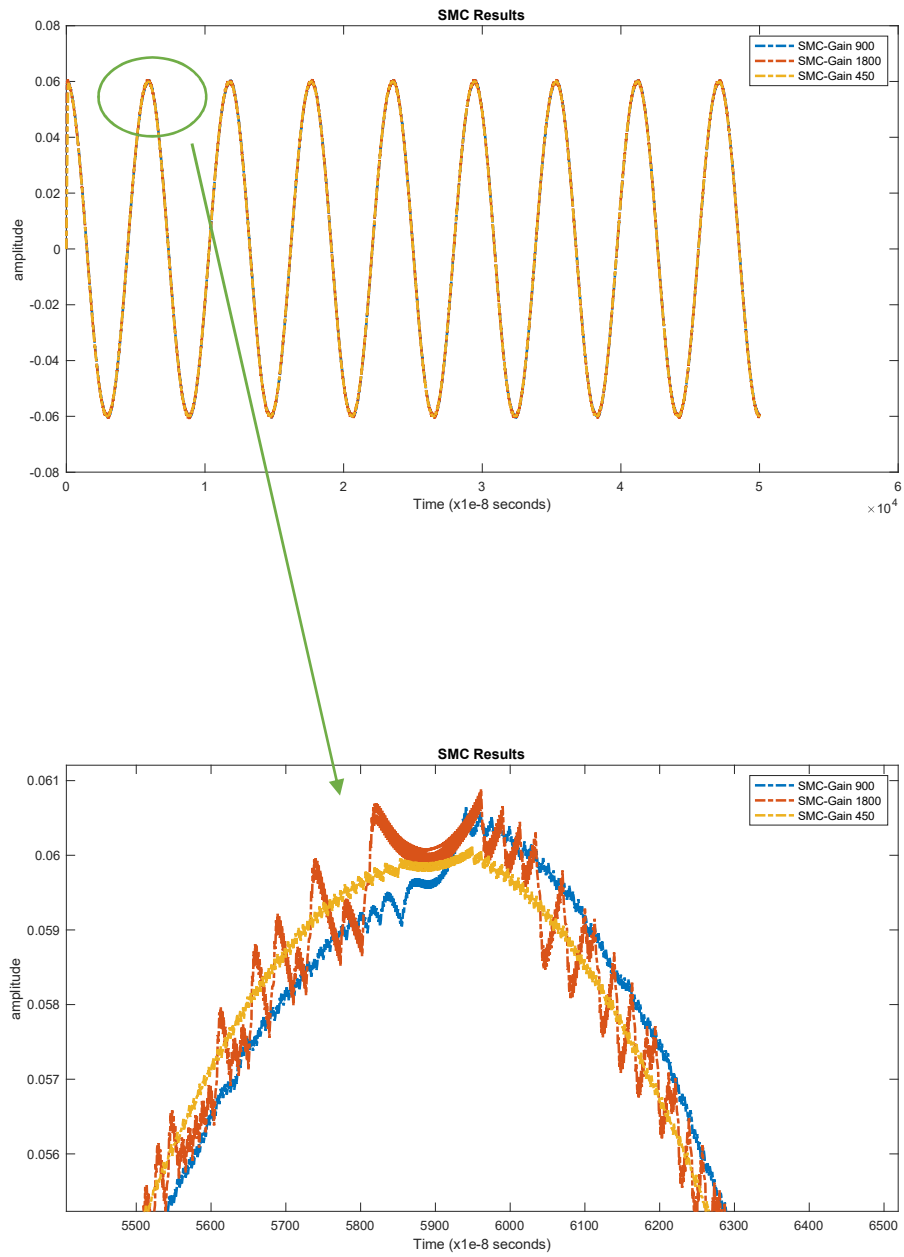


Figure 5.10 Effect of Q on the SMC Tracking Performance

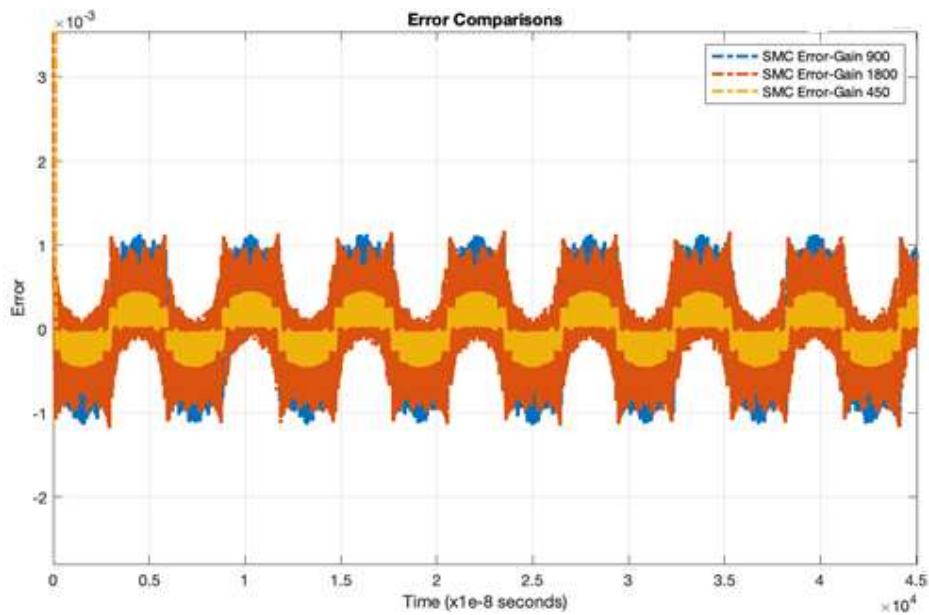


Figure 5.11 Effect of Q on the SMC Error Performance

Finally, effect of boundary layer thickness is investigated. ϕ is increased and decreased between 0.11 and 0.46. Determining an appropriate value for the boundary layer thickness ϕ is crucial; it directly affects tracking and robustness performance. A narrow boundary layer cannot solve the chattering problem, and a too wide boundary layer causes degradation in tracking performance and robustness.

According to Figure 5.12 and Figure 5.13 $\phi = 0.23$ gives the optimum solution for chattering and tracking performance. Tracking performance degradation is observed with the wide boundary layer.

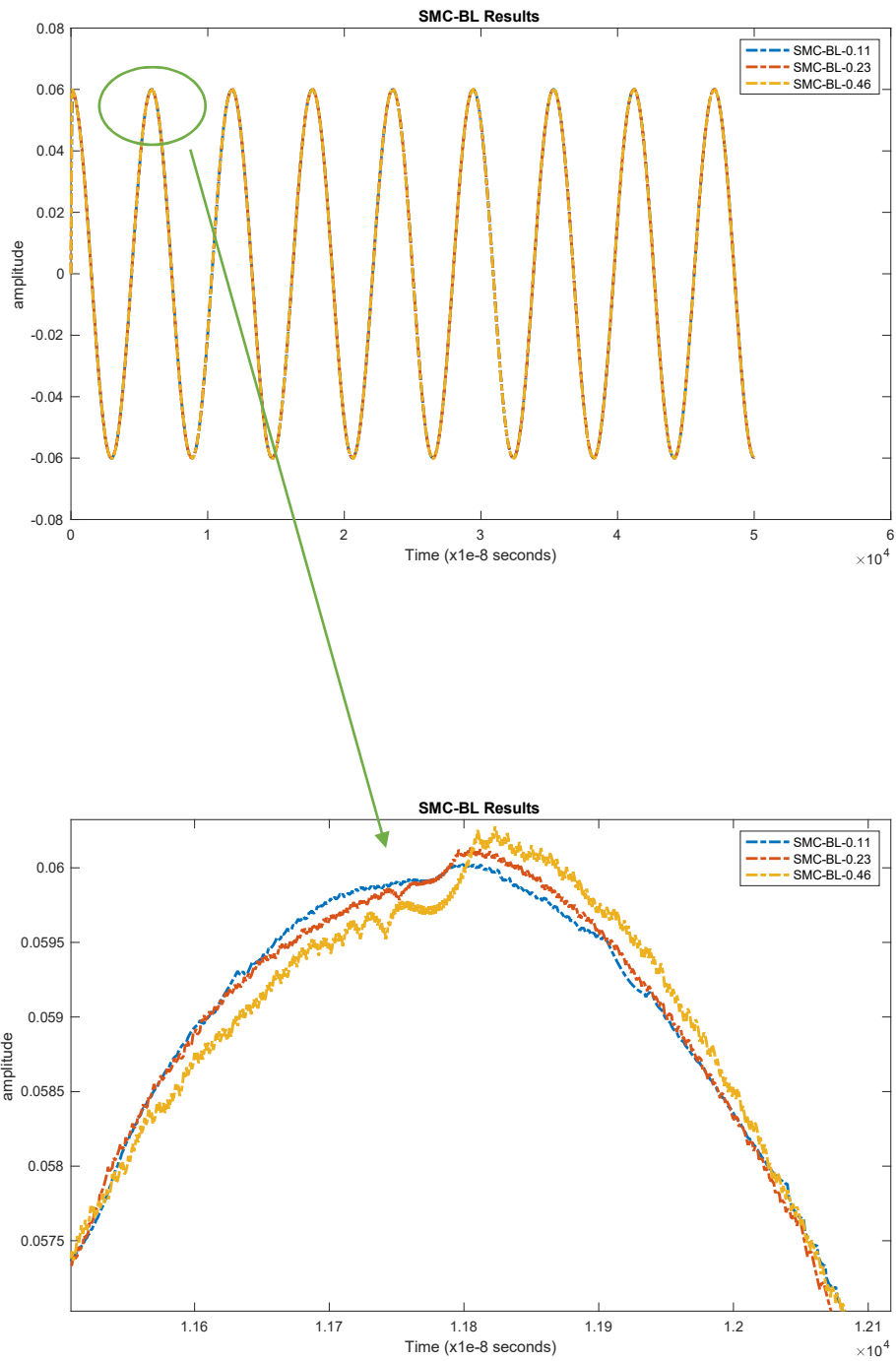


Figure 5.12 Effect of ϕ on the SMC Tracking Performance

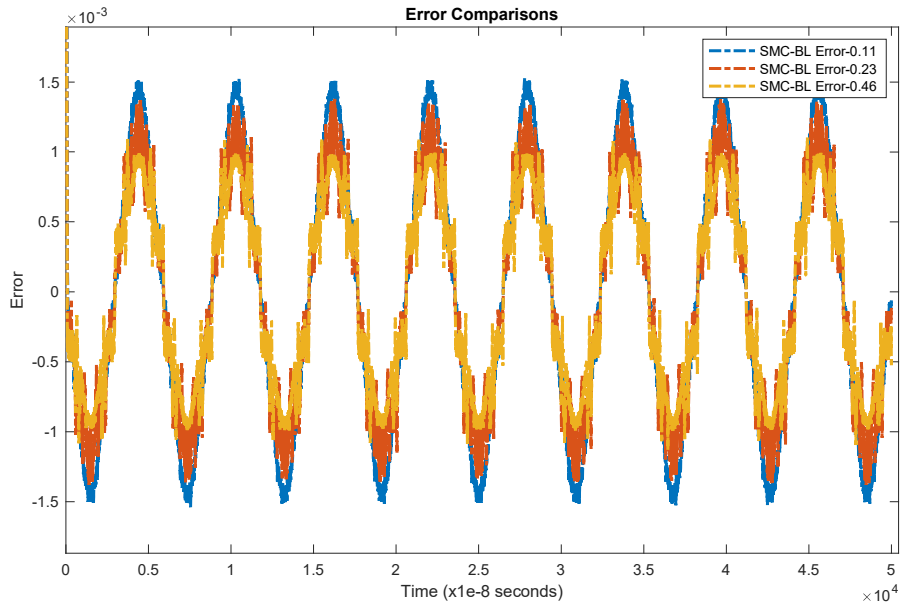


Figure 5.13 Effect of ϕ on the SMC Error Performance

5.3 Error Performance Comparison for Different Angular Rate Input

Two different angular rates are applied to the system during the experimental studies. And it is observed that a change on the input angular rate does not cause a significant change in the controller performance. This situation confirms the effect of controller usage on proportionality coefficient error.

Error measurements under input rates are summarized in Table 5.2.

Table 5.2 Angular Rate Total Error Comparison for Different Input Rates

Parameter	<i>PID</i>	<i>SMC</i>	<i>SMC-BL</i>	<i>PBSMC</i>	<i>W-FF</i>
Maximum Error for 10 deg/s	-31.1341 deg/h	-27.5947 deg/h	-26.9839 deg/h	-22.8719 deg/h	-24.1894 deg/h
Maximum Error for 20 deg/s	-32.2484 deg/h	-28.5214 deg/h	-26.9830 deg/h	-23.6921 deg/h	-24.1882 deg/h

Controller tracking performance and error comparison figures for 10 deg/s input rate are given in Chapter 4, and comparisons for 20 deg/s input rate are shown in Figure 5.8, Figure 5.9, and Figure 5.10.

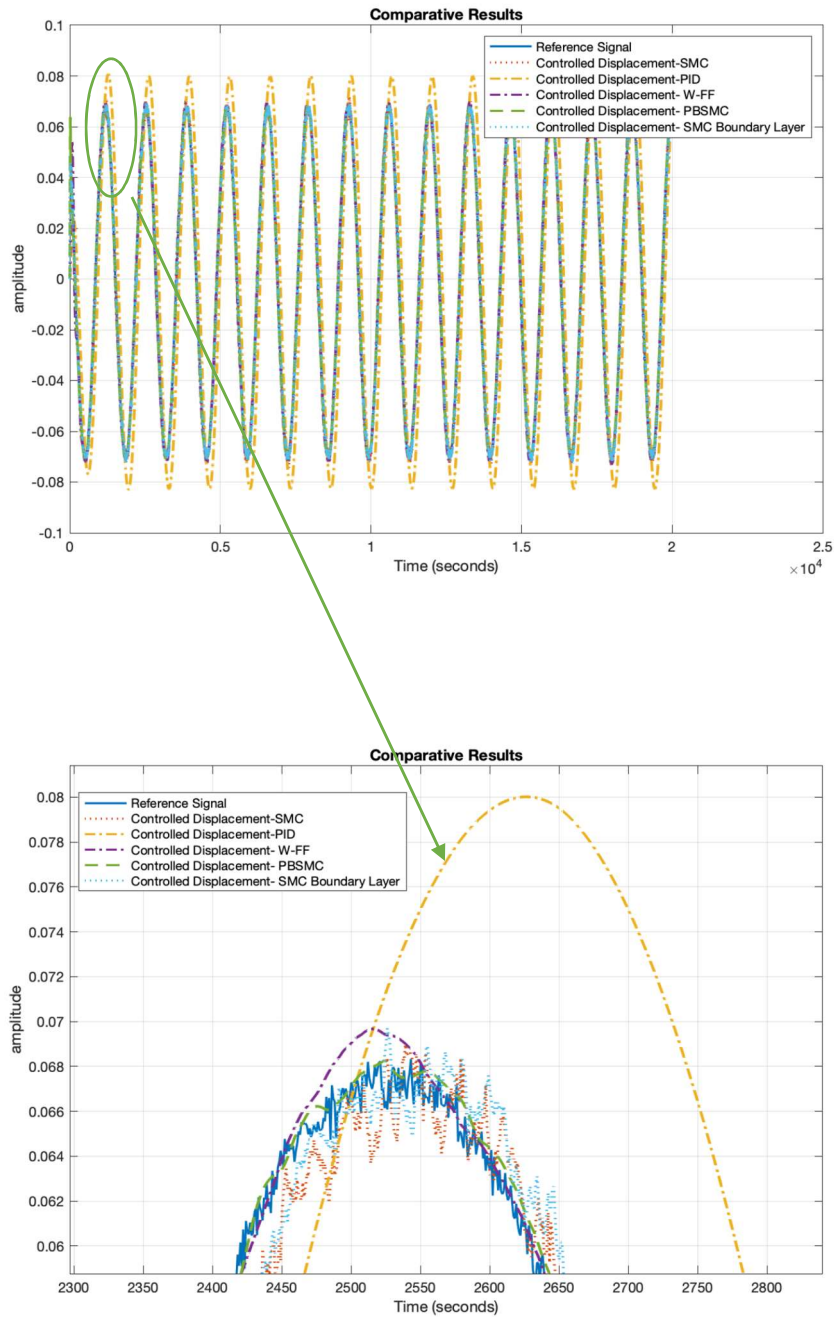


Figure 5.14 Controller Tracking Performance for Drive Axis Control – Experimental Data 20 deg/s input rate

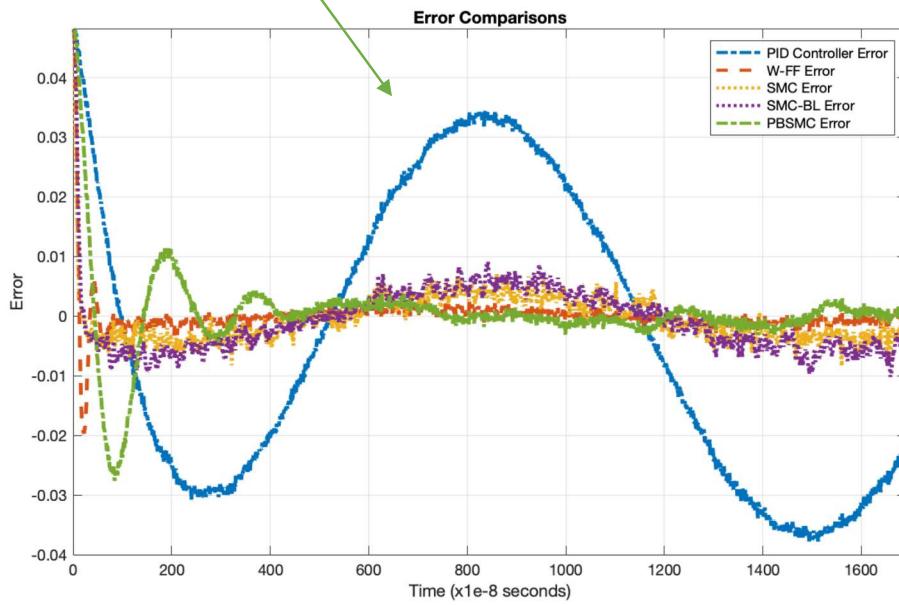
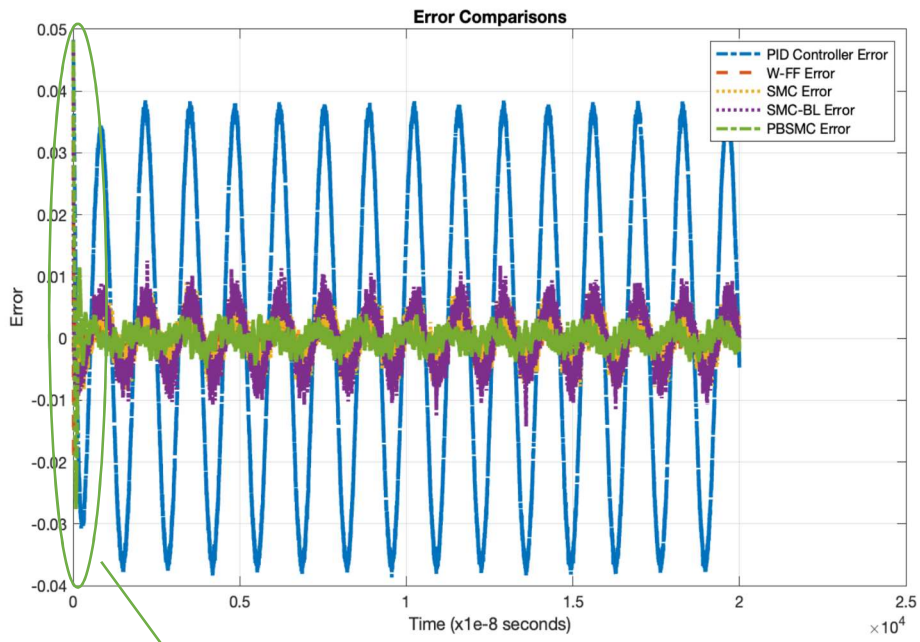


Figure 5.15 Error Comparisons - Experimental Data 20 deg/s input rate

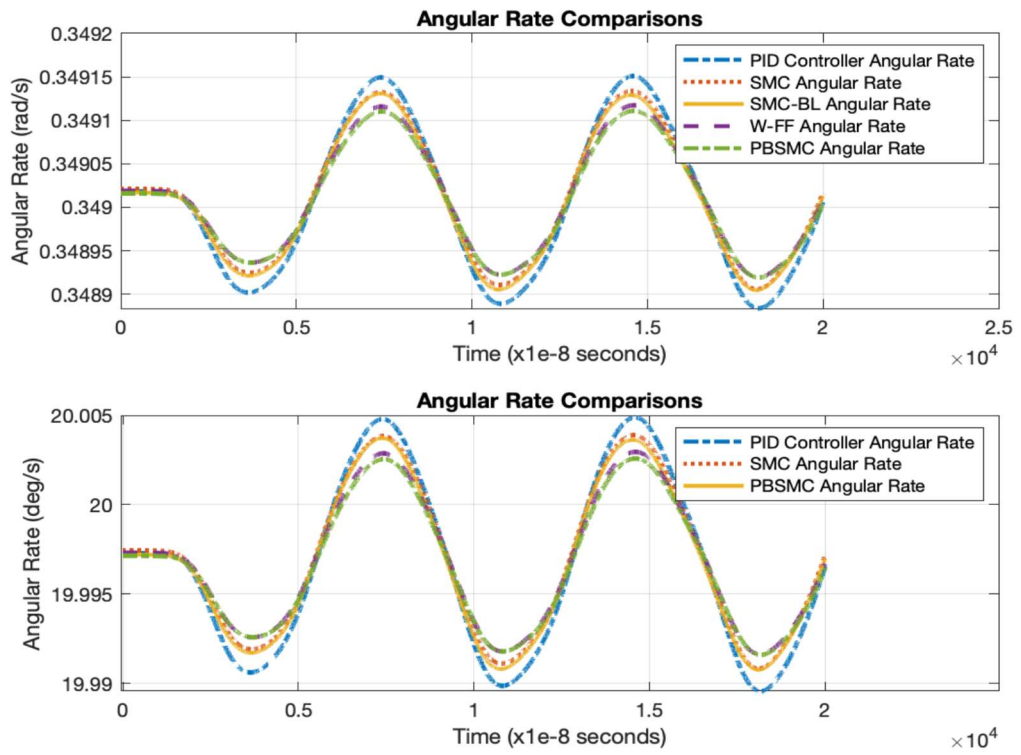


Figure 5.16 Angular Rate Measurement Comparison-Experimental Data 20 deg/s input rate

CHAPTER 6

CONCLUSIONS AND FUTURE WORK

6.1 Conclusions

In this thesis work, two different and new generation control methods are proposed. It is aimed to get more accurate angular rate measurement performance by controlling the proof mass displacement.

Weighted Feedforward Controller and Proxy Based Sliding Mode Controller are proposed, and a SMC and PID controllers are implemented to compare the classical techniques and proposed methods. And classical methods perform worse than the proposed method.

Weighted Feedforward Controller performance is observed to be better than others in ideal conditions. However, Proxy Based Sliding Mode Controller is more robust under disruptive effects.

With the use of the proposed controllers, it is expected that there will be improvement in scale factor linearity, especially. This situation will provide high accuracy, especially under high angular rates, and reduce the total angular rate and angle error.

Both methods overwhelm the other methods on literature by the fact that they are easily implemented on low-cost CPU and microcontrollers. This also brings smaller and low power units which is important in new applications.

In addition to increasing the sensor performance, it is expected that the need for calibration of the sensor will decrease by means of the developed methods. This will contribute to providing a cost-effective solution.

6.2 Future Works

As a future work, temperature and vibration tests can be conducted using this sensor in a sealed case. It is expected that PBSMC will perform better than other controllers, and the performance difference between W-FF will increase.

A large number of tests can be carried out with the proposed controllers by producing in large quantities designed sensor prototypes. This test study aims to collect statistical data on sensor and controller performance under different conditions. Thus, information about the error mean and distribution of the sensor and controller can be obtained. As a result of this study, it is expected that the sensor errors will appear in a characteristic that converges to the Gaussian distribution.

In addition to the above studies, for the dynamic modeling of the gyroscope, it is considered that the performance of Weighted Feedforward Controller can be increased by adding a method that runs online and dynamically estimates the sensor parameters unlike the unit step response.

REFERENCES

- Acar, C., & Shkel, A. (2008). *MEMS Vibratory Gyroscopes Structural Approaches to Improve Robustness*. Springer.
- Apostolyuk, V. (2016). Coriolis vibratory gyroscopes: Theory and design. In *Coriolis Vibratory Gyroscopes: Theory and Design*. Springer International Publishing. <https://doi.org/10.1007/978-3-319-22198-4>
- Asad, Y. P., Shamsi, A., & Tavoosi, J. (2017). Backstepping-Based Recurrent Type-2 Fuzzy Sliding Mode Control for MIMO Systems (MEMS Triaxial Gyroscope Case Study). *International Journal of Uncertainty, Fuzziness and Knowledge-Based Systems*, 25(02), 213–233. <https://doi.org/10.1142/S0218488517500088>
- Batur, C., Sreeramreddy, T., & Khasawneh, Q. (2006). Sliding mode control of a simulated MEMS gyroscope. *ISA Transactions*, 45(1), 99–108. [https://doi.org/10.1016/S0019-0578\(07\)60069-X](https://doi.org/10.1016/S0019-0578(07)60069-X)
- Bu, F., Fan, B., Xu, D., Guo, S., & Zhao, H. (2021). Bandwidth and noise analysis of high-Q MEMS gyroscope under force rebalance closed-loop control. *Journal of Micromechanics and Microengineering*, 31(6), 065002. <https://doi.org/10.1088/1361-6439/abf32e>
- Cerone, V., Milanese, M., & Regruto, D. (2007). Robust feedforward design for a two-degrees of freedom controller. *Systems & Control Letters*, 56(11–12), 736–741. <https://doi.org/10.1016/j.sysconle.2007.04.010>
- Cui, M., Huang, Y., Wang, W., & Cao, H. (2019). MEMS Gyroscope Temperature Compensation Based on Drive Mode Vibration Characteristic Control. *Micromachines*, 10(4), 248. <https://doi.org/10.3390/mi10040248>
- Devices Analog. (2017). *ADXRS646 High Stability, Low Noise Vibration Rejecting Yaw Rate Gyroscope*. Analog Devices.

- Draženić, B. (1969). The Invariance Conditions in Variable Structure Systems. *Automatica*, 5(3), 287–295. [https://doi.org/10.1016/0005-1098\(69\)90071-5](https://doi.org/10.1016/0005-1098(69)90071-5)
- Durmaz, B. (2009). *Sliding Mode Control Of Linearly Actuated Nonlinear Systems A Thesis Submitted To The Graduate School Of Natural And Applied Sciences Of Middle East Technical University*.
- Edwards, C., & Spurgeon, S. (1998). *Sliding Mode Control: Theory And Applications*. Taylor & Francis .
- El-Sheimy, N., & Youssef, A. (2020). Inertial sensors technologies for navigation applications: state of the art and future trends. *Satellite Navigation*, 1(1), 2. <https://doi.org/10.1186/s43020-019-0001-5>
- Emcore Navigation. (2020). *Glossary of Inertial Sensing Terms*. Emcore Navigation and Inertial Sensing. <https://emcore.com/glossary-inertial-sensing-terms/>
- Emelyanov, S. (1957). *Variable Structure Control Systems*.
- Erbatur, K., & Çallı, B. (2009). Fuzzy boundary layer tuning for sliding mode systems as applied to the control of a direct drive robot. *Soft Computing*, 13(11), 1099–1111. <https://doi.org/10.1007/s00500-008-0383-z>
- Fei, J., & Yuan, Z. (2013). Dynamic Sliding Mode Control of MEMS Gyroscope. *IEEE International Conference on Control Applications (CCA)*.
- Fitzgerald, A. M. (2021). *MEMS Inertial Sensors* (, James J. Spilker Jr., Bradford W. Parkinson, Sherman Lo, Grace Gao Frank van Diggelen. T. Jade Morton, Ed.). The Institute of Electrical and Electronics Engineers. <https://doi.org/https://doi.org/10.1002/9781119458555.ch45>
- Geen, J. A., Sherman, S. J., Chang, J. F., & Lewis, S. R. (2002). Single-chip surface-micromachined integrated gyroscope with 50°/hour root allan variance. *2002 IEEE International Solid-State Circuits Conference. Digest of*

Technical Papers (Cat. No.02CH37315), 346–539.

<https://doi.org/10.1109/ISSCC.2002.992288>

Greiff, P., Boxenhorn, B., King, T., & Niles, L. (n.d.). Silicon monolithic micromechanical gyroscope. *TRANSDUCERS '91: 1991 International Conference on Solid-State Sensors and Actuators. Digest of Technical Papers*, 966–968. <https://doi.org/10.1109/SENSOR.1991.149051>

Grinberg, B., Feingold, A., Furman, L., & Wolfson, R. (2016). High precision open-loop and closed-loop MEMS accelerometers with wide sensing range. *2016 IEEE/ION Position, Location and Navigation Symposium (PLANS)*, 924–931. <https://doi.org/10.1109/PLANS.2016.7479789>

Groves P.D. (2003). *Principles of GNSS, Inertial, and Multisensor Integrated Navigation Systems*. Artech House.

Gu, G. Y., Zhu, L. M., Su, C. Y., Ding, H., & Fatikow, S. (2015). Proxy-Based Sliding-Mode Tracking Control of Piezoelectric-Actuated Nanopositioning Stages. *IEEE/ASME Transactions on Mechatronics*, 20(4), 1956–1965. <https://doi.org/10.1109/TMECH.2014.2360416>

Hexagon, N. (2022, May 10). *Attitude*. Hexagon Novatel. <https://novatel.com/solutions/attitude#:~:text=Attitude%20provides%20information%20about%20an,%3A%20roll%2C%20pitch%20and%20yaw.>

Honeywell Aerospace. (2017). HG4930 Inertial Measurement Unit (IMU) Performance and Environmental Information. In *Honeywell Aerospace*.

IEEE 528-2019. (2019). IEEE Standard for Inertial Sensor Terminology. In *IEEE*. IEEE Standard Association.

IEEE 1431-2004. (2010). IEEE Standard Specification Format Guide and Test Procedure for Coriolis Vibratory Gyros. In *IEEE*. IEEE Standards Association.

- IEEE Standard for Sensor Performance Parameter Definitions IEEE Electron Devices Society Sponsored by the Microelectromechanical Systems Standards Development Committee. (2017). In *IEEE Std 2700-2017 (Revision of IEEE Std 2700-2014)*. <https://doi.org/10.1109/IEEESTD.2018.8277147>
- Looney, M. (2015). *The Basics of MEMS IMU/Gyroscope Alignment*. Analog Devices.
- Marlin, T. (2000). *Process Control: Designing Processes and Control Systems for Dynamic Performance*. McGraw-Hill.
- Mizov, A. (2015). *A Model-Free Control Algorithm Derived Using the Sliding Model Control Method*. Rochester Institute of Technology.
- Moyer, B. (2020, October 28). Are Today's MEMS Gyros "Good Enough"? *Semiconductor Engineering*.
- Passaro, V. M. N., Cuccovillo, A., Vaiani, L., de Carlo, M., & Campanella, C. E. (2017). Gyroscope technology and applications: A review in the industrial perspective. In *Sensors (Switzerland)* (Vol. 17, Issue 10). MDPI AG. <https://doi.org/10.3390/s17102284>
- Patel, C., & McCluskey, P. (2012, May). Modeling and simulation of the MEMS vibratory gyroscope. *13th InterSociety Conference on Thermal and Thermomechanical Phenomena in Electronic Systems*. <https://doi.org/10.1109/ITHERM.2012.6231524>
- Pistorio, F., Saleem, M. M., & Somà, A. (2021). A Dual-Mass Resonant MEMS Gyroscope Design with Electrostatic Tuning for Frequency Mismatch Compensation. *Applied Sciences*, *11*(3), 1129. <https://doi.org/10.3390/app11031129>
- Preethi, B., Sujatha, L., & Selvakumar, V. S. (n.d.). *Design and Analysis of MEMS Gyroscope*.

- Qing Zheng, Lili Dong, Dae Hui Lee, & Zhiqiang Gao. (2009). Active Disturbance Rejection Control for MEMS Gyroscopes. *IEEE Transactions on Control Systems Technology*, 17(6). <https://doi.org/10.1109/TCST.2008.2008638>
- Rahmani, M., Rahman, M. H., & Nosonovsky, M. (2020). A new hybrid robust control of MEMS gyroscope. *Microsystem Technologies*, 26(3), 853–860. <https://doi.org/10.1007/s00542-019-04584-z>
- Raman, J., Cretu, E., Rombouts, P., Weyten, L., & Weyten, 'a, L. (2009). Closed-Loop Digitally Controlled MEMS Gyroscope With Unconstrained Sigma-Delta Force-Feedback. In *IEEE Sensors Journal* (Vol. 9, Issue 3).
- Saqib, M., Mubasher Saleem, M., Mazhar, N., Awan, S., & Shahbaz Khan, U. (2018). Design and Analysis of a High-Gain and Robust Multi-DOF Electro-thermally Actuated MEMS Gyroscope. *Micromachines*, 9(11), 577. <https://doi.org/10.3390/mi9110577>
- Shi, G., Yang, S., & Su, Z. (2011). Random Drift Suppression Method of MEMS Gyro Using Federated Kalman Filter. *3rd International Conference on Advanced Computer Control*.
- Slotine, J. J., & Sastry, S. S. (1983). Tracking control of non-linear systems using sliding surfaces with application to robot manipulators. *1983 American Control Conference*, 132–135. <https://doi.org/10.23919/ACC.1983.4788090>
- Slotine, J.-J., & Li, W. (1991). *Applied Nonlinear Control*. Prentice-Hall.
- Tronics. (2021). Tronics Gypro3300. In *Tronic's Microsystems S.A.*
- Trusov, A. A., Schofield, A. R., & Shkel, A. M. (2009). Performance characterization of a new temperature-robust gain-bandwidth improved MEMS gyroscope operated in air. *Sensors and Actuators A: Physical*, 155(1), 16–22. <https://doi.org/10.1016/j.sna.2008.11.003>

- Utkin, V. I. (2002). First Stage of VSS: People and Events. In *Variable Structure Systems: Towards the 21st Century* (pp. 1–32). Springer Berlin Heidelberg.
https://doi.org/10.1007/3-540-45666-X_1
- Vectornav Navigation. (2020). *IMU Specifications*. Vectornav Navigation Library.
<https://www.vectornav.com/resources/inertial-navigation-primer/specifications--and--error-budgets/specs-imuspecs>
- Wang, C. (2013). Reconfigurable Closed-Loop Digital $\Delta\Sigma$ Capacitive MEMS Accelerometer for Wide Dynamic Range, High Linearity Applications. *International Journal of Information and Electronics Engineering*.
<https://doi.org/10.7763/IJIEE.2013.V3.262>
- Wang, C., Yu, H. H., Wu, M., & Fang, W. (2007). Implementation of phase-locked loop control for MEMS scanning mirror using DSP. *Sensors and Actuators, A: Physical*, 133(1), 243–249. <https://doi.org/10.1016/j.sna.2006.03.026>
- Wheeler, J. M., & Digonnet, M. J. F. (2021). Demonstration of Strategic-Grade Noise in an Optically Gated Laser-Driven Fiber Optic Gyroscope. *Optical Fiber Sensors Conference 2020 Special Edition*, W4.75.
<https://doi.org/10.1364/OFS.2020.W4.75>
- Xia, D., Hu, Y., & Ni, P. (2016). A digitalized gyroscope system based on a modified adaptive control method. *Sensors (Switzerland)*, 16(3).
<https://doi.org/10.3390/s16030321>
- Yazıcı, İ. (2008). *Model Referans Kayan Kipli Kontrolör Tabanlı Güç Sistem Kararlayıcı Tasarımı* .

CURRICULUM VITAE

PERSONAL INFORMATION

Surname, Name: Ünsal Öztürk, Derya
Nationality: Turkish (TC)
Date and Place of Birth: 19 September 1986, Ankara
Marital Status: Married
email: derya.unsal@metu.edu.tr

EDUCATION

Degree	Institution	Year of Graduation
MS	METU, Electrical and Electronic Engineering	2012
BS	Baskent University, Electrical and Electronic Engineering	2008
High School	Mehmet Emin Resulzade Anadolu High School, Ankara	2004

WORK EXPERIENCE

Year	Place	Enrollment
2008-Present	Roketsan Roket Sanayi ve Ticaret A.Ş.	Engineer

FOREIGN LANGUAGES

Advanced English

PUBLICATIONS

1. Ünsal Öztürk, D.; Erkmen, A.M. Coriolis Vibratory MEMS Gyro Drive Axis Control with Proxy-Based Sliding Mode Controller. *Micromachines* 2022, 13, 446. <https://doi.org/10.3390/mi13030446>.
2. Altinöz, B.; Unsal, D. "Determining efficient temperature test points for IMU calibration," 2018 IEEE/ION Position, Location and Navigation Symposium (PLANS), 2018, pp. 552-556, doi: 10.1109/PLANS.2018.8373426.
3. Unsal D.; Dogan M., "Implementation of identification system for IMUs based on Kalman Filtering," 2014 IEEE/ION Position, Location and Navigation

Symposium - PLANS 2014, 2014, pp. 236-240, doi: 10.1109/PLANS.2014.6851381.

4. Altinöz, B.; Unsal, D., "Look up table implementation for IMU error compensation algorithm," 2014 IEEE/ION Position, Location and Navigation Symposium - PLANS 2014, 2014, pp. 259-261, doi: 10.1109/PLANS.2014.6851384.

5. Günhan, Y.; Unsal, D., "Polynomial degree determination for temperature dependent error compensation of inertial sensors," 2014 IEEE/ION Position, Location and Navigation Symposium - PLANS 2014, 2014, pp. 1209-1212, doi: 10.1109/PLANS.2014.6851494.

6. Unsal D.; Demirbas K., "Estimation of deterministic and stochastic IMU error parameters," Proceedings of the 2012 IEEE/ION Position, Location and Navigation Symposium, 2012, pp. 862-868, doi: 10.1109/PLANS.2012.6236828.

7. Unsal D., "MEMS Ataletsel Ölçüm Biriminin Deterministik ve Olasılıksal Hata Parametrelerinin Kestirimi", Savtek 2012.

8. Unsal D.; Dogan M., "Kalman Süzgeci ile Sistem Tanımlama" TOK'08(Member of IFAC)-Otomatik Kontrol Ulusal Toplantısı, İstanbul, Turkey, 2008, pp. 846-852.